FINAL REPORT

DTPH56-13-T-000003
"INO Technologies Assessment of Leak Detection System for Hazardous Liquid Pipelines"

SUBMITTED BY: Team Project Manager
Deborah Jelen
Electricore, Inc
27943 Smyth Drive, Suite 105
Valencia, CA 91355
Telephone: (661) 607-0230
E-mail: jelen@lelectricore.org

TEAM TECHNICAL COORDINATOR: Team Technical Coordinator
Jean-François Gravel
INO
2740, rue Einstein
Quebec (Quebec) GIP 4S4 Canada
Telephone: (418) 657-7006
E-mail: jean-francois.gravel@ino.ca

TEAM PARTICIPANTS: INO
TransCanada

SUBMITTED TO: U. S. Department of Transportation
Pipeline and Hazardous Materials Safety Administration
Mr. Max Kieba
Technical Program Manager
Max.Kieba@dot.gov

SUBMITTED ON: August 13, 2015

Table of Contents

1.0 Executive Summary 6
1.1 Executive Summary Report 1- Liquid Petroleum Pipeline Leak Detection by Means of Optical Remote Sensing; Concept of Operations (CONOPS) and Feasibility Study 6
1.2 Executive Summary Report 2 - Preliminary Test Results and Refined Feasibility 8
1.3 Executive Summary Report 3 - Limits of Detection, Choice of Platforms and Lifecycle Cost Analysis 9
1.4 Executive Summary Report 4 – IR Database, Raman System Modifications and In Depth Testing 10
1.5 Executive Summary Report 5 – INO Technologies Assessment as Leak Detection Systems for Hazardous Liquid Pipelines; Results of simulated field testing 12
2.0 Technical Status 17
3.0 Results and Conclusions 20
3.1 Report Content 21
3.2 Compositions of Targeted Liquid Petroleum Products 22
3.2.1 Saturated Hydrocarbons 22
3.2.2 Aromatic hydrocarbons 23
3.2.3 Soil Types and Characteristics 23
3.2.4 Targeted Molecular Species Concentrations in the Vapor Phase 23
3.2.5 Spectral Characteristics of Targeted Molecular Species 24
3.2.6 CONOPS as Defined in Report 1 25
3.3 Hardware Description and Return on Limit of Detection Estimates 26
3.3.1 Hardware for UV-Raman LiDAR 27
3.3.2 Hardware and Operating Principles of UV-DiAL 29
3.3.3 Hardware for IR absorption LiDAR (DiAL) 33
3.4 Test Set-Ups 36
3.4.1 Intermediate scale set-up (INRS) 36
3.4.2 Outdoor Set-Up 43
3.5 Results and Discussion 47
3.5.1 Intermediate scale testing 47
3.6 Outdoor Set-Up 64
3.7 Conclusion 68
4.0 References 74
5.0 Appendix 1 - Petroleum Hydrocarbon Leak Simulation in a Realistic Intermediate Scale Physical Model 76

List of Tables

Table 1 : Physical Characteristics of Selected Alkanes 22
Table 2 : Physical characteristics of selected aromatics 23
Table 3 : Average composition over the last 5 years of all crude oil types (light to heavy) logged @ crudemonitor.ca 24
Table 4 : Parameters for the as built enhanced UV Raman LiDAR 29
Table 5. Parameters for the IR-DIAL platform 36
Table 6. Timeline of the experiments done on the intermediate scale leak simulator 42
Table 7. List of wavelengths to be used in a multi-wavelength LiDAR scheme and their cross-section normalized to the pentane maximum cross-section 60

List of Figures

Figure 1. Photo of the UV-Raman platform 27
Figure 2. Configuration of the UV Raman LiDAR system as used for the simulated field testing. 28
Figure 3. UV-DiAL breadboard prototype in mobile laboratory. 32
Figure 4. Configuration of the UV-DiAL system as used for the simulated field testing. 33
Figure 5 : Photos of the camera (left) and the breadboard of the system in the mobile laboratory (right). 34
Figure 6 : Double seeded IR DiAL LiDAR; M: mirror; DM; dichroic mirror; PM: parabolic mirror; PD: photodiode for power measurements; MA: motorized actuator for focus. 35
Figure 7. Tank layout prior to sand filling (not to scale). 37
Figure 8. Underground leak simulator container with polyethylene tent. 38
Figure 9. Soil vapor monitoring wells in the leak simulator container. Top view (a) and cross-sectional view (b). 39
Figure 10. Air monitoring ports above the sand surface (not to scale) 39
Figure 11. Schematic illustration of the intermediate scale setup for Raman LiDAR and IR absorption LiDAR measurements. 40
Figure 12. Drawing of the windowless gas cell. 44
Figure 13. Photograph of windowless gas cell in an outdoors setting. 44
Figure 14. Schematic illustration of the outdoor setup for UV-DiAL measurements. 45
Figure 15. Photograph of outdoors set-up with mobile laboratory, folding mirror, windowless gas cell and aluminum target 46
Figure 16. Raman signal from leak simulator for different alkane concentrations. 49
Figure 17. Return curves with offset and mirror reflection corrected 49
Figure 18. Return waveform of Raman plus ground fluorescence 50
Figure 19. Evolution of the average with respect to number of pulses 51
Figure 20. Integrated Raman signal with respect to time after start of diesel injection 52
Figure 21. Differential absorption measurements for alkanes in leak simulator 54
Figure 22. Absorbance of a 10 cm cell of pentane at 7320 ppm with a FTIR spectrometer. 1 cm^{-1} optical resolution. 58
Figure 23. Absorbance of 10 cm cell of a sample of crude with a FTIR spectrometer. 1 cm^{-1} optical resolution 58

Figure 24. Superposition of atmospheric transmission (red), pentane normalized cross-section (black) and wavelength pairs (magenta and green vertical lines) satisfying conditions #1 to #6 59
Figure 25. UV absorption spectrum of benzene above a heated gasoline pan. 66
Figure 26. UV absorption spectrum of benzene in a 10 ppm-m reference gas cell. 68

List of Acronyms

Abbreviation	Term
BTEX	Benzene, Toluene, Ethylbenzene, Zylences
CONOPS	Concept of Operations
DOAS	Differential Optical Absorption Spectroscopy
FID	Flame Ionization Detector
GPS	Global Positioning System
ICCD	Intensified CCD Camera
IMU	Inertial Measurement Unit
INO	Institut National d'Optique / National Optics Institute
INRS/RDDC	Institut National de la Recherche Scientifique / National Scientific Research Institute [GRAVEL Jean-Francois] Recherche et Développement pour la Défense Canada / Research and Development Canada (DRDC)
IR-LiDAR	Infrared Light Detection and Ranging
LiDAR	Light Detection and Ranging
LDS	Leak Detection System
LOD	Limit of Detection
MCT	Mercury Cadmium Telluride (detector)
MCP-PMT	Microchannel Plate Photomultiplier Tube
ms	Milliseconds
MWIR	Mid-wavelength Infrared
NA	Numerical Aperture
OPG	Optical Parametric Generator
OPO	Optical Parametric Oscillator
PID	Photoionization Detector
PMT	Photomultiplier Tube
PPLN	Periodically Poled Lithium Niobate
SWIR	Short-wave Infrared
TDT	Thermal Desorption Tubes
UV	UltraViolet
UV-DiAL	UltraViolet Differential Absorption LiDAR
UV-LIF	UltraViolet Laser Induced Fluorescence
UV-fluorescence LiDAR	UltraViolet Fluorescence Light Detection and Ranging
UV-Raman LiDAR	UltraViolet Raman Light Detection and Ranging
VOC	Volatile Organic Compound

1.0 Executive Summary

This Final Report summarizes work completed on the U. S. Department of Transportation (DOT) Pipeline and Hazardous Materials Safety Administration (PHMSA) contract DTPH56-13-T-000003 completed by Electricore, Inc., National Optics Institute (INO) and TransCanada on optical remote detection of leaks in hazardous liquid petroleum product pipelines.

Current leak detection systems for pipelines are not only unreliable in the detection of minute leaks, but often expensive and/or dangerous to run. This is an unacceptable standard for pipeline operators and leak detection service providers. Electricore, Inc. and INO with support from TransCanada and National Scientific Research Institute (INRS/RDDC) conducted a new research effort consisting of the development of a transportable leak detection system (LDS) demonstrating the ability to externally locate, identify, and assess small liquid and gaseous leaks (weeper/seepers) from a safe standoff distance.

1.1 Executive Summary Report 1- Liquid Petroleum Pipeline Leak Detection by Means of Optical Remote Sensing; Concept of Operations (CONOPS) and Feasibility Study

INO's first contribution was in studying the possible vapor plume extent and content over a leak location and in determining the optical properties of the molecular species in the plume. TransCanada was instrumental in defining a concept of operations for an optical remote leak detection system. With the help of the conclusions of the plume modeling and the concept of operations, INO determined the feasibility of using broadband Infrared Light Detection and Ranging (IR-LiDAR), UltraViolet Fluorescence Light Detection and Ranging (UV-fluorescence LiDAR) or UltraViolet Raman Light Detection and Ranging (UV-Raman LiDAR) for the detection of leaks along long stretches of pipeline.

There has been work done on optical remote leak detection, some sponsored by the US DOT. All of the previous concepts relied on some form of infrared spectroscopy, active (with lasers) or passive, all of them having been originally demonstrated on natural gas pipelines (methane detection). In particular, the classical two wavelength differential absorption LiDAR in the IR has been demonstrated to be able to detect leaks of liquid petroleum products. The working concepts of INO's platforms differ from these previous remote optical leak detection systems either by the approach (resonant UV fluorescence or UV Raman of the volatile hydrocarbons in the vapor plume) or by the principle of operation (broadband IR absorption). But, whatever the approach, it was suggested to INO by a pipeline operator (TransCanada) that a successful optical remote leak detection system (LDS) would need to detect leaks as small as an LDS pig does, that is: 0.1 L/min (~1 barrel per day).

In the absence of a usable model for the formation of a vapor plume above a liquid petroleum product leak (in almost every case, a buried leak), a simplified model of a liquid filled pan at the ground surface was used. To determine which substances to expect in the vapor plume, INO surveyed the molecular content of typical crude oils extracted in Canada, from light to heavy, sweet to sour and conventional to unconventional over the last 5 years. Analysis showed that most petroleum products will contain similar molecular species, but at differing relative levels. To simplify the modeling and to better control the upcoming experimental tests,

emphasis was put on alkanes and aromatics as they are the main components of petroleum products. Butane is gaseous at normal temperature and pressure and pentanes have a fairly high vapor pressure. In light of the model, ***pentane*** was used for the feasibility study of broadband IR LiDAR and UV Raman LiDAR, being the most abundant and having the highest vapor pressure of the liquid alkanes (at normal temperature and pressure). ***Benzene*** was used for the feasibility of the UV-fluorescence LiDAR, being the most abundant and having the highest vapor pressure of the molecular species having optical resonances in the usable UV.

The quantities used are those of an average crude oil seeping at 0.1 L/min.

The plume is a flattened hemisphere, the aspect ratio of which depends on the molecular species studied, with the maximum concentration above the leak location and diminishing outwards.

The model gives substantial concentrations of pentanes over a measurement volume (hundreds of ppm). Benzene is much less abundant (a few ppm).

Having determined what was to be measured, the following parameters were used for the feasibility study;

- Airborne platform (fixed wing or helicopter)
- Flight height: 150 to 300 ft. (50 to 100 m)
- Flight speed: 80-120 knots (150 -220 km/hr.)
- Flight trajectory: Along the pipeline ROW, slightly to the side (~15 ft. (5 m) from center)
- Flight length: hundreds of miles (hours of data)
- Lateral field of view: All of ROW (60 to 90 ft. (20 to 30 m))
- Simultaneous positioning by Global Positioning System (GPS) and Inertial Measurement Unit (IMU)
- Frequency of inspection for oil pipeline: every two weeks
- Data product: leak zone size and geographical position
- Smallest detectable leak: 0.1L/min (ideal)
- Spatial resolution/detection accuracy: 30 ft. (10 m)
- Time from survey to delivery of data products: 12 hours.
- Cost: $25-30/km of pipeline + cost of aerial platform.

The feasibility was done with the lower airspeed and the closer distance between the aerial platform and the ground (80 knots and 50 m). In order to respect the spatial resolution, a measurement time of 250 milliseconds (ms) was chosen. Most of the parameters for the measurement platforms are those of INO platforms as they are at this point in time. The optical laser sources parameters are realistic.

For the IR absorption platform: it was determined that optical absorption from alkanes would be significant. The strength of the return signal depends on the reflectivity of the ground. Unfortunately, alkanes have a very broadband spectral signature in the 3.4 to 3.6 µm

range. This spectral signature could be difficult to distinguish from that of the ground's spectral reflectivity. In spite of this drawback, ***it is very feasible to detect small weeper/seeper leaks using broadband IR absorption LiDAR with return from the ground***. ***For the UV–Raman platform***: again the signal from alkanes was considered. All alkanes (and aromatics) present in crude oil have a Raman peak in the vicinity of 3000 cm^{-1}. If the optical measurement integrates the Raman returns in a sufficiently large spectral band, all the hydrocarbons will contribute to the signal. Raman LiDARs do not depend on a reflection from the ground and are independent from excitation wavelength. The major drawback is the very small Raman cross-sections. In order to have a measurable signal in 250 ms, the laser at 355 nm needs to be relatively high power (the feasibility used 10 W). ***It is feasible to detect small weeper/seeper leaks using a 355 nm Raman LiDAR at a distance of 50 m and flying at 80 knots.***

For the UV-LIF platform; in contrast with the other two platforms, the UV-LIF platform's feasibility was done using benzene concentrations and optical characteristics. Benzene has useable absorption and fluorescence peaks in the deep UV region, between 225 and 270 nm. Although it would be possible to study the feasibility of optical absorption as a means of detecting leaks, INO proposed the use of fluorescence, practically the same hardware being used in both cases. Although the concentration of benzene is much lower than that of alkanes, the fluorescence return signal is very strong (the feasibility used 2 W of tunable light). The unknown element is the quantum efficiency of fluorescence for a given wavelength range, and it is more difficult to calibrate a quantitative measurement of concentration. ***It is feasible to detect small weeper/seeper leaks using a 253.7 nm fluorescence LiDAR at a distance of 50 m and flying at 80 knots.***

This preliminary work shows that detecting weeper/seeper leaks is feasible with any of the techniques studied if the platform is designed with sufficient optical source power and realistic but optimal system transmission and detection quantum efficiency. The information contained in this first report was used for the next step of cost analysis and laboratory testing.

1.2 Executive Summary Report 2 - Preliminary Test Results and Refined Feasibility

INO performed preliminary testing of its breadboards in order to further the feasibility and prove or disprove crude modeling done in previous phases. INO tested broadband IR-LiDAR, UV-fluorescence LiDAR and UV-Raman LiDAR for the detection of vapors of benzene, toluene, ethylbenzene, and xylenes (BTEX) molecules and of alkanes in a laboratory setting.

To better control the experimental testing, emphasis was put on alkanes and aromatics as they are the main components of petroleum products. Butane is gaseous at normal temperature and pressure and pentanes have a fairly high vapor pressure. In light of the model of report #1, pentane was used for the feasibility testing of broadband IR LiDAR and UV Raman LiDAR, being the most abundant and having the highest vapor pressure of the liquid alkanes (at normal temperature and pressure). Benzene was used for the feasibility of the UV-fluorescence LiDAR, being the most abundant and having the highest vapor pressure of the molecular species having optical resonances in the usable UV.

For the IR absorption platform: it was confirmed that optical absorption from alkanes is significant, but the strength of the return signal will depend on the reflectivity of the ground along with the detection limit. Unfortunately, alkanes have a very broadband spectral signature in the 3.4 to 3.6 µm range. This spectral signature could be difficult to distinguish from that of the ground's spectral reflectivity. In spite of this drawback, it is very feasible to detect small weeper/seeper leaks using multi-wavelength IR absorption LiDAR with return from the ground.

For the UV–Raman platform: again the signal from alkanes was considered. All alkanes (and aromatics) present in crude oil have a Raman peak in the vicinity of 3000 cm^{-1}. If the optical measurement integrates the Raman returns in a sufficiently large spectral band, all the hydrocarbons contribute to the signal. Raman LiDARs do not depend on a reflection from the ground and are independent from excitation wavelength. The major drawback is the very small Raman cross-sections.

In order to have a measurable signal in 250 ms, the laser at 355 nm needs to be relatively high power.

The laboratory testing confirmed the initial modeling and it is feasible to detect small weeper/seeper leaks using a 355 nm Raman LiDAR at a distance of 50 m and flying at 80 knots.

For the UltraViolet Laser Induced Fluorescence (UV-LIF) platform; in contrast with the other two platforms, the UV-LIF platform's feasibility was done using benzene. Benzene has useable absorption and fluorescence peaks in the deep UV, between 225 and 270 nm. Although it would be possible to study the feasibility of optical absorption as a means of detecting leaks, INO proposed the use of fluorescence, practically the same hardware being used in both cases. The expected concentration of benzene is much lower than that of alkanes, and it was shown that at atmospheric pressure, in nitrogen, there is very strong quenching of the fluorescence; an unexpected result. It would be close to impossible to detect small weeper/seeper leaks using a fluorescence LiDAR. It is not the best approach, by far.

This preliminary work shows that detecting weeper/seeper leaks would be best performed using the Raman Effect with a platform designed with sufficient optical source power and optimal system transmission and detection quantum efficiency. The final choice will be done in the next phase. The information contained in this second report will be used for the next step of cost analysis.

1.3 Executive Summary Report 3 - Limits of Detection, Choice of Platforms and Lifecycle Cost Analysis

Report #3 presents limits of detection (LODs) and arguments for the choice of the most adequate approach. It follows preliminary testing INO performed on its breadboards and the feasibility of detecting weeper – seeper leaks with the underlying techniques. INO tested broadband IR-LiDAR, UV-fluorescence LiDAR and UV-Raman LiDAR for the detection of vapors of BTEX molecules and of alkanes in a laboratory setting.

For the IR absorption platform: The strength of the return signal depends on the reflectivity of the ground, as does the detection limit. Moreover, alkanes have a very broadband spectral signature in the 3.4 to 3.6 µm range. This spectral signature could be difficult to distinguish from that of the ground's spectral reflectivity and adversely affects the LOD. Not all grounds have the same spectral signature, which is an added problem. Wet ground is almost spectrally flat, but has a low reflectivity. Dry ground has much higher reflectivity, in general, but a complex signature. Vegetation is somewhere in between. LOD is variable and it is a challenge to give a unique number. In spite of this drawback, ***there are ways to enhance the LOD and broadband IR absorption LiDAR but the required effort to make it possible is unknown. INO therefore decided to leave aside this approach for the remaining phases of this project.***

For the UV–Raman platform: All alkanes (and aromatics) present in crude oil have a Raman peak in the vicinity of 3000 cm^{-1}. If the optical measurement integrates the Raman returns in a sufficiently large spectral band, all the hydrocarbons contribute to the signal. Raman LiDARs do not depend on a reflection from the ground and are independent from excitation wavelength. The major drawback is the very small Raman cross-sections. In order to have a measurable signal in 250 ms, the laser at 355 nm needs to be relatively high power, and may cause security issues. ***This is the simplest and most straightforward approach. Modeling and LOD determination are simple. UV Raman LiDAR is retained for follow-on testing using 355 nm laser light***.

For the UV-LIF platform; in contrast with the other two platforms, the UV-LIF platform relies on benzene and other aromatics. These are very variable in proportion in the different crudes. In addition, it was found that the fluorescence yield is minute. ***It would be close to impossible to detect small weeper/seeper leaks using a fluorescence LiDAR. It was not used for follow on work.***

Both IR absorption LiDAR and UV-Raman LiDAR have a realistic potential as far as life cycle cost goes. However, this preliminary work shows that detecting weeper/seeper leaks would be best performed using the Raman Effect with a platform designed with sufficient optical source power and optimal system transmission and detection quantum efficiency. The information contained in this third report will be used for designing upgrades and adaptations to the selected breadboard.

1.4 Executive Summary Report 4 – IR Database, Raman System Modifications and In Depth Testing

Report #4 presents modifications done to the Raman platform in order to upgrade the design for the task of VOC detection and to enhance the LOD. It also presents a series of tests done to characterize these modifications. It follows preliminary testing INO performed on its breadboards and the feasibility of detecting weeper – seeper leaks with the underlying Raman technique. As a reminder, INO tested broadband IR-LiDAR, UV-fluorescence LiDAR and UV-Raman LiDAR for the detection of vapors of BTEX molecules and of alkanes in a laboratory setting in order to determine that Raman would be the best choice.

For the UV–Raman platform: All alkanes (and aromatics) present in crude oil have a Raman peak in the vicinity of 3000 cm^{-1}. The Raman platform was modified so that the optical measurement covers (adds) the Raman returns over a sufficiently large spectral band for all the hydrocarbons to contribute to the signal. For the different iterations of modifications presented here, the Raman signal was measured over 650 cm^{-1}. Raman LiDARs do not depend on a reflection from the ground but ground fluorescence is an interfering process as will be shown in the results. The major modifications were thus on the optical filtering unit, the optical detectors and the detection electronics. The aim of the modifications was for a simplified system with an enhanced limit of detection. The simplified system would cost less to manufacture and maintain. Raman signals are independent from excitation wavelength and for this iteration, 355 nm was conserved as the excitation wavelength. In order to have a measurable signal in 250 ms, the laser at 355 nm needs to be relatively high power, and may cause security issues. For this round of testing a relatively low power of ~ 300 mW was used, along with averaging over sufficiently long measurement times. Simple scaling will ultimately determine the required power for use in the determined Concept of Operations (CONOPS).

This is the simplest and most straightforward approach.

Testing was done both in an indoors setting and an outdoors setting. The indoors setting was mainly to verify that all modifications worked as planned. The more telling tests were done outdoors, after installing the Raman breadboard in a mobile laboratory. A special windowless gas cell was designed and manufactured for this phase of testing. Optical windows do not allow for realistic testing as they interfere in the measurement, in particular through fluorescence interference. A first iteration in modifications and testing showed that some optical components and the electronics chosen for the detection were in part inadequate because of ambient light and fluorescence from the background. In subsequent iterations, the detection footprint on the ground was reduced, spatial resolution (the volume over which the optical measurement are done) was enhanced (smaller volume) and the effect of the fluorescence return from the ground and the aerosols was lowered. In spite of these enhanced modifications, there was still an important contribution from ambient light reflecting on the background, as was expected. This confirmed the simple model that the measurements are photon shot noise limited, and especially the shot noise due to ambient light. It also indicated that the final platform would need to be further enhanced by using gating on the detectors, smaller optical detection bandwidth and smaller detection footprints on the ground. This was not done because of lack of time. So, in order to measure a LOD from which scaling could be performed, INO used a black non-reflecting background for the final measurements presented here. ***Tests were performed on concentrations of about 3 - 4 000 ppm*m for pentane, 1 500 – 2 000 ppm*m for gasoline and 100 ppm*m for diesel. The results indicate that the LOD of the system would be below 1 500 ppm*m for all hydrocarbons, which is the target for the system.***

For the IR absorption platform: The strength of the return signal depends on the reflectivity of the ground, as does the detection limit. Moreover, alkanes have a very broadband spectral signature in the 3.4 to 3.6 µm range. This spectral signature could be difficult to distinguish from that of the ground's spectral reflectivity and adversely affects the LOD. Not all grounds have the same spectral signature, which is an added problem. Wet ground is almost spectrally flat, but has

a low reflectivity. Dry ground has much higher reflectivity, in general, but a complex signature. Vegetation is somewhere in between. LOD is variable and it is a challenge to give a unique number. In spite of this drawback, there are ways to enhance the LOD and broadband IR absorption LiDAR but the required effort to make it possible is unknown. INO therefore decided to leave aside this approach for the remaining phases of this project except for the signature database. This report thus also presents work on a signature database for the various ground reflectivities in the IR.

As mentioned in the third report, both IR absorption LiDAR and UV-Raman LiDAR have a realistic potential as far as life cycle cost goes. This preliminary work with a modified and enhanced Raman platform and tests done outdoors on an open windowless gas cell shows that detecting weeper/seeper leaks is realistic if our crude vapor plume model stands-up to reality in the next testing phase with simulated underground leaks.

1.5 Executive Summary Report 5 – INO Technologies Assessment as Leak Detection Systems for Hazardous Liquid Pipelines; Results of simulated field testing

Report #5 presents the detailed information about the testing strategy and installations used during the simulated field testing of the UV Raman LiDAR approach, previously selected as the most promising technique for the application considering simplicity of the approach and of the data analysis. Detailed information about the operating conditions and complete results analysis is also included in this report. It also includes work done in the additionally funded framework for IR-LiDAR and UV-DiAL testing and for the hydrocarbon vapor diffusion model description.

A successful optical remote leak detection system would need to be airborne and able to generate data every 300 ms in order to be able to accurately map the right of way of hazardous liquid pipelines. After preliminary tests in a laboratory environment, INO selected UV-Raman as the best approach to put forward for intermediate scale testing. Modifications have been brought to the platform in order to improve both its sensitivity and its transportability.

For the UV–Raman platform: All alkanes (and aromatics) present in crude oil have a Raman peak in the vicinity of 3000 cm^{-1}. The Raman platform was modified so that the optical measurement covers (adds) the Raman returns over a sufficiently large spectral band for all the hydrocarbons to contribute to the signal. For the different iterations of modifications presented here, the Raman signal was measured over 650 cm^{-1}. Raman LiDARs do not depend on a reflection from the ground but ground fluorescence is an interfering process as shown in the results. The major modifications were thus on the optical filtering unit, the optical detectors and the detection electronics. The aim of the modifications was for a simplified system with an enhanced limit of detection. The simplified system would cost less to manufacture and maintain.

Testing done outdoors showed there was still an important contribution from ambient light reflecting on the background, as was expected. This indicates that the final platform would need to be further enhanced by using gating on the detectors, smaller optical detection bandwidth and

smaller detection footprints on the ground. It was not possible to implement these upgrades to the system within the timeframe of the project. So in order to measure a LOD from which scaling could be performed, INO used a black non-reflecting background for measurements.

Test performed on concentrations of about 3 000 - 4 000 ppm-m for pentane, 1 500 – 2 000 ppm-m for gasoline and 100 ppm-m for diesel in the outdoors suggested a LOD of the system below 1 500 ppm-m for all hydrocarbons, which was the target for the modified system.

Although UV-Raman was preferred at this step of the project, IR-absorption showed great sensitivity for hydrocarbons detection. And as mentioned in the third report, both IR absorption LiDAR and UV-Raman LiDAR have potential as far as life cycle cost goes. The major concern with IR is that the strength of the return signal depends on the reflectivity of the ground, so it may be difficult to distinguish between variations of the ground reflectivity versus hydrocarbons presence. But because of its high sensitivity, it was decided to test both IR-absorption and UV-Raman systems during the intermediate scale testing phase. In addition, UV-DiAL was tested as a method of detection for benzene in INO's open-cell setup.

The intermediate scale tests were performed at Institut National de la Recherche Scientifique (INRS) where an underground leak was simulated in a large sand container. Simulation of airborne measurements was achieved from ground based installation thanks to a tilted mirror mounted 5 m over the contaminated soil top layer. Analysis of the air composition above soil and under the soil surface during the whole experiment duration with a commercial Photoionization Detector (PID) / Flame Ionization Detector (FID) instrument allowed for the monitoring of hydrocarbon concentration at various locations in the simulator. These are used as reference measurements to correlate with the UV-Raman / IR-absorption data. Analysis of these reference measurements showed a major concern as to the validity of the vapor plume model used in the previous phases. ***There is a strong vertical concentration gradient with the highest concentration very close to the ground.*** This was not observed in the outdoors tests performed in the previous phase because measurements were done through a 2 m long windowless gas cell horizontally, which made for a uniform 2 m of interaction. Although this has no effect on the estimates of limits of detection in terms of number of molecules, it does have an impact on the estimate of the number of molecules an excitation laser beam will interact with. ***It has an impact on the minimum detectable leak size***. It also has an impact on the eventual design of an optimized measurement hardware. Moreover, the use of a tent to enclose the vapor plume likely reduced the gradients with respect to what it would be without the tent, in open air, with drafts and wind. Pipeline operators' interest is to measure a leak of a given size. However, the leak detection systems proposed here, as do many others, measure concentration of hydrocarbons in the vapor phase around a leak. And as the intermediate scale testing showed, ***it is clearly a challenge to correlate a measured concentration to an actual leak size.*** To elaborate a

standardized testing procedure for leak detection system would be beneficial for the industry as it would allow the comparison in performances of different systems.

For UV-Raman platform, tests confirmed the importance of using gating on the detectors and smaller optical detection bandwidth. The problem is that a large number of the molecules to be detected are very close to the ground. The hardware, as built, could not resolve the portion just above ground where the concentration is at its highest. It is recommended to go with the transient digitizer and a laser with a shorter pulse length (<1 ns) unless a fast gateable Microchannel Plate Photomultiplier Tube (MCP-PMT) is used with the current integrator. Both these avenues raise the cost of the hardware. In addition, and as stated in the previous reports, a high pulse energy, high power (10 W) laser is needed. However, even with the platform as is, with the transient digitizer, and without the contribution of the molecules closest to the ground, ***Raman could eventually detect better than concentration length products between 100 and 500 ppm-m*** as measured with the PID and FID if measurement time was not an issue.

In light of the additional cost of the proposed hardware, and of the weak concentration encountered over the simulated leak, INO suggests to abandon the Raman technique for remote leak detection from an airborne platform.

For IR-absorption platform, intermediate scale tests confirmed the sensitivity of the approach. Moreover, this approach does allow measurement of the very high concentration of hydrocarbons encountered next to the soil surface. An important effort was then placed on ground variation study combined with different measurement strategies. The results showed that ***it is not possible to ascertain that the measured signal is due to absorption by hydrocarbons when the concentration obtained is below 250 ppm-m of actual molecules. When the measured concentration is higher than 250 ppm-m, it is indicative of the very probable presence of alkanes.***

In light of this, IR LiDAR should be revisited as a viable approach to leak detection as long as one is looking for a leak generating a vapor concentration higher than 250 ppm-m.

For UV-absorption platform, open-cell tests allowed to determine a limit of detection of benzene around ***1.5 to 2.5 ppm-m of benzene molecules***. Although its principle is similar to IR absorption, it should not be affected by the ground reflectivity because of the very small difference in wavelength between ON and OFF absorption transition wavelength. However, benzene represents only a small and variable fraction of the overall hydrocarbons composition of petroleum products and we evaluate that this represents an LOD of about 100 ppm-m in alkane equivalent.

In light of this, UV-DiAL of benzene would be the most sensitive approach, even though the effective LODs of the different techniques are all in the same range (if we consider the performance limitations related to type of soils and background for IR-DiAL).

Because of the work done in this phase, the assumption that using Raman scattering would have the best sensitivity has to be revisited. Raman still has the advantage of being scalable with laser power. IR and UV absorption do not have that advantage. However, this is only an advantage on paper because using very high power UV lasers would be an issue. Limit of detection is not the only parameter to take into account, although one of the most important. The three techniques are very close when looking at vapor plume detection, be it through alkanes or aromatics or both. Other requirements such as cost, mass, size, power, false alarms, and ease of use need to be considered.

Moreover, the right technique might differ from pipeline to pipeline, depending on vapor migration through the ground, soil temperature (in particular frozen ground), soil cover (in particular snow) and other similar parameters. None of this is considered in the feasibility presented here. Clearly, leak detection through a generated vapor plume will work best in warm climates.

As in many instances, only field trials will determine the most adequate approach. ***Follow-on work could focus on looking at better ways of detecting through absorption in the UV***. There could be ways to simplify the approach by not using costly stabilized laser systems. INO is looking into promising alternatives and would appreciate the opportunity to participate in field trials, on simulated leaks or real pipelines.

Finally, in the course of this project, we determined that there is not much vapor over an underground leak spot and that there is a strong concentration gradient over the soil surface; the most concentrated fraction being in the first several centimeters over the surface. To ensure maximum sensitivity, the chosen technique should be able to collect signal coming from every centimeter along the probing path. This gives serious advantage to absorption technique; Raman and fluorescence are therefore abandoned. Although UV-DiAL seems very interesting at this point, the technique has not been studied in details within this project. Having a better idea of vapor behavior over a leak, it would be valuable to complete a new pros and cons exercise considering only the two absorption techniques.

Considering these conclusions, INO's recommendations for further studies would be concentrated around simulated tests and studies of absorption measurements only. For IR absorption, the uncertainty lies in the encountered soils reflectivity variations. Validation of INO's theoretical evaluation is therefore proposed as a future development. Experimental measurements of ground reflectivity over a pipeline right-of-way are proposed. For UV

absorption technique, more tests are proposed. The data analysis algorithm needs to be refined and independence of the approach to soil variation is also to be demonstrated. At this point, measurements done over a given number of soil types may be sufficient. UV source alternatives also need to be evaluated in order to reduce size, cost and complexity of the actual laser source. Suggested tasks for a follow-on work on optically remote leak detection would be:

- To investigate UV light source alternatives for DiAL applications
- To perform more tests using the UV-DiAL approach in realistic conditions
- To refine the analytical approach and algorithm
- To take measurements of the ground reflectivity in the IR along a typical right-of-way
- To complete a new pros and cons analysis of the approaches using information gathered during this last test campaign
- Based on the pros and cons results, to adapt the selected platform for further testing
- To perform tests on simulated or real leaks

2.0 Technical Status

The team completed the following technical activities prior to completion of the project. All of the technical activities, results and conclusions are detailed in Section 3, Results and Conclusions.

Task 1: Project Kickoff
The project team, consisting of Electricore, Inc. and INO, held the required Kick Off meeting via teleconference and webinar on Monday, September 30, 2013 with DOT/PHMSA's Technical Program Manager, Mr. Max Kieba.

Task 2: Requirement Analysis
The project team conducted the following activities during Task 2, Requirement Analysis:

- Document use cases for on-shore pipeline operating conditions, infrastructures and environments.
- Determine composition and characteristics of targeted vapors from hazardous liquid pipeline leaks.
- Determine the characteristics of leak occurrences and range of targeted vapor concentrations for each substance with respect to leak size and leak environment, such as soil type, soil humidity and soil temperature in the case of underground leaks.
- Obtain the spectral characteristics of the targeted chemical vapor compounds present in leaks.
- Validate use cases and establish CONOPS for realistic use of the selected technology for monitoring extended lengths of pipeline.
- Carry out refined feasibility analysis.
- Write Report #1.

Task 3: Initial Laboratory Testing
The project team conducted the following activities during Task 3, Initial Laboratory Testing:

- Write a test plan and set up the existing hardware for testing.
- Proceed to tests.
- Analyze data.
- Determine pros and cons of each approach.

Task 4: Platform Analysis
The project team conducted the following activities during Task 4, Platform Analysis:

- Assess the detection limits
- Assess the need for upgrade for the platforms
- All of the important results obtained during Tasks 4 are discussed and included in Report #3. Main conclusions of the report are summarized in Section 2 above.

Task 5: Life Cycle Cost Analysis
The project team conducted the following activities during Task 5, Life Cycle Cost Analysis:

All of the important results obtained during Task 5 are discussed and included in Report #3. Main conclusions of the report are summarized in Section 2 above.

Task 6: Platform Modification
The project team conducted the following activities during Task 6, Platform Modification:

- The selected instruments were merged, modified and adapted to meet the detection and CONOPS requirements and for eventual simulated / field testing.
- Modifications plan, execution and testing, along with data analysis (Tasks 6 and 7) were presented in the report #4.
- Report #4 was written documenting Task 6 and 7 accomplishments.

Task 7: Prototype Optimization
The project team conducted the following activities during Task 7, Prototype Optimization:

- Write a complete test plan, set-up the hardware for tests, and conduct in-depth testing of the technological solution to optimize instrument detection parameters for a few selected petroleum products and simulated background settings.
- Carry out data analysis.
- Establish database of return signal signatures of leaked substances and possible background interference.
- The hardware was set up and proceeded to in-depth testing of the modified instrument.
- The data analysis was carried out.
- The database of return signal signatures of leaked substances and possible background interferents was established. (Note: This is not practical for the Raman approach but still a work in progress for IR platform as an in-kind effort).
- Report #4 was written documenting Task 6 and 7 accomplishments.

Task 8: Simulated Field Testing
The project team conducted the following activities during Task 8, Simulated Field Testing:

- Ready the ruggedized breadboard instruments for simulated field deployment.
- Prepared for September simulated field deployment at INRS facilities.
- Elaborate test plan and select test site and CONOPS.
- Finalize the test plan.
- Carry out test campaign.
- Complete results analysis
- Analyze results; assess the technology as well as the CONOPS.
- Analyzing results; assess the technology as well as the CONOPS.
- Describe diffusion model.
- Write Report #5

Task 9: Industry Workshop

The project team conducted the following activities during Task 9, Industry Workshop:

- The Electricore team participated in the PHMSA Research & Development Forum in Chicago, IL August 6 and 7, 2014.
- Petroleum Technology Alliance Canada (PTAC) presentation.
  Standoff Stack Emissions Monitoring and Weeper/Seepers Detection in Oil Pipelines Using Photonics Sensing Modalities (Calgary, Dec 9, 2014).
- Saskatchewan Research Council (SRC) (Saskatoon, February, 2015).
- A presentation was given to Conoco Phillips, Talisman Energy and Husky Energy
- Results were shared with Exxon Mobile, APC Pipelines Canada.
- Final results were presented to our partner TransCanada.
- INO disseminated the results to industry and in particular to CFER, (through our partner TransCanada Corp.); an organization devoted to testing leak detection systems (under and above ground).

Task 10: Project Management and Reporting

The project team conducted the following activities during Task 10, Project Management and Reporting:

- The project team held regular teleconference meetings with INO to track performance, schedule and budget.
- The project team completed and submitted the required status reports documenting accomplishments.
- The project team participated in the Research Project Peer Review on May 20, 2014.
- On October 6, 2014, the Electricore project team submitted a request for a contract modification to incorporate additional scope of work and funding in the field testing phase at INRS under Task 8 to the program; this request was granted.
  - Derivation of a vapor migration model in the soil over a diesel leak
    - ✓ Vapor plume diffusion model for diesel
    - ✓ Allow having a better estimate on time between the leak occurs and vapors appear over soil surface
  - Complete compositional characterization of the gas phase in soil and in air for diesel vapor
    - ✓ Component wise reference concentration through experimentation
    - ✓ Experimental validation of the model
  - Experimental testing of the previously described IR absorption LiDAR platform over the simulated leak
  - Experimental testing of a new UV absorption LiDAR platform (benzene detection oriented)
  - Additional note on timing associated with weather conditions in Canada: INO and INRS performed outdoor tests in December 2014. The leak simulation setup is located inside the INRS building and a large door allows INO to "shoot" their LiDAR from outside the building. Of course, snow fall would prevent INO from measuring with the LiDAR but we have the same limitation during summer when it rains. In conclusion, the testing during the beginning of winter is not a major concern even though we prefer to perform the campaign when the temperature is above -10 Celsius.

3.0 Results and Conclusions

Pipeline operators cannot easily and efficiently detect small weeper/seeper leaks over extended lengths of pipeline. Some pipelines have distributed sensors (flow, temperature, pressure) that relay measurements to a software that raises an alarm when changes in the measurements indicate a leak. Unfortunately, these systems cannot detect leaks smaller than approximately 1% of the total flow, which can be a significant loss. Weeper/seepers thus go undetected. Specialized leak detection systems such as vapor permeable sensor tubes, optical fiber sensor networks, or electrical sensor cables fitted along the pipeline are hugely expensive on a per mile basis and are only installed on new pipeline and/or over environmentally sensitive terrain. If weeper/seepers are to be detected over the entire length of pipeline, it must be through other means. A point sensor network would be very expensive. The best and most feasible external weeper/seeper detection system is a standoff, mobile sensor that regularly surveys the pipeline from the ground or air. The response time is consequently not that for larger leaks, but is significantly cheaper than the aforementioned specialized approaches.

Small leaks could indicate the imminence of much larger leaks and their detection will reduce the consequential costs (loss of life, loss of product, prolonged down time, irreversible environmental damage, remediation, legal, manpower, security, etc.). Even though the survey period is long, detecting the leaks at early stages allows for a better management of risks and consequences. The platforms that INO is developing are based on principles put forward by most remote leak detection specialists. INO is striving to bring the platforms to a technological level which renders the standoff monitoring at an acceptable price point, both at the purchase level and at the maintenance/operations level.

Electricore, Inc. and National Optics Institute (INO) in partnership with TransCanada proposed a new research effort to develop a transportable leak detection system (LDS) which should demonstrate the ability to externally locate small liquid leaks from a safe standoff distance. The final outcome should be a mobile sensor for monitoring of new and existing onshore pipelines.

The objective of this project was to assess the stand-off capabilities of INO developed instruments for the detection of vapors from liquid petroleum pipeline leaks. The prototype sensor on a mobile platform was to include one or more of three spectroscopic instruments: 1) UV Fluorescence LiDAR, 2) UV Raman LiDAR, and 3) IR absorption LiDAR remote sensor. Remote capability up to 100 yards was to be evaluated for several concentrations of vapor from petroleum products (typically transported by pipelines) in a laboratory and in a simulated pipeline setting. As a final note, INO added UV absorption LiDAR in some of its analysis and testing, the hardware not being very different from UV fluorescence.

3.1 Report Content

The first tasks of the project were mainly literature review and a global analysis of pipeline leak detection. Another task was to document use cases for targeted on-shore pipeline environments, infrastructures, and operating conditions. Information on typical crude oil composition was summarized as well as expected vapor compositions and concentrations over a pipeline leak. Physical properties and spectral characteristics of the most interesting vapor species were listed in Report 1.

Along with TransCanada, a preceding task was the development of a realistic CONOPS for a future remote leak detection system. Finally, using the CONOPS as a guideline for realistic parameters definition, a theoretical feasibility study was done for the three systems proposed – UV fluorescence LiDAR, UV Raman LiDAR and IR absorption LiDAR.

Report 2 yielded results of preliminary laboratory testing and confirmation or disproof of the theoretical analysis. The molecules used for testing were benzene and toluene for UV-fluorescence (and UV-Absorption), and pentane for UV-Raman and IR-absorption. In addition, a sample of crude was vaporized to have results more closely related to oil products. Pros and cons of the different approaches were summarized, in the context of the CONOPS developed in the previous phase, using the results from the experiments.

Report 3 gathered the pros and cons, the results of the preliminary laboratory testing, the results of modeling and the results of a lifecycle cost analysis to determine the best approach for weeper/seeper leak detection using the CONOPS determined in Task 2. It was determined that the best approach was the Raman approach. Using realistic parameters for a future platform, it was determined that 1500 ppm-m was a realistic LOD.

In the fourth report, modifications to the Raman platform are described and explained. An outdoor test set-up that uses a windowless gas cell is described and results obtained are analyzed. A database of IR ground signatures was compiled and presented.

In this fifth report, we repeat most of the information contained in the previous reports for completeness; summary of the defined CONOPS, crude oil composition, spectral characteristics useful for all the platforms. Modifications to the platforms are described and explained. An in depth analysis of the IR spectral databases was completed in order to better quantify the impact of the ground reflectivity variations previously discussed. Most of all, the intermediate scale testing campaign is described and the results obtained are analyzed. This was done both for UV-Raman and IR-DiAL systems. In addition, preliminary results using UltraViolet Differential Absorption LiDAR (UV-DiAL) approach are presented.

For the intermediate scale leak simulation, the instrument was installed about 40 meters away from the leak simulator and laser probing was done from the air using reflection from a mirror. This simulates well the airborne approach envisioned for the final application. Vapors generated were optical interrogated and light returns were recorded. Finally, assessment based on the capability to detect and identify leaked products for a range of realistic concentrations and patterns is done.

3.2 Compositions of Targeted Liquid Petroleum Products

From crude oil to premium gasoline, a wide range of petroleum products are transported in three major types of pipelines around the globe. Our approach is to detect leaks using the vapor generated over the leak location and therefore, the more volatile the product the easier the detection. Crude oil was used for the purpose of the feasibility analysis, which is probably the most difficult product to detect using the vapor because of its relatively low volatility when compared to the other types of petroleum products.

3.2.1 Saturated Hydrocarbons

Saturated hydrocarbons, also called alkanes, are a major part of any crude oil. Most of them are linear carbon chains but cycles are also possible within the structure; therefore they are called cyclo-alkanes.

Alkanes are organic compounds composed exclusively of singly bonded carbon and saturated with hydrogen atoms. Table 1 summarizes the most important physical characteristics of the 8 shortest alkanes.

Table 1 : Physical Characteristics of Selected Alkanes

Number of carbon atoms	Alkane	Molecular weight (g/mol)	Boiling point (°C)	Vapor pressure @ 25°C (torr)
C1	Methane	16.04	-162	gas
C2	Ethane	30.07	-89	gas
C3	Propane	44.10	-42	gas
C4	Butanes	58.12	-12 - 0	gas
C5	pentanes	72.15	28 – 36	521.6
C6	Hexanes	86.17	37 – 69	151
C7	Heptanes	100.20	70 - 98	46.2
C8	Octanes	114.23	99 – 126	10 @ 20°C

According to reference data, crude oil contains only a small fraction of propane and shorter hydrocarbons, for the simple reason that this very light fraction is gaseous at normal temperature and pressure. Because of the high affinity of hydrocarbons with each other, a considerable fraction of butanes is still found in typical crude oil although their boiling point is near 0 °C. The vapor pressure of a component is an indicator of a liquid's evaporation rate. A higher vapor pressure results in a higher fraction of this component in the gas phase over the liquid/gas

interface. When a leak occurs, the components likely to be found in the gas phase over the leak are the most volatile species.

3.2.2 Aromatic hydrocarbons

The most frequently encountered are benzene, toluene, ethylbenzene, xylenes and are often referred to as BTEX. They are of particular interest because of their high toxicity. BTEX are an important part of gasoline and, because of their volatility and partial water solubility, are some of the first species to be depleted when a leak occurs. We can therefore consider that they are good potential candidates to be found in the gas plume surrounding a petroleum leak.

Table 2 : Physical characteristics of selected aromatics

Number of carbon atoms	Aromatic	Molecular weight (g/mol)	Boiling point (°C)	Vapor pressure @ 25°C (torr)
C6	benzene	78.11	80.1	95.8
C7	toluene	92.14	111	28.3
C8	ethylbenzene	106.17	136	9.5
C8	xylenes	106.17	138 - 144	6.7 – 8.7

3.2.3 Soil Types and Characteristics

A significant amount of research has already been conducted on the oil plume spreading behavior in soil and air after a spill or a leak [1-4]. It is not the purpose of the present project to understand or predict the spreading behavior of the petroleum plume in soil or air. However, as presented at the results section of this report, intermediate scale simulation of an underground leak allowed for interesting observation of the vapor plume propagation behavior in soil as well as in air above leak.

For the UV based leak detection systems proposed in this project, the soil properties are expected to have a low impact on the measurements, mainly affecting the resulting vapor concentration over the leak location. Because UV Raman LiDAR is a range resolved technique, it is possible to directly measure the vapor in the air, with minimal, if any, contribution/interference from the soil/ground. However, because the IR absorption technique uses light diffused from the ground, the spectral characteristics of the ground will directly impact the performance of the platform. For example, it is well known that both the nature and humidity of the soil strongly affect the reflectivity in the IR region [5, 6].

3.2.4 Targeted Molecular Species Concentrations in the Vapor Phase

The average compositions have been calculated from the analytical information of each crude sample found on the website crudemonitor.ca. Average proportions in Table 3 are based on 51 different samples each representing an average over the last 5 years.

Table 3 : Average composition over the last 5 years of all crude oil types (light to heavy) logged @ crudemonitor.ca

	Weighted average composition on all crude oil types	Vapor pressure @ 25°C (torr)	Calculated partial vapor pressure@ 25°C (torr)
Methane, ethane, propane	0.22	Gas	Gas
Butanes	2.29	Gas	Gas
Pentanes	3.85	521.6	17.43
Hexanes	5.03	151	5.77
Heptanes	5.25	46.2	1.64
Octanes	5.42	10 @ 20°C	0.33
Nonanes	4.34	10 @ 20°C	0.24
Decanes	2.08	1.5	0.02
Benzene	0.22	95.8	0.24
Toluene	0.57	28.3	0.15
Ethyl Benzene	0.20	9.5	0.02

Interestingly, in crude, it can be noted that the pentanes in the vapor phase are expected to have the highest concentration of all liquid molecular species. For BTEX, it is benzene that is expected to be found in higher concentration, even if the proportion in crude oil is not as high as toluene or xylenes. Once again, it is the vapor pressure that dominates in the calculation of concentration in the vapor phase.

The partial vapor pressure calculated for individual hydrocarbons over crude oil are only for the immediate gaseous region covering the liquid crude, or the concentration one would find in the gas phase surrounding the crude in a closed container. As already mentioned, the composition of the petroleum product reaching the surface at a leak location is not known. However, it can be assumed that the vapor phase composition over the leak location should lie somewhere between the vapor pressure of the pure state of the lightest fraction of hydrocarbons and the calculated partial vapor pressure over the crude oil mixture.

3.2.5 Spectral Characteristics of Targeted Molecular Species

IR Absorption

In *IR spectroscopy*, every species has its own absorption spectrum related to rovibrational transitions and direct measurement of absorption in a sample can lead to quantitative analysis. Detailed information about pentane, benzene and other hydrocarbons IR absorption characteristics can be found in references [7-11].

Raman Scattering

Raman spectra are signatures of molecules and differ from one to the other. An important difference with respect to absorption, Raman scattering can be generated at any excitation wavelength. Detailed information about pentane, benzene and other hydrocarbons Raman cross-sections and frequencies can be found in references [12-16].

UV Absorption

Similar to IR absorption but for electronic transitions, in *UV spectroscopy*, every species has its own absorption spectrum and direct measurement of absorption in a sample can lead to quantitative analysis. Detailed information about pentane, benzene and other hydrocarbons IR absorption characteristics can be found in references [7-11].

3.2.6 CONOPS as Defined in Report 1

Having determined what was to be measured, characteristics and operating capabilities of a useful remote leak detection system were defined with the input of TransCanada. The following parameters were used for the feasibility study and were also used as a reference for realistic definition of the testing phases completed throughout this project.

- Airborne platform (fixed wing or helicopter)
- Flight height: 150 to 300 ft. (50 to 100 m)
- Flight speed: 80-120 knots (150 -220 km/hr)
- Flight trajectory: Along the pipeline ROW, slightly to the side (~15 ft. (5 m) from center)
- Flight length: hundreds of miles (hours of data)
- Lateral field of view: All of ROW (60 to 90 ft. (20 to 30 m))
- Simultaneous positioning by Global Positioning System (GPS) and Inertial Measurement Unit (IMU)
- Frequency of inspection for oil pipeline: every two weeks
- Data product: leak zone size and geographical position
- Smallest detectable leak: 0.1L/min (ideal)
- Spatial resolution/detection accuracy: 30 ft. (10 m)
- Time from survey to delivery of data products: 12 hours.
- Cost: 25 to 30 $/km of pipeline + cost of aerial platform.

The feasibility was conducted with the lower airspeed and the closer distance between the aerial platform and the ground (80 knots and 50 m). In order to respect the spatial resolution, a measurement time of 300 ms was chosen.

Although it was first determined using calculations that any of the UV-LIF, UV-Raman or IR-DiAL platform could potentially be used as a weeper/seeper leaks detection platform,

preliminary experiments showed that UV-LIF did not offer sufficient sensitivity for the application.

It was than determined that weeper/seeper leak detection would be best performed using the Raman Effect with a platform designed with sufficient optical source power and optimal system transmission and detection quantum efficiency. UV-DiAL was finally added as an additional option during the last testing phase.

3.3 Hardware Description and Return on Limit of Detection Estimates

This section describes the hardware modifications brought to the UV Raman platform in order to enhance the sensitivity and to simplify the hardware for it to have a lower cost of purchase and of ownership. The modifications also reduce the size and weight of the platform, rendering it more transportable; although for it to be really man-transportable, the laser would need to be changed. The required lasers exist commercially but were out of budget for this project. The original platform had an optical spectrograph and a gated Intensified CCD Camera (ICCD). This allowed for enhanced molecular identification using a full spectral measurement. INO decided to abandon the "identification" aspect of the platform in this redesign and simplification. Thus the platform now detects all volatile organic compounds (VOCs) without discrimination, and all compounds that have C-H bonds that generate a Raman signal in the 2925 ± 325 cm^{-1} window. The hypothesis was made that over the pipeline right of way, there would be essentially only VOCs from pipeline leaks. This hypothesis will be confirmed after multiple test campaigns in real conditions. This design raises the probability of false positives, which, in INO's opinion, is acceptable in the context of this application. The design described here uses only two detection channels; while the ICCD used in the first design allowed 1024 detection channels. It is certainly possible to add a few more channels to reduce false alarm rate if deemed necessary.

There are databases of Raman signatures, mostly of solids and liquids. The Raman signatures do not change significantly between the liquid state and the gas state; where they can change is when a different excitation wavelength is used. There are very few published Raman spectra using an excitation wavelength of 355 nm.

These considerations do not change the LOD modeling as this modeling does not account for interference from other Raman signal generating molecules in the atmospheric volume being remotely sampled.

This section recalls the LOD as presented in report 3. This limit was evaluated considering platform improvements to best meet the CONOPS parameters. The LOD was evaluated considering an aerial platform surveying at near 50 m above ground and at a mean speed of about 200 km/h, as determined during the CONOPS efforts. The end-data-product is an effective ground sampling of about 10 m (300 ms observation time).

In Report 1, a simplified hydrocarbon diffusion model was use to predict that a 0.1 L/min leak would produce a "cloud" of equivalent pentane concentration of 300 ppm. Considering the "cloud" dimension (~5 m radius), this translates to an effective concentration-length product of 1500 ppm-m, the relevant quantity for the Raman LiDAR instrument to detect.

Raman signals were obtained on alkanes using the hardware, parameters and protocol described in Report 2. Raman signals can be generated with almost any excitation wavelength. The use of 355 nm light seems to be optimal, hardware wise. All alkanes, and part of the aromatics, will generate a Raman signal in the wavelength band to be detected. It is a simple system consisting of a single wavelength emitter and a reduced wavelength band receiver. The resulting Raman signal is detected by a receiver located near the excitation laser. For this application, the Raman excitation laser beam of the LiDAR would propagate through the vapor plume.

3.3.1 Hardware for UV-Raman LiDAR

Report 4 described modifications to the Raman platform. The configuration used for the testing phase is the one described as iteration number 3. It is presented in Figure 1 and Figure 2, and is briefly explained in the following section.

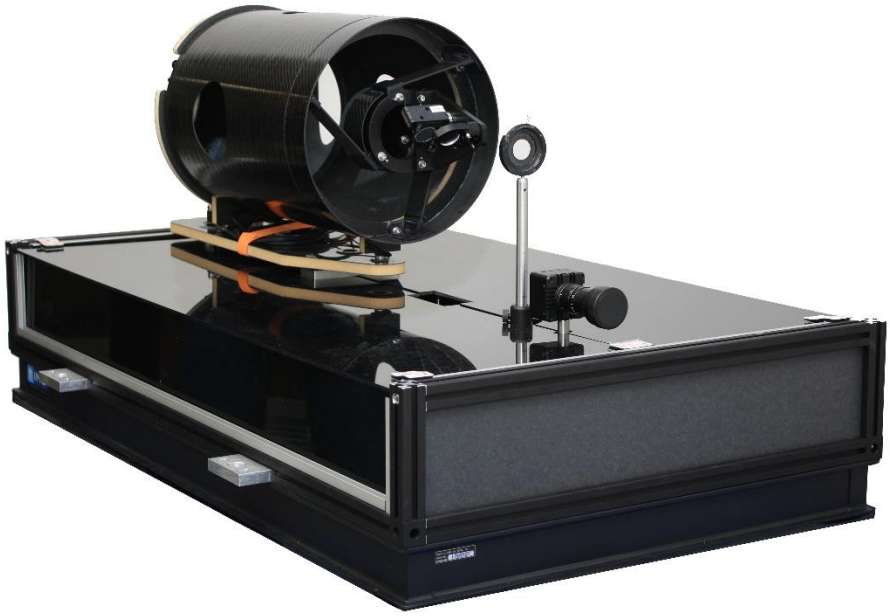

Figure 1. Photo of the UV-Raman platform

As Implemented in Iteration 3 Of The Modifications (Report 4)

The platform has a modular design. The optical head includes a large collection telescope mounted in a lightweight carbon fiber enclosure, an emission beam expander mounted in front of and on the same optical axis as the receiver telescope and as a low power, medium pulse energy 355 nm laser beam. INO decided that a high power 355 nm laser was not necessary at this point.

Scaling was done using the results of the testing. The laser is pulsed to ~ 6-7 ns, in order to minimize the effect of daylight and for range resolved measurements. A 365 µm core optical fiber, having a numerical aperture (NA) of 0.22, with one end in the image plane of the receiver telescope connects the collection telescope to an optical filtering unit. Filtering out of the elastic return (the signal at the wavelength of the laser returned by hard surfaces or aerosols) is done inside the telescope, before the input face of the optical fiber. The Raman signal coming from nitrogen molecules is kept for calibration and quantification purposes. The filtering unit isolates the Raman return of nitrogen from the Raman return of hydrocarbons and partly isolates the Raman return form hydrocarbons from other ambient light sources. The filtering unit is ~10 nm in bandwidth for the nitrogen return and ~10 nm for the Raman centered at 395 nm. The filtering unit is made of thin film filters. Although not optimally implemented at this stage, this is commensurate with weight and volume reduction of the filtering unit. Thin film filters have a better transmission than grating spectrometers. There are two detectors which are high quantum efficiency photomultiplier tubes, one for the Raman from nitrogen and one for Raman from hydrocarbons. The detectors are not gated, as was the ICCD in the preliminary experiments. Instead, they were directly connected to the input of a high bandwidth transient digitizer or a gated integrator. The transient digitizer is synchronized with the laser pulse, as is the gated current integrator. The transient recorder is a 14 bits system. A block diagram of the system can be found at Figure 2.

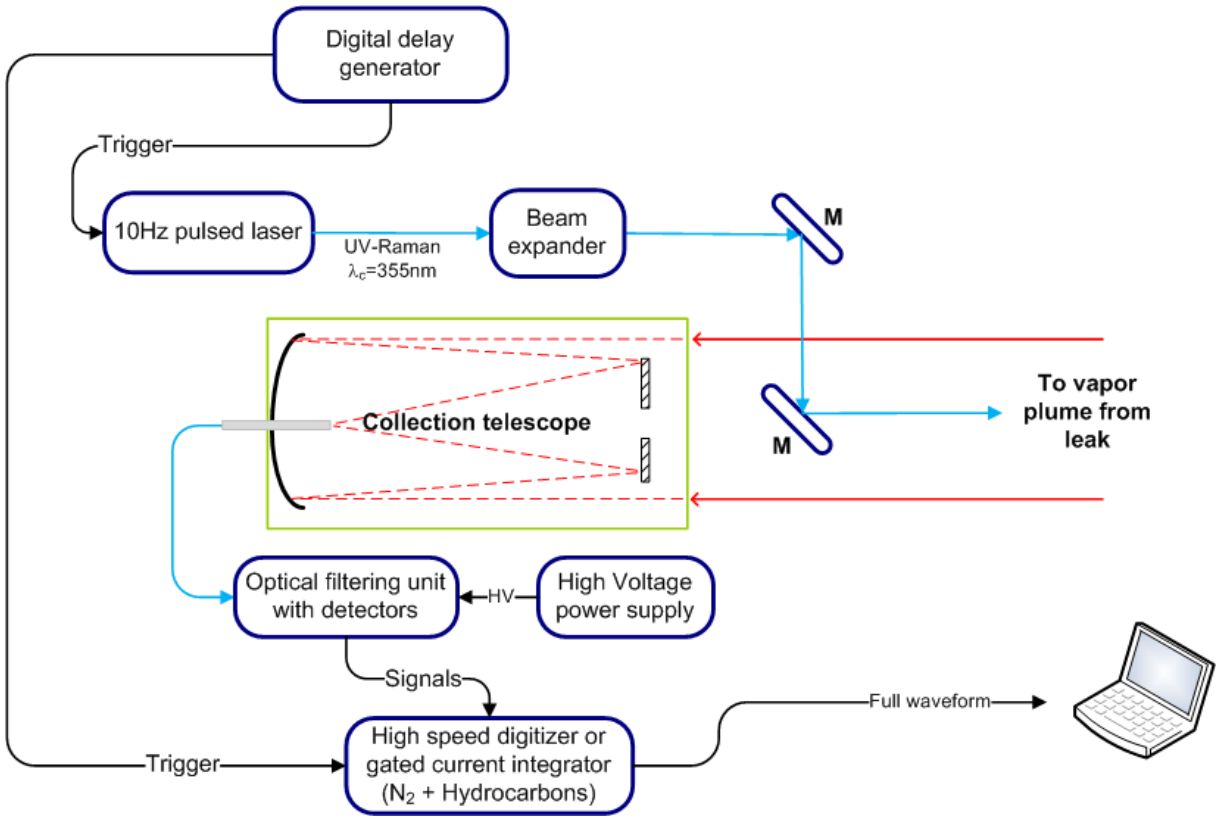

Figure 2. Configuration of the UV Raman LiDAR system as used for the simulated field testing.

The sampling method using the **transient digitizer** is called full-waveform measurement. This is the usual LiDAR set-up, as LiDARs measure spatially resolved concentration profiles. The **gated current integrator** allows integration of signal during a temporal window limited to ~ 60 ns or more. The detection electronics are comprised of the fast gated current integrator and control electronics and software. Again, the use of the gated current integrator is for a high sensitivity at a reduced cost and complexity when compared to the use of a scientific ICCD. Summary of the platform specifications and parameters used for calculation are presented in Table 4.

The cross-sections are those measured in the previous phase. A column as also been added to describe the ideal platform as suggested by INO for the application (details can be found in report 4 of the current project).

Table 4 : Parameters for the as built enhanced UV Raman LiDAR

Parameters	INO UV Raman platform	Ideal platform
Laser energy per pulse (E)	~0.020 J	0.1 J
Laser pulse repetition rate (PRF)	10 Hz	50 Hz
Emission wavelength (λ)	355 nm	355 nm
Laser linewidth	Less than 0.05nm	Less than 0.05nm
Laser pulse width (FWHM)	6.4 ns	6 ns
Laser beam quality factor	BPP < 8 mm-mrad	M^2<2 (BPP < 0.26 mm-mrad)
Detection footprint on ground	0.091 m in diameter	0.1 m in diameter
Pentane Raman cross section	1.25×10^{-29} cm^2/sr	1.25×10^{-29} cm^2/sr
Measurement time	300 ms	300 ms
Length of range cell (L)	~10 m	5 m
Distance to gas cell (R)	50 m	50 m
Receiver area (A)	0.03 m^2	0.03 m^2
Efficiency of detection system (η)	0.26	0.2
Wavelength of detection (λ)	395 nm	395 nm
Detection band width	10 nm	4 nm
Overall system detection efficiency	0.26	0.35

3.3.2 Hardware and Operating Principles of UV-DiAL

Although UV-DiAL is closely related to the fluorescence approach and was presented as a potential option in Report #3, it was not initially planned as a part of this project because fluorescence is usually easier to measure than absorption. Fluorescence is an emission process that is only possible after absorption occurs, which means that fluorescence cannot exist without absorption. However, in this specific case, fluorescence emission is spectrally broader and of lower efficiency than expected, bringing the detection sensitivity to a level that is not sufficient

for the application as defined in the CONOPS. Because an important amount of benzene is found in the vapor phase of gasoline, and because the absorption spectrum contains strong selective features, the UV-DiAL approach was added in the project scope as a modality to be tested.

UV-DiAL, in its usual form, implies having a tunable optical source or at least two wavelength stable laser sources. To perform UV-DiAL measurements, INO decided to use a tunable optical source. The tunable laser is a pulsed 355 nm laser followed by an OPO tunable in the visible spectral range. This light is then doubled in frequency to reach the UV range through a second harmonic generation process. Tuning is done by rotating crystals in synchronicity. For these tests, changing the wavelengths was achieved with calibrated motorized actuators. The laser light from the tunable laser was monochromatic (a single well defined wavelength), but with a finite linewidth on the order of 0.017 nm. In order to get an absorption profile, the laser wavelength is scanned across the absorption feature, which takes time. In our implementation of LiDAR absorption measurements, the technique relies on laser return coming from scattering from the ground.

There are methods to simplify the use of a tunable deep UV laser for absorption measurements. The first method is to not build the complex wavelength stabilization sub-system usually found in DiAL setups. These wavelength stabilization units are necessary when the absorbing molecule has a spectral feature which is very sharp and when only two wavelengths are used. The "ON" wavelength, the wavelength that is most absorbed, preferably has a spectral linewidth smaller than the spectral feature's spectral width for maximum change in return signal. This requires a special sub-system, usually by injecting the light of a reduced linewidth semiconductor laser in the tunable laser cavity. Moreover, small shifts in wavelength, common in tunable lasers, must be avoided, thus the necessity of stabilizing the wavelength.

INO did not follow this approach. The goal is to have and demonstrate as simple a system as possible. Although injection seeding could be envisioned at a later time, when a more advanced fieldable prototype will be designed and built, it was not considered in this phase of the work. The mentioned sub-systems are for ultimate sensitivity and selectivity, but they are not always necessary or they do not always bring more sensitivity and selectivity. This depends on the absorption features' spectral widths and also on the density of the features, as will be seen in the results and analysis section. The density of spectral features in benzene or toluene and the spectral width of the resolvable absorption features did not warrant these complex sub-systems in INO's view.

Furthermore, in order to enhance selectivity, INO adopted a measurement scheme that required multiple wavelengths, so the laser wavelength was scanned to cover multiple wavelengths. It would be preferable that changing wavelength did not require mechanical movement of crystals, but this can be addressed at a later date. This use of multiple wavelengths is such that the

measurement is more like a differential optical absorption spectroscopy (DOAS) than like the conventional DiAL. No effort has been made for quantifying the vapor concentration as the described experimental effort was mainly done to confirm that absorption measurements could be possible in the context of this project.

There are a number of benzene absorption features that could have been used. INO decided to use the 253nm feature because it is relatively strong and because there is no interference from ambient light.

The laser pulse energy is only ~1 mJ at this UV wavelength, and the laser is pulsing at 10 Hz, for an average optical power of ~10 mW, depending on the exact wavelength. This optical power can fall if the second harmonic generation crystals do not move in synchronicity while the laser is scanned in wavelength. The pulse length is approximately 6 ns, meaning the LiDAR return comes from a volume close to 1 m in length providing the electronic detection bandwidth is sufficient. In this case, the bandwidth is 250 MHz and the sampling rate is 500 MS/s (a point every 2 ns or every ~ 0.3 m), more than sufficient to resolve the 6 ns pulse from the laser. The spatial resolution of the system is thus ~ 1 m. For the application at hand and because of the use of the reflection from the ground, there is no need to improve this resolution further.

The platform used for UV-DiAL, shown in Figure 3, shares a lot of components with the UV-Raman platform. The laser system cannot be seen, being in the bottom box (black box on table). The emitting optics is inside the box. The laser beam is expanded and routed out of the box. The emitted laser beam strikes a folding mirror in front of the receiver telescope. The cylindrical form on the top is the receiver telescope with a parabolic collection mirror 20 cm in diameter. Both the emitted beam and the return signal are on the same optical axis. The output laser light can be changed from the 215 mW of 355 nm light for Raman measurements to the tunable deep UV light at <10 mW for UV-DiAL. The telescope optics are coated with aluminum for use in the deep UV. The light is collected by a non-solarizing optical fiber and routed to an optical setup that couples the return light to a grating monochromator and a photomultiplier tube (PMT) for measuring the return signal. The monochromator bandpass is approximately 2.2 nm with the output slit. Optical filtering is necessary for isolating the return from the ambient light, but also to isolate the backscattered light from the generated fluorescence or Raman signals. There is a mismatch in numerical aperture between the grating monochromator and the receiver telescope. This should be corrected in the future for optimum signal recovery.

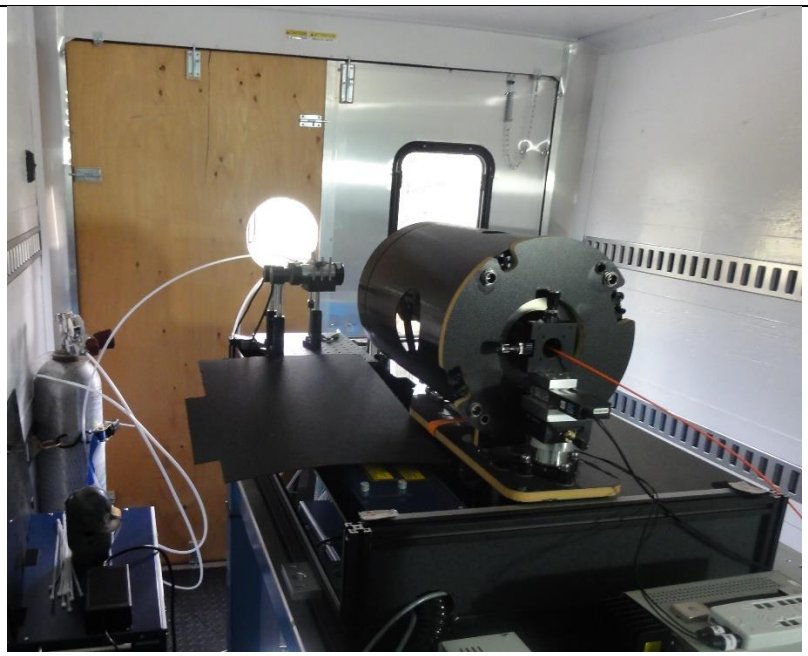

Figure 3. UV-DiAL breadboard prototype in mobile laboratory.

The incoming light on the PMT generates a signal that is digitized at 500 MS/s. The PMT amplifies the signal generated by the return photons to a level such that the digitization circuit is not a significant contributor to measurement noise. Not seen on the photo are the laser controller and the grating monochromator with PMT.

Other components that are seen on the photograph are a calibrated gas bottle, gas routing hardware and a reference gas cell. Figure 4 shows a drawing of the UV-DiAL setup. The laser output is routed to the exterior using multiple folding mirrors. After the last folding mirror there are two glass wedges that pick up part of the laser beam. A first deflected beam goes through the reference gas cell to a pyroelectric detector and a second deflected beam goes directly to another pyroelectric detector. The exact configuration is not important because components can be moved around for the best work performance.

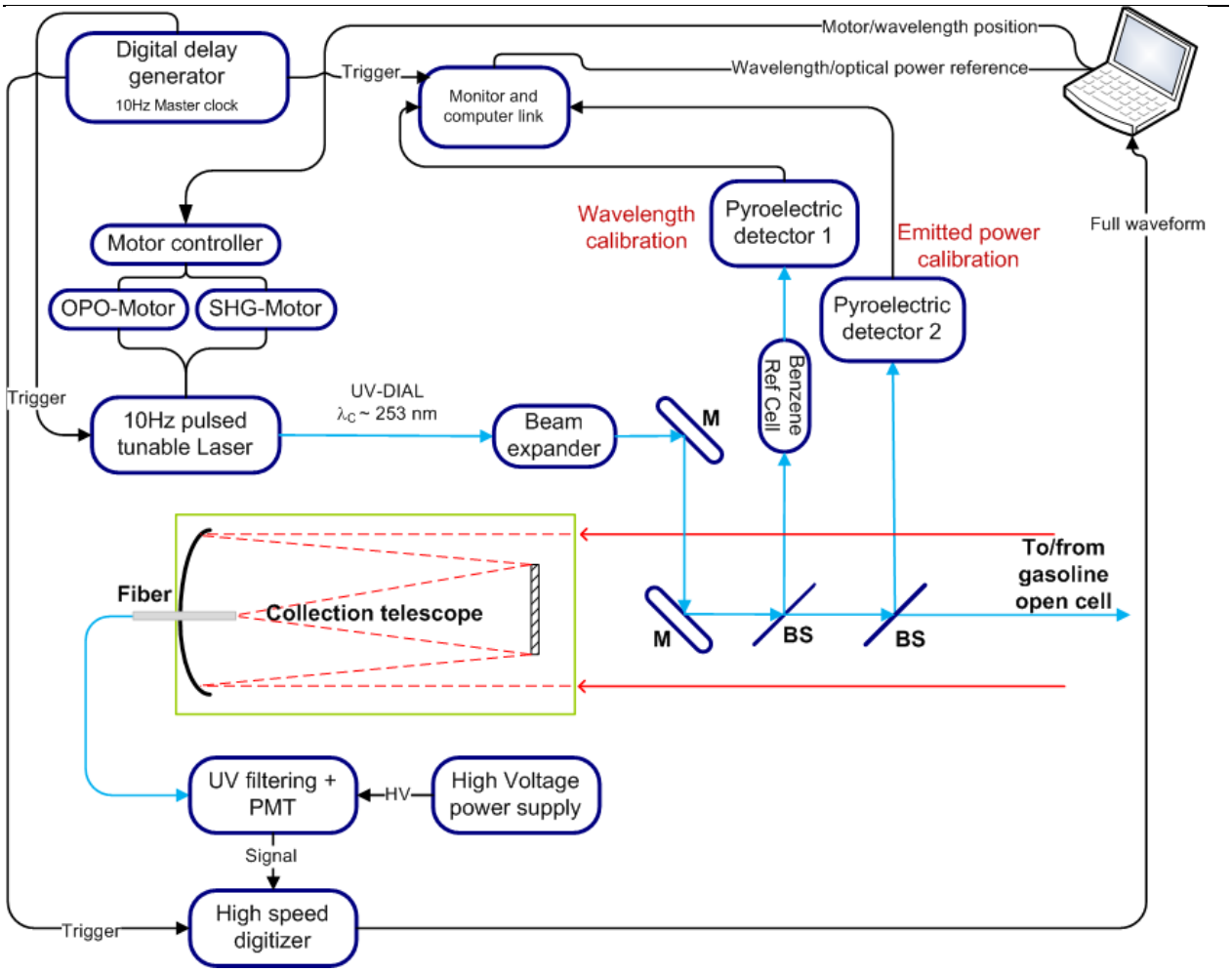

Figure 4. Configuration of the UV-DiAL system as used for the simulated field testing.

3.3.3 Hardware for IR absorption LiDAR (DiAL)

The INO instrument can be operated in two different ways: path integrated and range resolved, but in the application at hand, even the range resolved mode will be used for path integrated measurements. This means the signal will depend on the absorption all along the laser beam path and back.

The INO IR-DiAL breadboard houses the laser head, routing and shaping optics to bring the laser beams to the beam expander and in between, optics, oven and crystals for Short-wave Infrared (SWIR) / Mid-wavelength Infrared (MWIR) generation. The laser beam expander and the output beam size are chosen to ensure the system is eye-safe and to be able to reduce the collection field of view for enhanced daytime capability. It also houses the receiver telescope, and return signal routing optics, an IR spectrometer, if required, and the detector(s) and detector electronics.

The IR system is similar to the UV systems but all detection, source and routing optical components operate in the SWIR/MWIR. The system operates with an optical parametric generator (OPG) designed and built at INO. It is a coherent, tunable (1.48-3.84 µm), broadband source based on 1064 nm pumping of Periodically Poled Lithium Niobate (PPLN) materials. A complete overview of the system can be found in [17]. For the application at hand, pentane and crude components in general are measured in the 3.4 to 3.6 µm range. The output power of the coherent MWIR beam could be as high as 0.5 W, effectively separated in short pulses of < 1 ns at a repetition rate of up to 100 kHz. This large amount of concentrated power allows the use of a Lambertian target instead of a retroreflector, or the use of any topographical target.

The OPG is seeded using tunable external cavity diode lasers at 1524.6 and 1533.4 nm. The seed powers are approximately 1 mW each. The seeds are inputted to the PPLN alternatively at every other pump pulse, hence seeding one at a time. So each seed operates at 2.5 kHz for a total pulse rate of 5 kHz.

One of the detector options is a camera developed at INO to maximize the sensitivity in the spectral region of interest (Figure 5). It can be operated under avalanche mode for detecting very small signals and be gated in order to reduce the background noise. In this case the laser system operates only at 150 Hz, the maximum image throughput of the camera. There is no on-chip accumulation at this time. When using this detector, the OPG is seeded simultaneously with both seed lasers.

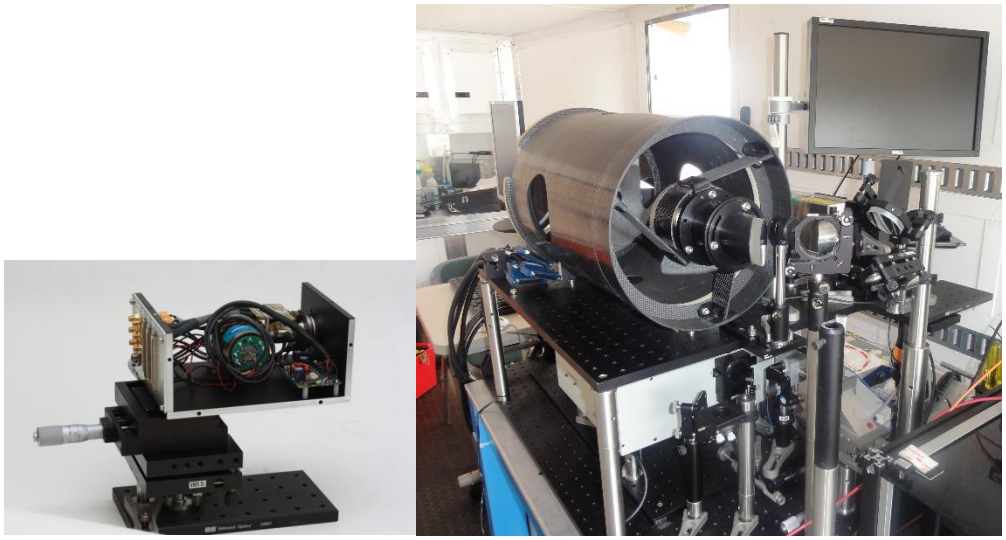

Figure 5 : Photos of the camera (left) and the breadboard of the system in the mobile laboratory (right).

The detector that has been used for the measurements presented here is a fast response immersion MCT detector. There is no input filtering. The signal from the MCT goes to a digitizing card and the whole of the return is digitized at 100 MS/s. The returns, from the same seed, are averaged over a large number of pulses. The triggering is synchronized with the pump laser pulses. A reference signal is picked off before the beam is sent into the atmosphere and routed to the MCT detector. This reference signal is separated from the return in time.

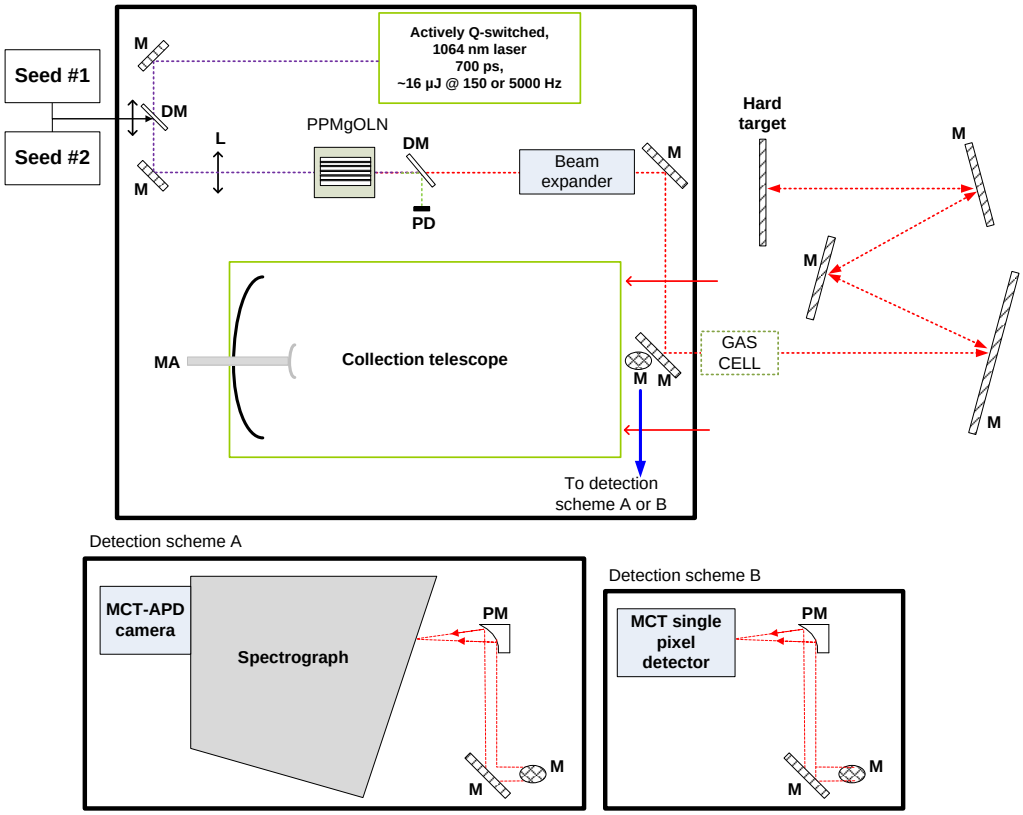

Figure 6 : Double seeded IR DiAL LiDAR; M: mirror; DM; dichroic mirror; PM: parabolic mirror; PD: photodiode for power measurements; MA: motorized actuator for focus.

The laser target used during testing is a sandblasted aluminum plate large enough to intercept the entire IR beam. The reflection is supposed lambertian (similar in all directions). The reflectivity of aluminum is close to 100% in the IR (the diffuse reflectance of our target was not measured), whereas in the application the ground would be closer to 5%. Table 5 summarizes the parameters of the IR-DiAL platform as used for the intermediate scale testing phase.

Table 5. Parameters for the IR-DIAL platform

Parameters	
Laser energy per pulse (E)	> 0.00001 J
Laser pulse repetition rate (PRF)	1 Hz to 100 kHz
Emission wavelength (λ)	1.48 µm to 3.84 µm
Laser linewidth (seeded)	~3 nm FWHM
Laser linewidth (unseeded, FWHM)	10 nm <$\Delta\lambda_L$<100 nm
Laser pulse width	~ 1 ns
Laser beam quality factor	Not measured
Distance to diffuse target (R)	~40 m
Receiver area (A)	0.03 m^2
Efficiency of detection system (Φ)	>0.08 at 50% coupling of return in detection system (low resolution)
Spectral coverage of camera system	120 nm
Spectral resolution of spectrographic system	0.6 nm < $\Delta\lambda_S$ < 10 nm

3.4 Test Set-Ups

In order to simulate field measurements for Raman LiDAR and IR absorption LiDAR, an intermediate scale set-up was designed and built in collaboration with Institut National de la Recherche Scientifique (INRS). A brief summary of the installation and protocol is presented here but the entirety of the INRS report is presented in Appendix 1. For UV-DiAL experiments, tests on benzene were conducted outdoors in an open gas cell setup different from the two other modalities (IR-DiAL and UV-Raman).

3.4.1 Intermediate scale set-up (INRS)

Based on the CONOPS, INO asked INRS to provide an intermediate scale model with the ability to simulate a diesel fuel leak under 1.2 m of dry sand. The requested simulator had to allow vapor monitoring in the ground as well as in the air column located above the sand surface up to a height of 5 m. The mandate also required that INRS monitor diesel vapor migration both in the sand and in the air column located above the sand during the experiment. At the same time INO performed measurements of volatile organic compounds using Raman LiDAR and IR absorption LiDAR.

Leak Simulator

The leak simulator used for the experiment was a rectangular watertight steel container lined with a flexible PVC membrane of 1/8in thick (Figure 7).

The sizes of the tank were:

- Interior height : 1.372 m (4 ft. 6 in)
- Width : 1.880 m (6 ft. 2 in)
- Length : 2.565 m (8 ft. 5 in)
- Area : 4.822 m^2 (52 ft^2)
- Internal volume : 6.616 m^3 (234 ft^3)

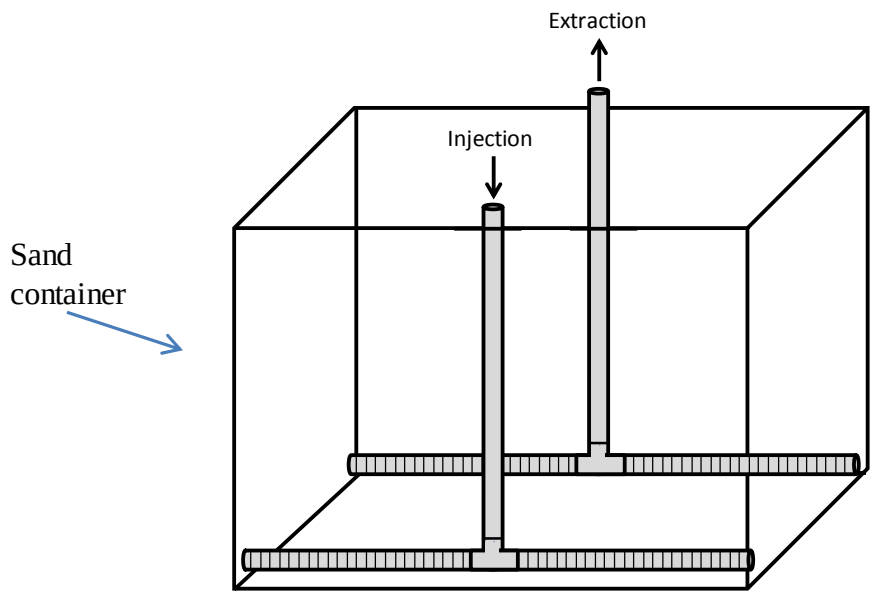

Figure 7. Tank layout prior to sand filling (not to scale).

A liquid petroleum product injection and extraction system was installed inside the container before it was filled with sand. The system was designed to simulate a continuous leak at the bottom of the sand container. The injection and extraction system is illustrated in Figure 7 and was composed of the following:

- Two horizontal wells located at the bottom of the container, on opposite sides. The wells were constructed with slotted 1-inch PVC pipe (slot size 0,010 inch). Both ends of each horizontal well were caped;

- Two vertical solid 1-inch PVC pipes connected to the middle of each horizontal well with a tee and rising along the container wall to a height of 1.5 m (59 in).

Finally, approximately 8 metric tons (8.8 US tons) of Temisca grade #18 silica sand (Opta Minerals) were used to fill the container employing a precise layer-by-layer compaction procedure. The end result is a homogenously compacted soil which is representative of a realistic ground.

Vapor Plume Control System

To allow control of the vapor plume above the simulated underground leak while allowing evaporation of the volatile fraction of the petroleum product, a 5 m high polyethylene tent was built over the leak simulator container. To limit the transport of vapor in the air outside the tent, the upper part was fixed to an air extraction unit.

Figure 8. Underground leak simulator container with polyethylene tent.

Monitoring Wells and Air Sampling Ports

Hydrocarbon vapor progression in the sand and in the air over the simulated leak is monitored using hollow sampling wells (in the ground) and sampling ports (in the air). Distribution of each is illustrated in Figure 9 and Figure 10.

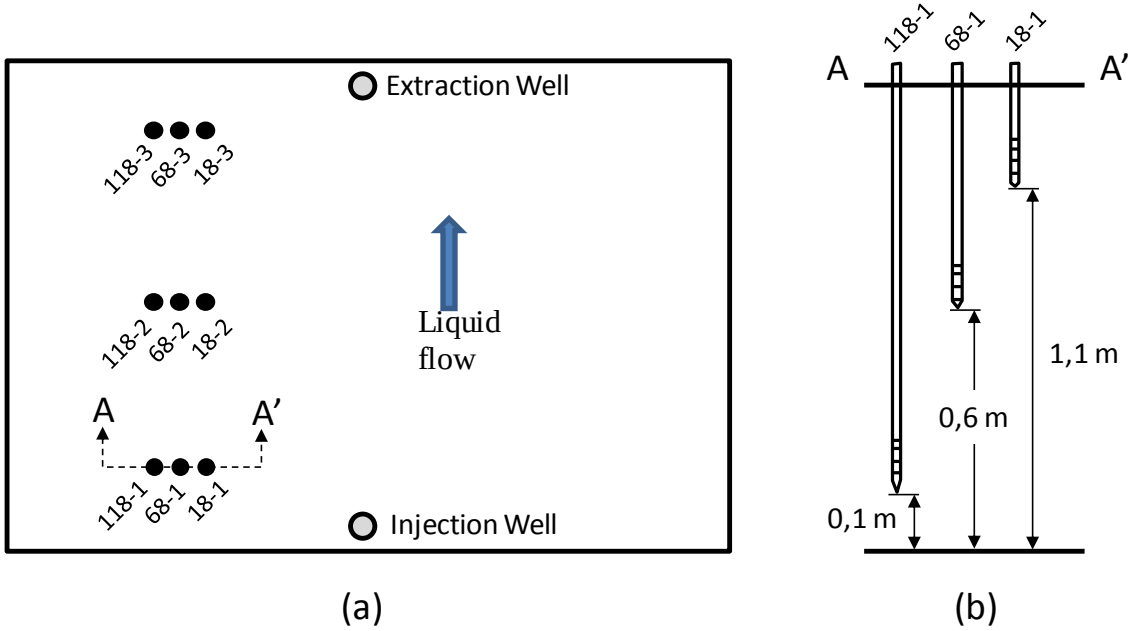

Figure 9. Soil vapor monitoring wells in the leak simulator container. Top view (a) and cross-sectional view (b).

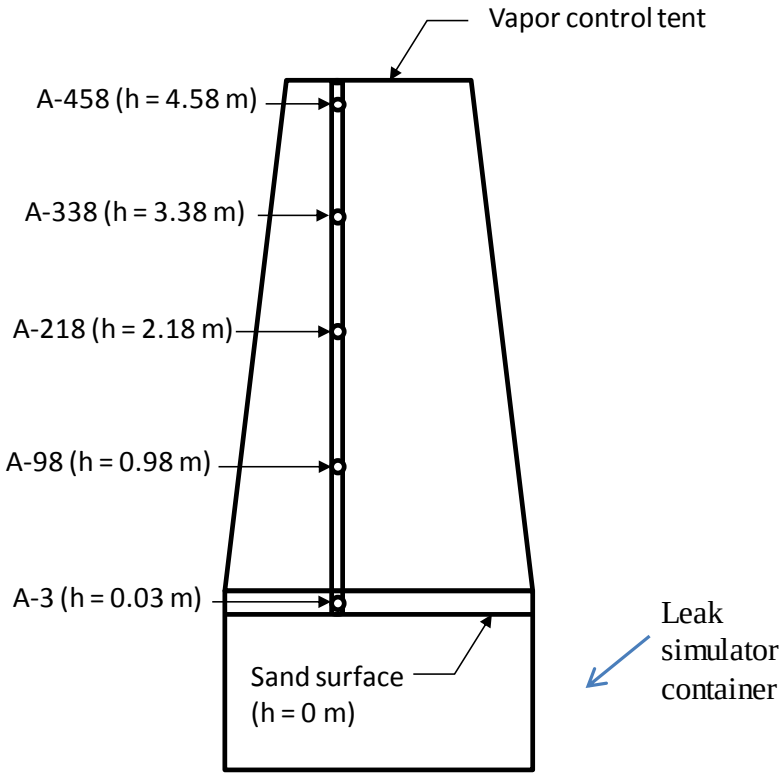

Figure 10. Air monitoring ports above the sand surface (not to scale)
(h = height measured from the sand surface)

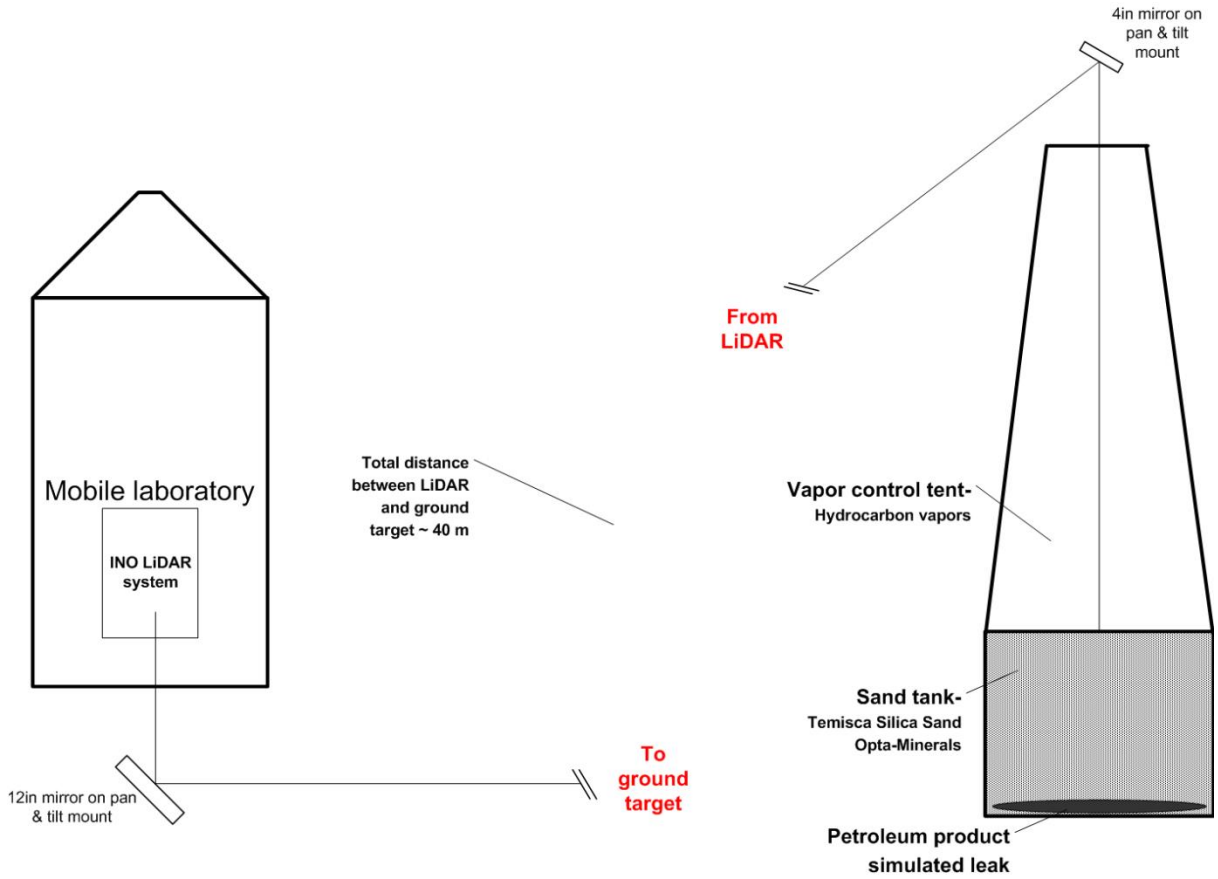

Figure 11. Schematic illustration of the intermediate scale setup for Raman LiDAR and IR absorption LiDAR measurements.

Reference Measurements

Each port is sampled and analyzed using both a flame ionization detector and a photoionization detector (FID/PID) from the same Thermo/Foxboro TVA 1000B Vapor Analyzer. This instrument allows for two (2) different measurements of the vapor concentration and is capable of concentration measurements as long it is sufficiently calibrated, which means that the composition of the vapor does not change. A fundamental difference between these two similar methods is that the FID is sensitive to short C-chain hydrocarbons such as methane, ethane and propane whereas PID is not.

Thermal Desorption Tubes (TDT) packed with Carbopack B were also used to get the composition of the vapor. Using a volume calibrated pump, the hydrocarbons contained in the sampled gas are adsorbed by the packing material of the tubes. These tubes are then analyzed by an independent lab (Cassen Testing Laboratories, Ont. Canada) and results are returned a few weeks later. 29 different compounds can be analyzed using this approach. However, this

approach is expensive and can only supply post-experiment results. This is why it is only used as a complement to the information provided by the FID/PID values.

Fuel Supply and Injection

Three types of fuel were used in the course of these tests: diesel fuel, pentane and unleaded regular gasoline. These compounds were either injected in the tank through the injection port or simply placed in open pans over the soil to allow rapid evaporation in air.

Two peristaltic pumps were used for injection and extraction of the diesel fuel. Flexible Viton and high density polyethylene tubings (¼ inch outside diameter) ran from each pump to their respective horizontal well (see Figure 7). During the injection phase of the experiment, the injection flow rate was an average of 0.30 kg/min or 0.36 L/min if a density of 0.83 kg/L is considered for diesel fuel. During the recirculation phase, the flow rate was set at 0.1 kg/min (0.12 L/min) for both injection and extraction pumps.

A pan experiment was also made where 5 to 6 pans (Pyrex pans of 30cm x 30cm x 5cm), filled with 1 cm of fresh product (diesel, pentane or gasoline) were uniformly set on the surface of the sand in the leak simulator container.

Hydrocarbon Leak Simulation Volumes and Timeline

Liquid petroleum products were injected for different time periods on different days. The leak simulator was characterized at the same time leak detection was performed: there was a significant learning curve. The injected volumes are presented in Table 6. There was no removal of the sand in the container. There was a continuous build-up and migration of the liquid petroleum and of the vapor in the sand. Vapor monitoring results presented in the following sections are reported with respect to the start time of injection on Day 1, in the cumulative column (hr), as presented in Table 6. There is a long interlude between the tests with pentane and those with the gasoline. During this period, the liquid petroleum product was allowed to migrate in the sand as was the vapor plume above the leak simulator container and measurements with the PID/FID were taken as were samples of the vapor. This was done to have a better model of vapor plume formation than the one used in the LOD estimates of the previous phases. Of course, the vapor plume model is impacted by the fact that the container is closed, as is the tent above the container.

Table 6. Timeline of the experiments done on the intermediate scale leak simulator

Date	Time	Cumulative time (hrs)	Event
2014-09-09	09:58	0.00	Start of diesel injection
2014-09-09	14:57	4.90	End of diesel injection (100 L injected)
2014-09-10	09:28	23.50	Start of diesel injection / extraction
2014-09-10	11:20	25.37	End of diesel injection / extraction (15 L)
2014-09-10	11:25	25.46	Start of diesel pans experiment (5 pans on sand)
2014-09-10	12:00	26.03	* Improvement of the sealing at the base of the tent
2014-09-10	15:12	29.23	End of diesel pans experiment
2014-09-10	15:25	29.45	Start of pentane pans experiment (5 pans on sand)
2014-09-10	16:00	30.03	End of pentane pans experiment
2014-09-18	11:05	217.12	Start of gasoline pans experiment (6 pans on sand)
2014-09-18	16:00	222.03	End of gasoline pans experiment

LiDAR Measurement Procedures

Figure 11 shows how the INO mobile laboratory was set-up for the tests. The mobile laboratory is a trailer equipped with scientific instruments and an optical table. The optical table is a rigid and robust steel table with the tabletop being a perforated steel slab. The holes are ¼-20 tapped and spaced by one or two inches. Ancillary equipment can be placed on a shelf underneath the table. The LiDAR platforms are attached to the tabletop pointing towards the back of the mobile laboratory. When in operation, the back doors are opened, and a panel with an oversized hole is installed (or not, depending on weather) in the door opening.

The laser beams exiting the LiDAR platforms are routed towards 12" diameter exterior optical grade mirrors mounted on tripods. The tripod mounted mirrors then route the laser beam towards a mirror mounted on a gantry crane, immediately above the vapor plume containment tent at 5 m from the surface. The mirror directs the laser beam towards the leak simulator sand (or soil) surface, through a hole on the top of the vapor plume containment tent. This is the same hole from which the vapors are extracted using vacuum pumps. The signals generated by scattering, fluorescence or Raman on and above the surface are routed in the opposite direction towards the LiDAR platforms by the same mirrors. The gantry mounted mirror is attached to a motorized pan

and tilt unit controllable from the ground. This allows precise alignment of the laser and return beams with respect to the leak simulator surface.

The tripod mounted mirrors are also used to route the laser beams towards other tripod mounted accessories, such as verification or calibration targets. These targets are used, in particular, to verify and optimize proper emitter/receiver alignment and effects of daytime lighting conditions on the measurement apparatus.

The leak simulator container and overhead tent are inside a large garage type laboratory, underneath the overhead gantry crane. The INO mobile laboratory is outdoors. The rollup garage doors are fully opened while LiDAR measurements are being taken. Once the LiDAR platforms are up and running, it takes several minutes to install the tripods and adjust the beams for useful aligned measurements.

LiDAR measurements are time stamped. Similarly, PID/FID measurements and TDT analysis reflect compositional values at a specific moment. All measurement parameters are logged along with the raw data for post-processing and analysis. Ambient lighting conditions do not greatly affect the measurements, nor do the wind conditions. Rain can have an impact on the measurements, with the beams traveling outdoors: no measurements were taken during in the rain.

3.4.2 Outdoor Set-Up

Windowless Gas Cell

Because of a component failure in the UV LiDAR platform and the closing of the test window at INRS, the UV-DiAL outdoors tests were performed at INO using the windowless gas cell described in Report #4. The use of a windowless gas cell is necessary due to the fact that the windows fluoresce and scatter. This interferes with the measurements and does not correctly simulate the CONOPS.

The windowless gas cell is simple in design. It is a Plexiglas box, 2 m in optical path length limited at each end with a Plexiglas wall, with a square cross-section ~40 cm on a side. At both ends of the optical path section are ~15 cm long Plexiglas extensions with the same ~ 40 cm per side square cross-section. ~10 cm diameter openings are cut into the two walls at each ends for the laser beam and return light to travel freely without encountering anything but the atmospheric air and the simulated vapor plume. A drawing is shown in Figure 12. Two other face-to-face ~10 cm diameter holes are cut in the extensions, perpendicular to the beam path, in order to flow outside air in these extensions and create an "air curtain" to minimally contain the hydrocarbon vapors. The flow is controlled with two face to face fans in the perpendicular holes on each ends.

The outside air and some vapor are routed away from the windowless cell not to interfere with measurements (see Figure 13).

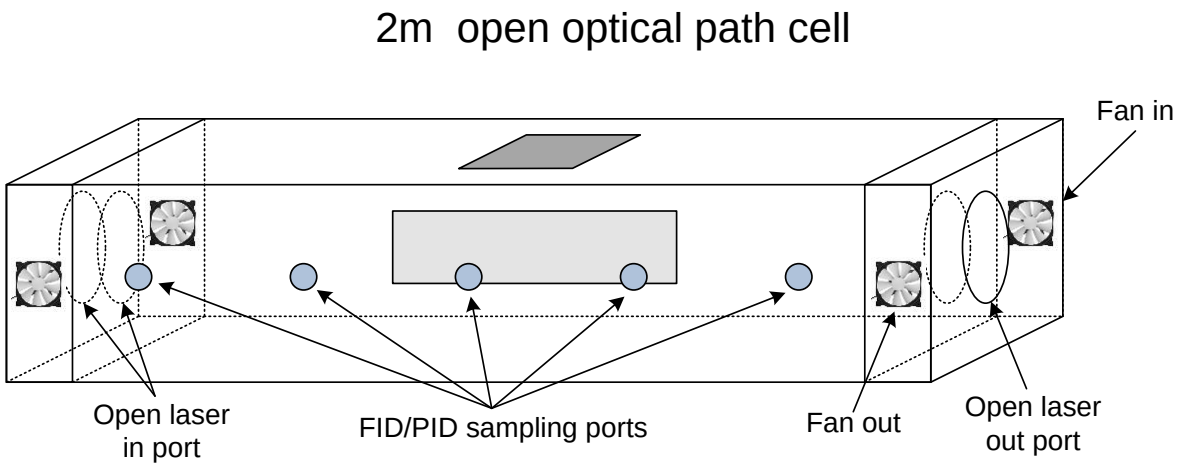

Figure 12. Drawing of the windowless gas cell.

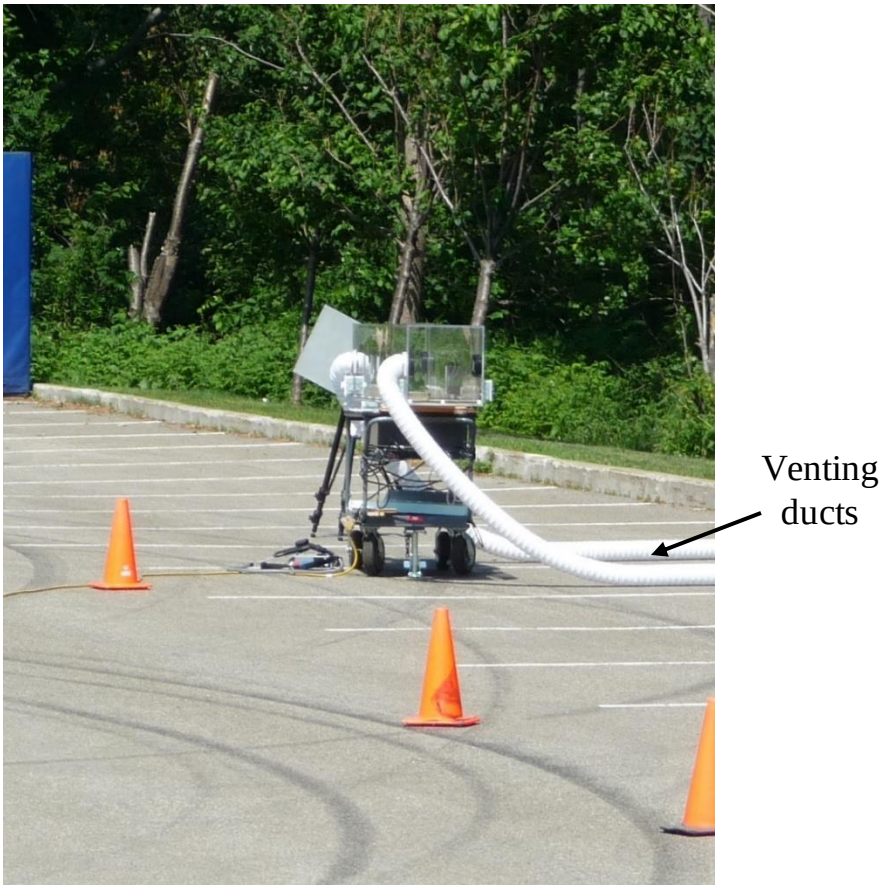

Figure 13. Photograph of windowless gas cell in an outdoors setting.

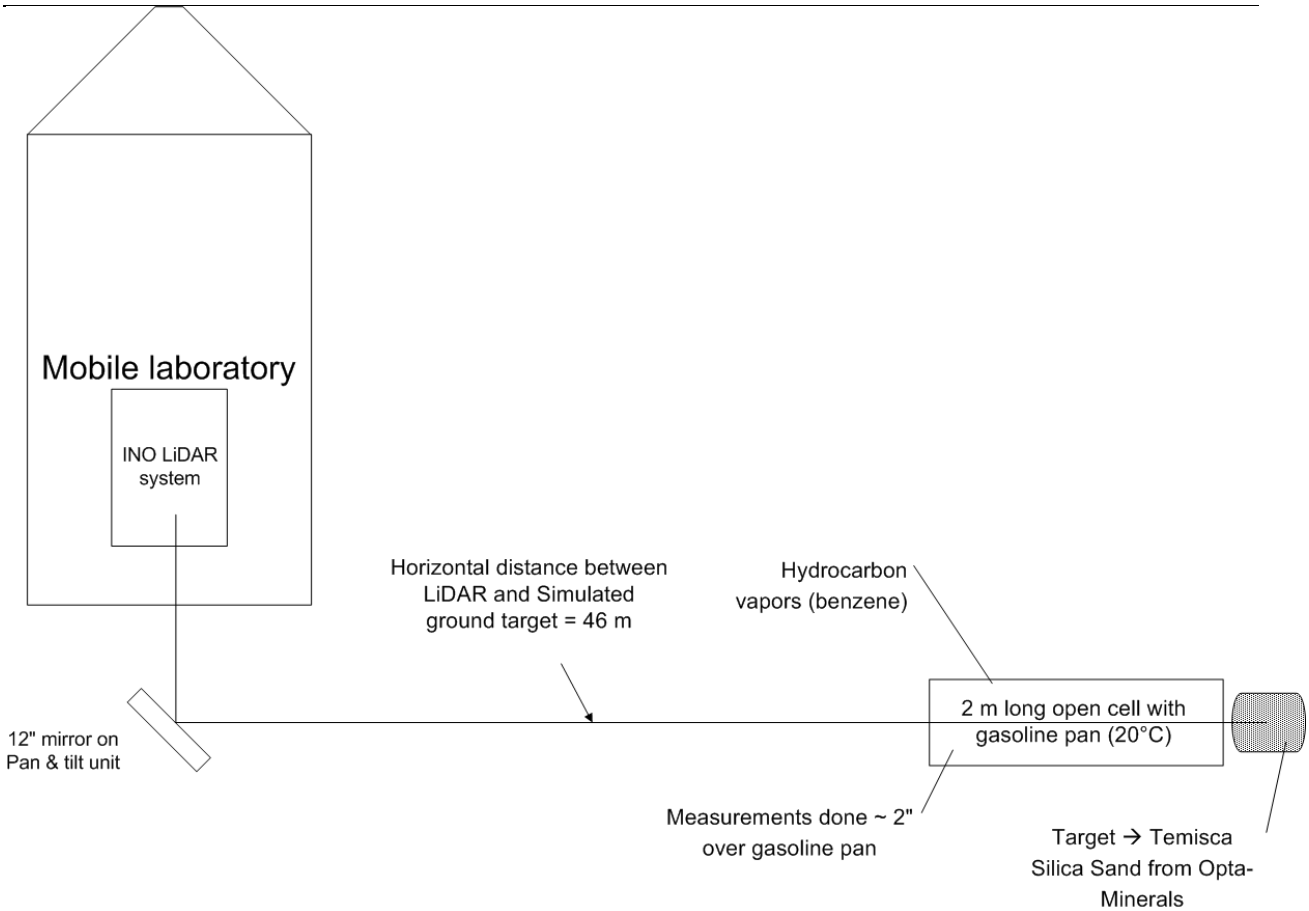

Figure 14. Schematic illustration of the outdoor setup for UV-DiAL measurements.

The vapor concentration inside the cell is measured with a calibrated flame ionization detector (FID) – photoionization detector (PID), model Thermo TVA 1000B, through small holes cut in the wall of the cell. There are five holes uniformly distributed along the 2 m optical path length, which are sealed when not in use. Measurements inside the windowless cell and outside the cell show that an insignificant amount of hydrocarbon vapor is in the optical path outside the cell itself. The FID-PID detector is used to give an estimate of the vapor concentration inside the windowless cell.

The use of the windowless cell is not without drawbacks. The tests are done in a parking lot adjacent to INO buildings in Quebec City, Canada. Days without strong intermittent winds are rare. These winds regularly flushed part of the vapor out of the windowless cell, directly or by affecting the speed of the fans in the "air curtains" on the ends of the cell. This gives rise to fluctuations in the measurements that can be interpreted as measurement noise. This must be taken into account when analyzing data. In order to have measurements in "quiet" conditions, the Raman platform in the mobile laboratory along with the windowless cell and ancillary hardware

would have needed to be moved to a remote location. This was not done for the measurements presented here.

In order to generate the vapor inside the windowless cell, a large pan containing the liquid from which plume is created is placed inside the cell through a large rectangular opening on the side. The opening is sealed once the pan is placed inside the cell. The concentration of vapor inside the cell depends on the vapor pressure of the liquid constituents. This in part depends on temperature and direct sunlight on the liquid because the cell is made out of Plexiglas. For the tests with gasoline presented here, a heater was added underneath the pan, the outside temperature being around -7°C. The resulting temperature of the liquid was set at 20°C.

Outdoors Measurement Procedures

The UV-DiAL platform was installed in a mobile laboratory (Figure 15). As in the previous case, the platform is installed on a rigid table. The laser beam exits the platform and is directed towards a large folding mirror on a tripod just in front of the back doors of the mobile laboratory. The laser beam is aligned so that it is reflected at the center of the large folding mirror. The laser beam can be scanned and aligned by adjusting the angular positions of the folding mirror. It then travels horizontally to the horizontal windowless measurement cell for a total of ~50 m of travel. It continues its travel until it hits an installed panel or other topographical target, in this case a target made of Temsica Silica Sand from Opta Minerals, the same as for the Raman and IR-DiAL measurements performed at INRS. The target is slightly slanted. The panel was mounted within 1 m from the exit of the windowless cell to simulate the laser hitting the ground (as would be the case when measuring from an airborne platform).

Figure 15. Photograph of outdoors set-up with mobile laboratory, folding mirror, windowless gas cell and aluminum target

The return signal is directed to the collection telescope by the large folding mirror and enters the collection optical fiber. At the other end of the fiber, light is optically filtered and detected as described in the hardware section. The current from the PMT is measured using the transient digitizer. The transient digitizer acquisition is synchronized to the laser pulse.

The acquisition is in fact triggered twice for every laser pulse. One trigger is for measuring the optical and electronic background noise without emitting a laser pulse and the other the sum of the noise and the actual integrated path UV-DiAL return while emitting a laser pulse. The background without laser pulse is subtracted from the return with laser pulse.

3.5 Results and Discussion

3.5.1 Intermediate scale testing

Raman LiDAR measurements

The main goal of the measurements with the leak simulator was to test the modified Raman platform in more realistic conditions. INO tested two of the platform configurations with the leak simulator: 1) using the current integrator; 2) using the fast transient digitizer. Otherwise, the remainder of the hardware was the same. A large amount of data was accumulated but only the most relevant part is presented here.

Figure 16 shows the ratio of the Raman of alkanes to that of nitrogen as defined in the hardware section with respect to distance from the platform. The Raman channels have an optical bandwidth of 10 nm. This is not ideal, but was deemed sufficient for the demonstration. The measurement's spatial resolution is limited by the laser pulse length of 6 to 7 ns which correspond to approximately 1 m (back and forth at light speed). The digitizer samples every 5 ns (200 MS/s). Figure 16 is a small portion of the returns where time elapsed between laser emission and return to the detector is transformed into distance from the platform. Between 32 and 35 m, there clearly is a signal in the alkanes channel. There is always signal in the nitrogen channel: there is nitrogen everywhere and at the same concentration, so it is used as the reference. The return coming from only the nitrogen channel is not shown but the signal varies because of the changing overlap between the field of view of the receiver and the laser beam footprint. It also changes because of the drop in return power due to the increasing distance from the platform. The ratio of the alkanes channel to the Raman channel, on the other hand, is relatively constant with distance when considering the region where the overlap is significant (>30 m). These are processed curves. Since there is a large peak when the pulse hits the ground, all curves can be corrected for timing jitter.

There should not be any alkanes in the atmosphere at these distances. The signal in the alkanes channel can be caused by a number of interfering phenomena. There is of course ambient light,

but this is an offset that is corrected for. Then there is the back-scattering at the excitation wavelength (355 nm). When designing a Raman system, care must be taken to insure that the laser emits only laser light in a very restricted laser linewidth and this light must be very well filtered on the return. INO used high end Raman filters, but the Raman signals are very weak with respect to the back-scattering (Mie and Rayleigh scattering) at 355 nm. It is very much possible that some amount of this light filters through the detection channels. Another likely interferent is the presence in the air of molecules that have part of their Raman signature within the 10 nm detection bandwidth of the alkanes, and possibly of nitrogen. Finally, but much less likely, there could be particulates in the air that fluoresce. Whatever the cause, this is a constant offset that can be subtracted.

Figure 16 also shows a peak between 36 and 38 m. This is scattering from the folding mirror placed on the gantry, above the polyethylene tent covering the leak simulator container. In the other graphs, this portion of the curve is ignored: there will be no mirror in a real life application with an airborne platform. The portion of the signal that is of interest is then from 38.6 m to 41 m. This is only 2.4 m, but the laser pulse length of 6 to 7 ns represents approximately 1 m. So, our measurement points would cover roughly 3.4 m. There is a clear rise from the mirror to the ground. These curves are for measurements with diesel or pentanes pans on the sand inside the tent. The important characteristic is that the Raman signal rises when approaching the ground. There is a concentration gradient, with the largest concentration being closer to the ground. Figure 17 shows the curves corrected for the offset and the mirror scattering.

These are very small signals compared to the reflection from the ground and subsequent fluorescence. This can be seen in Figure 18. This graph has the time axis before transformation to distance and with the mirror scattering removed. The important characteristic here is the very large return from the ground which seems to be a sum of different returns followed by fluorescence. The peak at ~235 ns is likely a sum of scattering at 355 nm leaking into the detection channel, Raman signals from nitrogen and alkanes and some fluorescence from the sand. The contribution from the scattering at 355 nm cannot be more than what is observed prior to the mirror; thus it is a small contribution. The contribution from fluorescence can be estimated by the signal from 260 ns and over. When the laser hits the ground, there is no longer any laser beam return: the laser light no longer exists. The signal that comes afterward is continuing fluorescence from the ground previously excited by the laser beam. The remaining contribution to the peak is Raman from alkanes or other ground molecules. The ground generates instantaneous Raman; it most likely contributes to the signals in the nitrogen and alkane Raman detection channels.

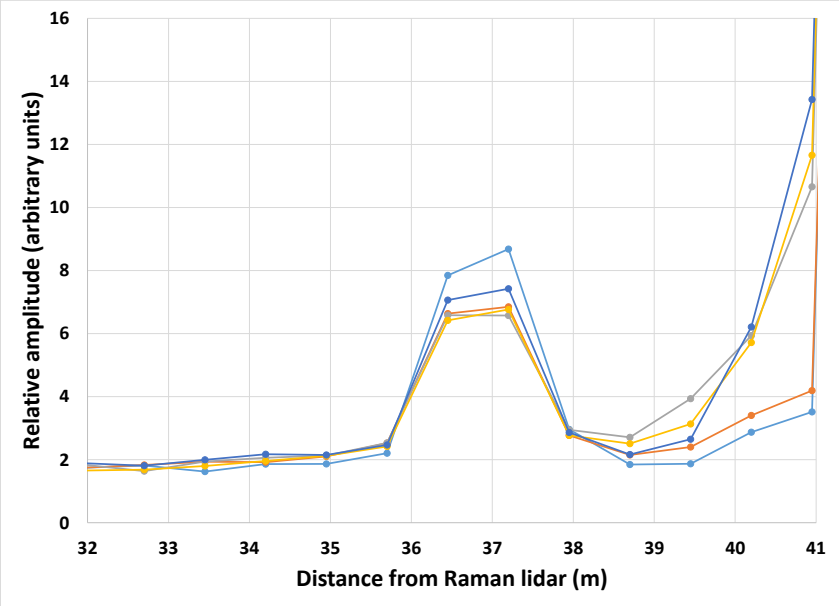

Figure 16. Raman signal from leak simulator for different alkane concentrations.

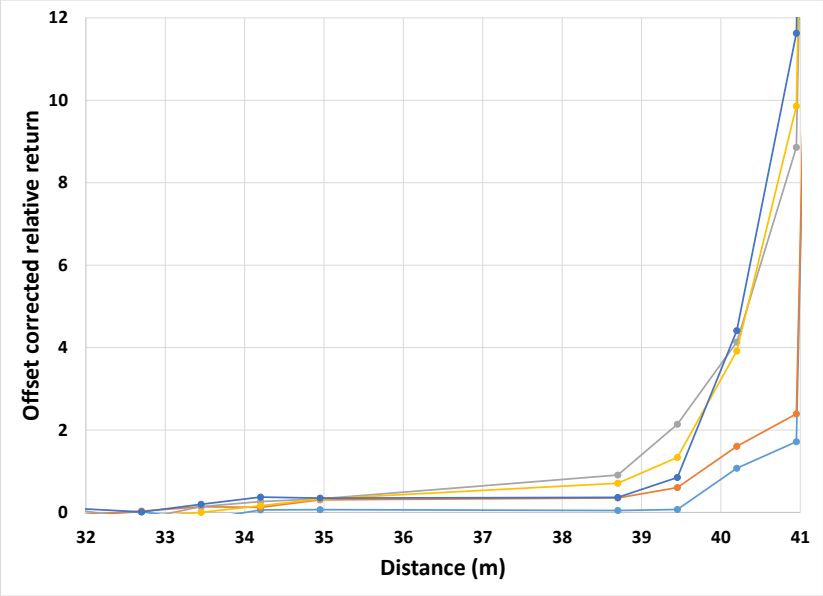

Figure 17. Return curves with offset and mirror reflection corrected

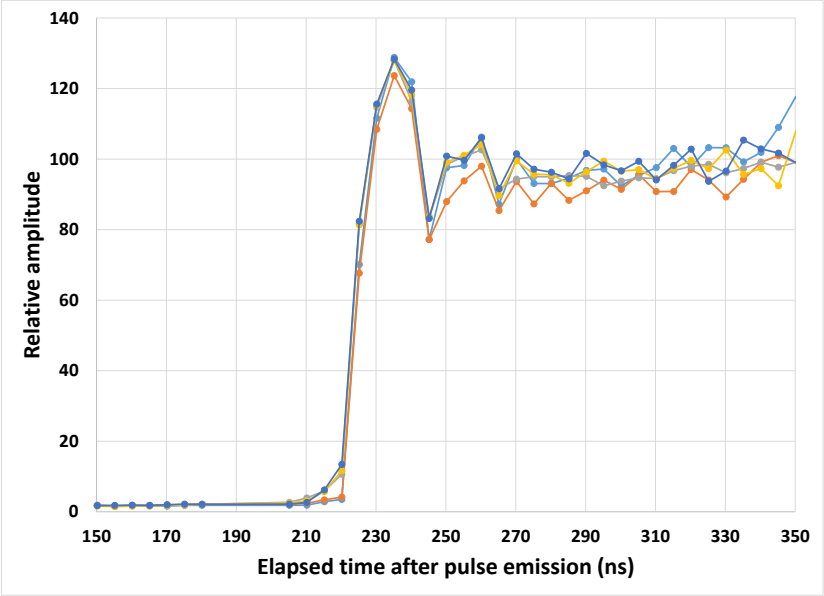

Figure 18. Return waveform of Raman plus ground fluorescence

All curves in Figure 18 peak at the same value except one. The differences in amplitude for the points prior to the peak are most likely varying signals from the alkanes' channel. These measurements show a good signal-to-noise ratio because they are the averages over multiple Raman returns. Each curve is the average over 963 returns (except for one at 855 returns). Each laser pulse is approximately 20 mJ just above the ground, which translate to ~20 J of energy: this is a huge amount of energy. In these experiments, this amount of energy was accumulated by measuring for 96 seconds, which is not in line with the CONOPS. It was estimated that the measurement should be done within 300 ms. For this to happen, the laser system would need to pulse at 5 kHz with 20 mJ per pulse, which is a huge laser power. It is 20 times more than the estimate made in previous reports. The signal-to-noise ratio might be too large, but not in excess, seeing the noise on the curves between 32 and 35 m. But going from an average over 100 pulses to an average over 1000 pulses only enhances the SNR by a factor of ~3, as can be deduced from the curve of Figure 19 when looking at the high frequency portion. This graph is the evolution of the average over 3.4 m of one of the curves with respect to number of pulses averaged. The return of every pulse is saved to disk. The results presented here are post processed. Averaging over 100 pulses or so should be sufficient. This then makes for a laser only twice as powerful as what was originally estimated, which is in line with the fact that the concentration of alkanes was much lower than expected.

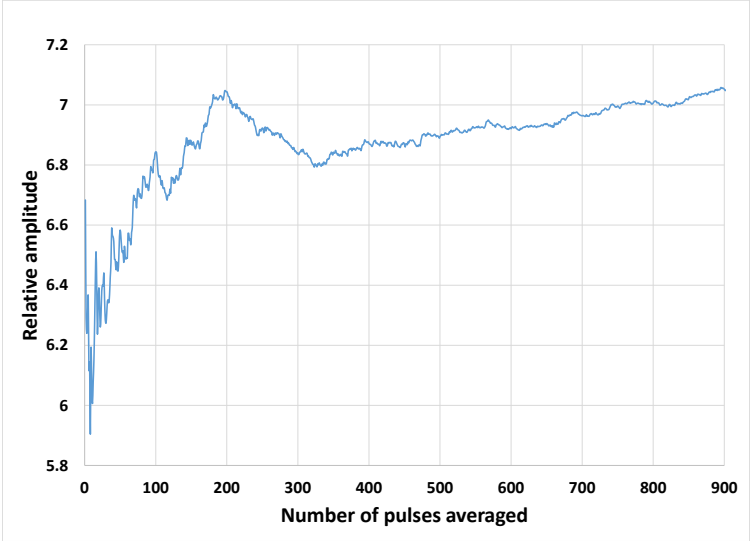

Figure 19. Evolution of the average with respect to number of pulses

In order to have a good separation between the interfering Raman/fluorescence from the ground and the return from the Raman of hydrocarbons, a much higher spatial resolution is required. Since most of the vapor stays close to the ground, having a 6 to 7 ns laser pulse length limits the separation between the ground and the Raman from hydrocarbons in the air. Fluorescence generated by the leading edge of the pulse will swamp the Raman very near the surface. In order to correct for this, a laser pulse length of less than 1 ns would be required, along with detection electronics that can resolve such rapid changes in signal. The hardware used in these tests can resolve such rapid signal changes: only the laser would need to be replaced. However, at the moment of testing, INO did not have such laser at hand.

In order to have a better estimate of the required laser power, a sum over the 3.4 m of linear space is done (the last four points before the rapid rise in signal caused by the ground). The result is shown in Figure 20 with respect to time after start of diesel injection at the base of the container. The rise by a factor of ~4 between the diesel pans and the pentane pans is in line with other measurements, in particular the PID measurements when the PID offset taken before start of diesel injection is factored in.

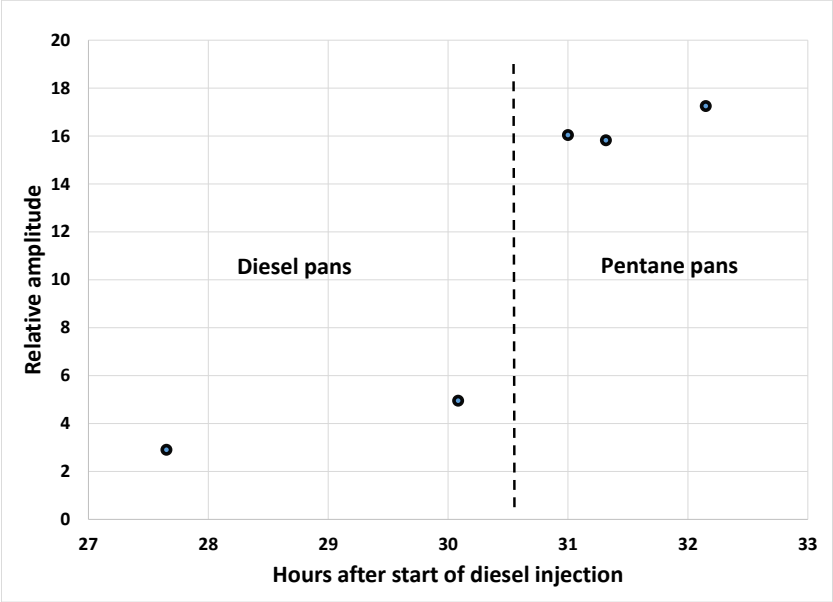

Figure 20. Integrated Raman signal with respect to time after start of diesel injection

The measurements with the current integrator were less convincing. The minimum current integrator gate is 50 to 60 ns at half maximum, which translates into 7 to 9 m of distance. When taking into account the rise time and the fall time of the gate and/or the laser pulse length, this extends roughly to 9 to 11 m. As for the approach with the transient digitizer, the gate must be timed to close significantly short of the ground in order for the Raman and the fluorescence from the ground to not interfere with the measurement. This entails that the return from the mirror is part of the measurement, along with some of the signal in the open air before the mirror. This generates a strong offset on which there is noise, especially from the mirror. Moreover, timing jitter cannot be corrected because the measurement approach eliminates all temporal information. Therefore some integrated measurements include part of the ground contribution. These must be processed out of the results, which is relatively simple, since these are measurements for which the ratios are large when compared to the average. But the slow closing of the integrator temporal window forces the elimination of a large portion of the alkane plume contribution next to the ground; which is the more concentrated section. As a consequence, the signal strongly depends on the concentration in the upper part of the tent, which is very variable and weak. For all these reasons, the results using this iteration will not clutter this report.

A more representative measurement with an integrator would require finding a current integrator with very fast gate opening and closing and with much smaller gate times. An alternative would be to use a micro-channel plate photomultiplier that can be gated to nanoseconds or less so that the gate time and rise and fall times would be driven by the photomultiplier. This is an expensive alternative, but some sort of gated photomultiplier would be welcomed for a more robust

operation with strong ambient light, as ambient light often forces operation at less than optimal signal-to-noise ratios.

In conclusion, *the use of Raman returns must be revisited because of the tendency of alkanes to stay close to the ground and the observation that the concentrations are lower than expected for a 0.1 L/min underground leak. If Raman is to have any success, it will be through the use of short pulse lasers (1 ns or less), high bandwidth electronics, transient digitizers and gated photomultipliers*, along with high pulse energy, high power lasers. This makes for a more expensive system.

IR Absorption LiDAR Measurements

The measurements procedure used with the leak simulator is very similar to that used for the outdoors measurements in the windowless gas cell. The IR LiDAR platform is installed in the mobile laboratory. The laser is directed towards a first routing/folding mirror as described in a previous section and then towards a folding mirror on a gantry crane just above the tent and the leak simulator container. The total distance is 40.5 m. The laser beam hits a sandblasted aluminum panel. This was done in order to better compare with previous measurements. The return could have been that of the sand, but this was not done in the iteration of the tests. The light returned from the ground is routed backwards through the same optical path, collected with the receiver telescope and routed/focused to/onto a MCT detector. The output from the detector is amplified and digitized with a high sampling rate digitizer. A series of pulse returns are measured and stored for post-processing.

Telecom grade tunable lasers are used as seeds to the optical parametric generator (OPG). The seed wavelengths are 1533.4 and 1524.6 nm. They are modulated on and off so that each consecutive pump laser pulse sees a different wavelength. Measurements were done with the IR LiDAR platform using the wavelengths 3476 and 3522 nm. The wavelengths are switched at every pulse. The laser linewidths are large, between 7 and 10 nm, with large pedestals.

An output pulse energy reference is generated by splitting part of the output beam at the platform and routing it to the same detector as that for the return. For each pulse, a ratio is made of the return from the ground over the reference pulse. Each of the pulse signals are in fact the area under the return/reference pulses. An average is made over a number of pulses. The system works at 5 kHz pump pulse frequency, and thus is 2.5 kHz per wavelength. A measurement average over 250 ms per wavelength gives a very good signal-to-noise ratio. A single differential absorption measurement could be done within 400 µs or less, the operating frequency being variable up to 100 kHz. The pulse energy is ~15 µJ on average.

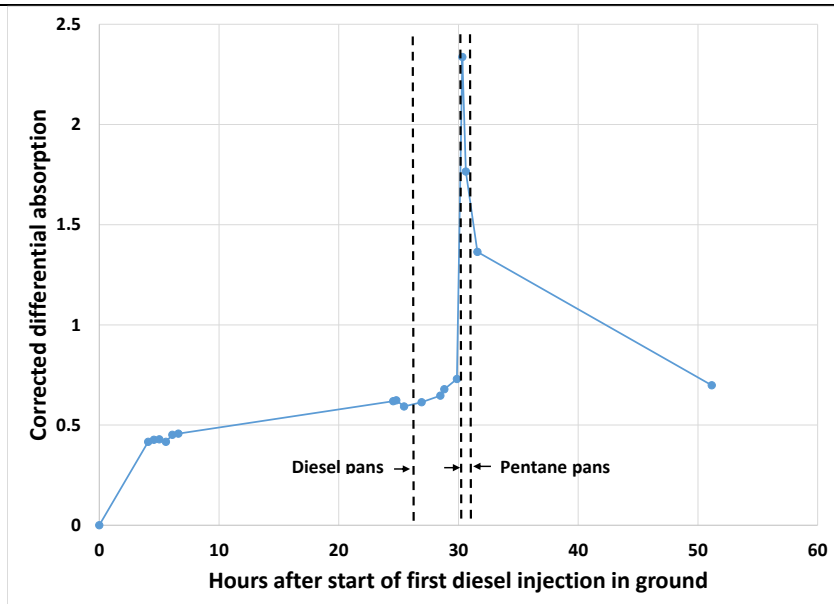

Figure 21. Differential absorption measurements for alkanes in leak simulator

Figure 21 shows the differential absorption measurements done on the leak simulator. The differential absorption is the natural logarithm of the ratio of the transmission at 3476 nm to that at 3522 nm. The differential is corrected for no alkane in the air by using a measurement done horizontally in the INO parking lot, using the same hard target at substantially the same distance. This measurement was done months before the leak simulator measurements, but was inserted at time "0". Nonetheless, it is a good approximate "zero". The goal is not to quantify the alkanes, but to detect a leak. For the measurements presented here, it is not the real zero. The polyethylene tarp used to enclose the vapor plume likely generates a substantial amount of alkanes or equivalent. This was also seen with the FID/PID measurements. The real zero would likely be the measurement inside the polyethylene tent, but before start of diesel injection. These measurements were done but are not on the graph. They are very similar to the first presented measurement points around 4 hours after diesel injection starts. This would then be the zero in the tent.

A constant rising slope is seen in the graph after start of injection. Injection was stopped at the end of the first day (4.9 hours after start of injection), and was restarted, along with extraction, for a few hours at the beginning of the next day (1 hour and 52 minutes). A total of 115 liters of diesel was in the leak simulator container. The amount of alkanes rose during the night. The drop before the placement of the diesel pans is probably due to opening of the polyethylene tent, start of vapor control systems or a mix of those. Once the pans are in the tent, the alkanes continue to rise, although it is not clear it is solely because of the pans. It is assumed that the vapor distribution and concentration above the leak simulator container and inside the tent tends towards a constant that is equivalent to that which would be obtained by using diesel pans

instead of injection into the sand. A continuous slow flow would probably be required to simulate an active leak. It is also clear that it takes a long time to establish some sort of equilibrium.

A constant and clear rise in signal is observed with alkane while concentration goes from very low concentrations to very high concentrations, as seen after the filling of the pans with pentane. The absorption cross-sections will vary when going from diesel vapor to pentane vapor, so that comparing the numbers in terms of concentration is slightly misleading. Also, the large laser linewidths come with interference from water vapor in the air. This effect was deemed not significant in the measurement presented here. Diesel seems to be a good simulant for determining sensitivities.

The wavelengths chosen are not at the maximum of the absorption spectrum of alkanes. Better sensitivity can be obtained by using other wavelengths, both in terms of absolute absorption difference and in reduction in interference from the varying ground spectral reflectivity. This is discussed in the next section.

In conclusion, *differential absorption is easily measured in the IR when the ground reflectivity does not change. This would be the best approach, if it were not for the varying ground spectral reflectivities*. This problem is further discussed in the next section.

Revisit of IR LiDAR Approaches

In light of the results obtained with the leak simulator and with the vapor plumes generated by the pans in the leak simulator, it was decided to revisit the conclusions of previous phases on the use of IR absorption. Recall that the major obstacle to the use of IR absorption was the large variations in ground spectral reflectivity (variation with respect to wavelength) for different soil types. At the time, only pairs of wavelengths were considered for the measurement procedure. In addition, there was no attempt at quantifying, statistically, the probability of having a false alarm for a given sensitivity.

Because of the slowly varying spectral absorption profile of alkanes, IR absorption of alkanes will never be as selective as IR absorption of methane or UV absorption of benzene for example. In real life situations, there will be strong spatial and spectral variations in ground reflectivity and absorption. The measurement of alkanes in the IR by integrated path absorption with reflection from the ground will always be limited by these last effects. Our goal in this revisit of IR absorption of alkanes is to mitigate the effects of the ground on the measurement. This was done in two ways:

1) Use the spectral databases of ground reflectivities and an estimated alkane absorption profile to select wavelength pairs that will minimize false alarms for a given sensitivity (a

given concentration-length product). An algorithm was developed and programmed to select the wavelength pairs. Parameters used in the algorithm will be discussed.

2) Investigate the use of more than two wavelengths, using the statistical algorithm, for enhancing sensitivity.

The idea behind the procedure is to systematically analyze the impact, in the context of a leak detection system for hazardous liquid pipelines, of spectrally non-uniform ground reflectance. The reflectance spectra are those of the ASTER SPECTRAL LIBRARY Ver. 2.0. The spectral library is a collection of spectra of natural and manmade materials (ref. http://speclib.jpl.nasa.gov/). The library contains 2445 spectral files out of which 1523 cover the IR range of interest, which is from 3.3-3.6 µm where alkanes have significant absorption levels, combined with relatively good atmospheric transmission and compatible with INO's SWIR/MWIR LiDAR technology. In this first attempt, the alkane absorption profile is represented by the pentane profile, for simplicity.

The algorithm works in two steps. It first searches for wavelength pairs that need to simultaneously satisfy the following conditions:

1. Atmospheric transmission > 95% (100 m of US standard atmosphere, 3.5 pm granularity, that is a spectral point at every 3.5 pm over 300 nm) as obtained from SpectralCalc website.
2. Pentane (C_5H_5) cross-section difference > 10% of its maximum value within that spectral range (i.e. > 50 000 cm^2/mol).
3. Minimum wavelength separation > 1 nm.
4. Maximum wavelength separation < 10 nm.

This first step gives tens of thousands of wavelength pairs, mostly due to the fine 3.5 pm granularity, most of the pairs being practically the same. Criteria #1 is necessary because of the multiple water absorption lines and methane absorption lines in the specified spectral range. The 100 m length of atmosphere is for a 50 m flight height, the laser beam having to go to the ground and back. The minimum and maximum wavelength separation are numbers that seem reasonable for a LiDAR system such as the one developed by INO. These criteria will be modified later on.

The second step is to explore the variability of the ground's spectral reflectivity. Using the spectral library, and for each wavelength pair determined in step 1, the standard deviation of the difference in ground reflectivity at the wavelengths of the wavelength pair is computed for every ground in the library. For each wavelength pair, there are thus 1523 differences in ground reflectivity, and the standard deviation of these differences is the parameter of interest. Moreover, for each wavelength pair, the difference in absorption cross-section is computed. The

goal is then to refine the selection process. Two new criteria are imposed on the wavelength pairs of step 1:

5. The standard deviation in ground reflectivity differences must be <20% of the maximum standard deviation value for all the wavelength pairs of step 1.
6. The pentane (C_5H_5) cross-section difference must be > 70% of maximum difference value found in the wavelength pairs of step 1.

This gives a few hundred wavelength pairs, but it is because of the granularity: this is really just one wavelength pair. The granularity helps in evaluating the accuracy with which the wavelengths must be generated. The wavelength pair would be 3372.3 ± 0.3 nm and 3379.5 ±0.2 nm.

This process maximizes the likelihood of choosing wavelengths for which the ground reflectivity will have a minimal impact. It does not give an estimate of false alarm rate with respect to alkane vapor detection sensitivity. Every ground in the library has the same weight in our model; in reality, this will not be the case. Weights will also vary with weather conditions (wet or dry ground, green grass or snow, etc.). Hardware wise, the hypothesis is that the laser in single-mode spectrally (the laser's spectral linewidth is at most a few pm). This reduces the chances of interference by water, methane or other molecules in the air. But this is not what is available at this point with the INO IR LiDAR. The 1064 nm is presently multimode and would need to be changed. This is technically feasible, but not in the scope of our work. At present, the linewidth is a huge 7 000 to 10 000 pm (7 to 10 nm).

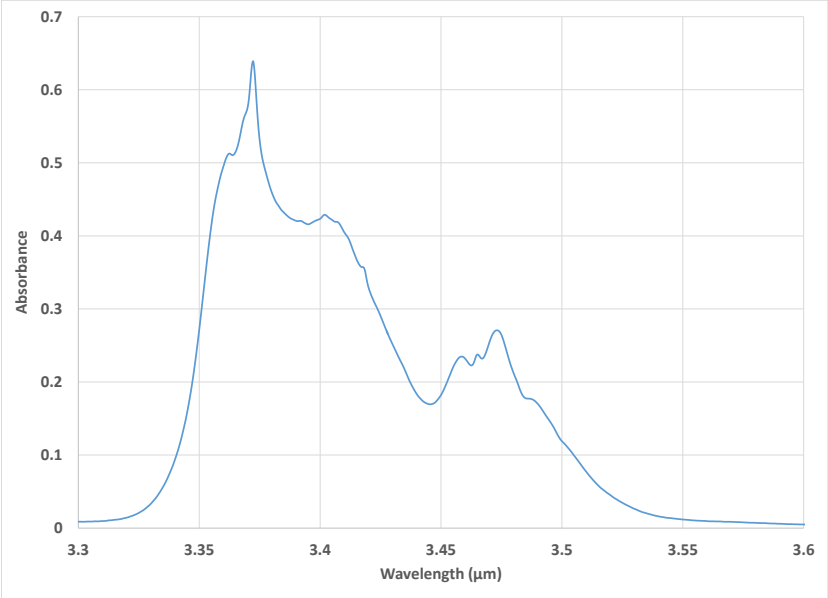

Figure 22. Absorbance of a 10 cm cell of pentane at 7320 ppm with a FTIR spectrometer. 1 cm^{-1} optical resolution.

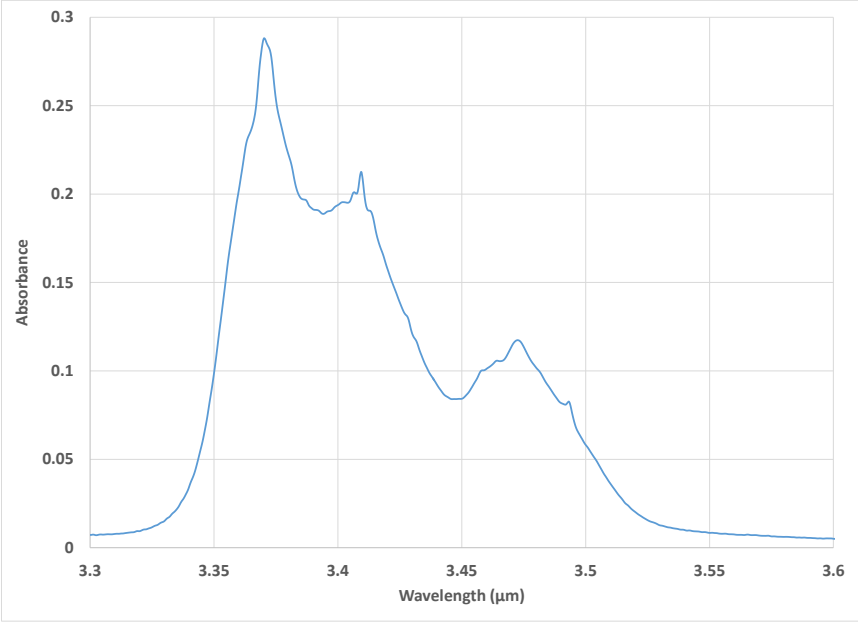

Figure 23. Absorbance of 10 cm cell of a sample of crude with a FTIR spectrometer. 1 cm^{-1} optical resolution

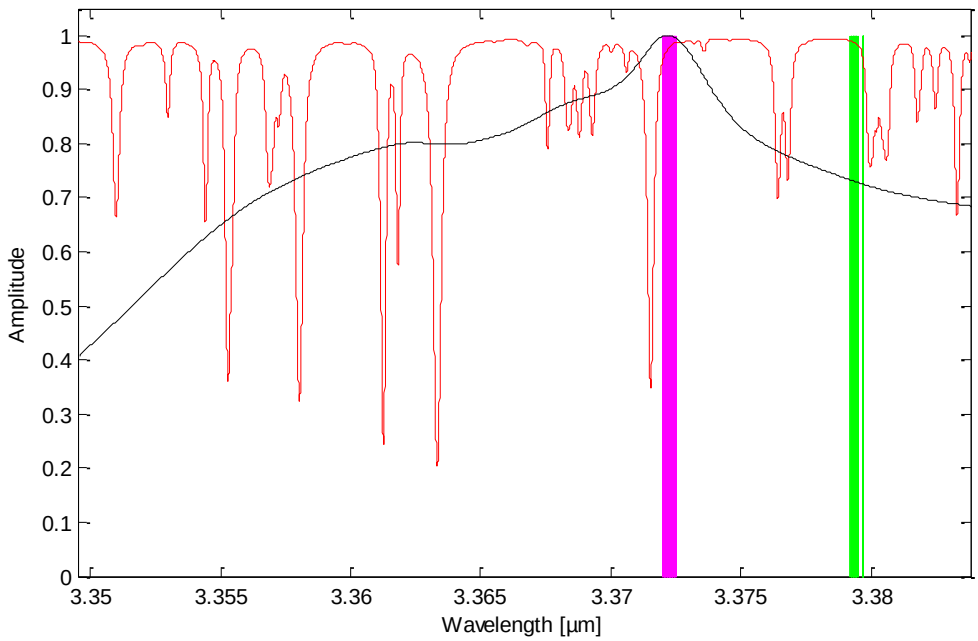

Figure 24. Superposition of atmospheric transmission (red), pentane normalized cross-section (black) and wavelength pairs (magenta and green vertical lines) satisfying conditions #1 to #6

In a second approach to modeling of the effect of the ground's spectral reflectivity variations on false alarms or on system sensitivity, the selection criteria were modified. It was determined that a LiDAR system with a simple laser system comprising a single PPLN to generate the required laser light could generate laser radiation up to 50 nm apart with two seed lasers. This does not render the system more complex. It is again a search for two wavelengths: the minimum number of wavelengths for absorption measurements. The granularity of the search was also modified to reduce the number of possible wavelength pairs. It was set at 122 pm. The first step is then:

1. Atmospheric transmission > 95% (100 m of US standard atmosphere) as obtained from down sampling the same SpectralCalc file as in the first approach.
2. Minimum wavelength separation > 1 nm.
3. Maximum wavelength separation < 50 nm.

There was no requirement on the minimum in pentane cross section difference. For every wavelength pair, the pentane cross section difference is computed. For each wavelength pair, the minimum and maximum in the logarithm of the reflectance ratio over the difference in cross section are searched within the spectral ground reflectivity library. Finally, using the sum of concentration–length products associated with the logarithm of the reflectance ratios for the maximum and minimum, a worst case concentration-length product is evaluated. *The results are*

481 ppm-m using the wavelength pair 3.3452 and 3.3565 µm. Again, there is some flexibility in the wavelength selection of a fraction of a nanometer (0.001 µm).

This second approach indicates that when an integrated amount of alkanes of more than 480 ppm-m is measured using the indicated wavelengths, there surely are alkanes on the ground, even though the exact amount is difficult to estimate. This still limits the sensitivity of the approach, but renders it comparable to the Raman and fluorescence approaches; it even surpasses them.

The third approach is very different; it does not rely on the return from only two wavelengths. It is DiAL at multiple wavelengths, more akin to DOAS. In fact, the signal processing is that of DOAS. The idea is to select a number of wavelength and build an artificial spectral response. The selected wavelengths must not be interfered with by water or methane in air. The wavelengths are chosen so as to construct a spectral response that has distinctive features. The zones with strong spectral changes are targeted.

The major problem with this approach is that the absorption spectrum of alkanes (exemplified by the spectrum of the crude oil, Figure 23) covers approximately 250 nm. In order to generate pulses of light rapidly across such a large spectral width requires a special laser system. The INO IR LiDAR system can generate the wavelengths, but not at the required speed: the CONOPS requires measurements within 300 ms. All the wavelengths must be generated within this timeframe. In order to do so, the laser system would need a number of parallel lines or a single line with a large optical parametric amplification bandwidth. It is technically feasible, but again not within the scope of this work. The hypothesis is made that such a laser system is commercially viable.

Remembering that different liquid petroleum products will have different proportions of alkanes and that the absorption spectrum will vary with these proportions, a good set of wavelengths would be as shown in Table **7**.

Table 7. List of wavelengths to be used in a multi-wavelength LiDAR scheme and their cross-section normalized to the pentane maximum cross-section

Wavelength (nm)	Approximate normalized absorption cross-section
3350	0.427
3358	0.750
3365	0.807
3371	0.945
3378	0.755
3414	0.591

3442	0.277
3473	0.424
3520	0.072

The selected wavelengths cover 123 nm. It might be possible to select only a subset of these wavelengths, but this will be analyzed at a later time. The spectra in the library of spectral reflectivities of grounds is used to rebuild, by extrapolation, a new library with points only at those selected wavelengths. These new spectra are used to compute equivalent absorption cross section times distance spectra, by normalizing the relative variations to 1 and making the logarithm (base e) of the resulting points. The hypothesis is again made that there is a uniform cloud 5 m in height. The standard deviation between the points in the spectra built from the reflectivities is compared with the spectrum of alkanes at the selected wavelengths. The spectrum with the smallest standard deviation is used for input to the DOASIS software that computes a concentration using the spectrum of alkanes as the reference spectrum. This should be an effective metric for the robustness of the selected wavelengths and measurement approach relative to varying ground spectral reflectivities. *The result is: 465 ppm-m.*

This is well within what should be emitted by a 0.1 L/min leak. Both the two wavelength approach and the multi-wavelength approach give approximately the same result.

The conclusion is still that the measurement is limited by the varying ground spectral reflectivity with approx. 250 ppm-m of molecules above ground.

Vapor Diffusion Model

Work with the leak simulator gave INO an insight into the behavior of a leaked liquid petroleum product in the ground. In the previous phases, INO used a model taken from the literature. This model assimilated a leaked substance to a pan of liquid of a certain size. This did not take into account gravity, liquid wetting of the ground, absorption by the soil, leak spreading and other factors. The model of the pan was useful, but did not give any indication of real vapor plume geometry or concentration gradient.

The leak simulator allowed for validation, at least in part, of the crude initial model. The testing was limited. Vapor diffusion through the sand used as a soil simulator was slow. Liquid spreading on the bottom of the container was also slower than expected. The design of the leak simulator container was correct for testing in the time frame available. A larger container would have required waiting for multiples days and even up to a week for a 0.1 L/min leak to spread evenly on the bottom of the container. On the other hand, a small container necessarily restrains the leak spreading. There is a balance to find between amount of soil to treat afterwards and accuracy of simulation when using this approach.

The dynamics of a leak would also need to be considered. In many cases, the leak grows from no leak at all to a significant leak. The goal was to establish if it was possible to detect a 0.1 L/min leak, but such a leak usually does not happen instantly. The ground around an evolving leak will allow liquid and gas phase hydrocarbons to migrate outwards from the leak. The ground will absorb some of the hydrocarbons. This will all depend on the type of soil, on humidity, on temperature, etc. When the leak reaches 0.1 L/min, the ground usually has already absorbed some hydrocarbons and some vapor is diffusing into the ambient air.

No one leak simulation model will cover all the possible leak scenarios. Pipelines are covered with different types of soils, at differing depths, and in varying terrain slopes. Leak will occur in wet or dry soil, in hot or frozen soils, and on bare or vegetation covered soils. All these parameters will affect the remote detection of leaks by optical techniques through the vapor plume they produce. Not that the sensitivity of the detection techniques vary, but the vapor plume itself could vary significantly in extent, concentration and composition.

It is not possible to give sensitivity in terms of L/min leaked unless an expert system is developed to equate concentrations of alkanes or aromatics in a plume to leak size considering pipeline depth, terrain slope, soil type, soil humidity and temperature, along with corresponding gradients.

In light of this, would it not be preferable to "simulate" a leak using standardized settings? If so, what would be the standardized settings? Before trying to answer these questions, the results from the leak simulator, as built and monitored, should be revised.

A report from INRS is presented in the appendix, along with compositional analysis of a number of vapor samples taken during the testing week. A large number of FID/PID measurements were done all along the testing cycle. These will be used to analyze the transient behavior of the vapor in the soil and above ground.

- FID/PID measurements of ambient air set a baseline for the instrument → no correction necessary.
- Measurements of air inside the tent gave a significant value both in FID and PID before starting the leak → the tent generates FID/PID detectable molecules that set a new baseline.
- The baseline generated by the tent is stronger the first and second day than the signal from the vapors generated by the simulated leak, except very near the surface of the sand.
- There was no strong transient at the beginning of the leak.
- 24 hours after start of injection of 100 liters of diesel at the base of the container at a rate of 0.1 L/min (~5 hours), the vapors were still diffusing slowly into the air.
- Vapor concentration was much higher in the soil around the leak than in the air above.
- Horizontal vapor diffusion (likely with the liquid) was complete within 8 hours at the bottom of the container.

- Vertical diffusion, as measured with the PID, is still evolving after 200 hours.
- Vertical diffusion, as measured with the FID, drops after 70 hours, signaling a change in composition, probably a drop in the more volatile compounds.
- There is a strong concentration gradient between 15 to 18 cm under the surface and 3 cm above the surface.
- In the air above the container, the concentration rises continuously for the first 25 to 48 hours, and is constant within the PID measurement accuracy afterwards (up to 140 hours).
- The same change in composition is seen in the air as in the ground.
- There is always a higher concentration at 3 cm above ground. Above 1m, gradients seem to disappear after 48 hours.
- After the initial spike in PID readings when filling the pans with diesel, the steady state concentrations and gradients with the pans filled resemble those without the pans, but with the diesel in the bottom of the container.
- Compositional analysis shows that pentane evaporates more rapidly than most other compounds in diesel, which is to be expected.
- In an enclosed tent, and without replenishing the diesel pool, pentane rises from ~20% in the fresh air vapor (in a jerrican or in the soil) to ~67% in the air above the sand container.
- When not sealed inside the tent, pentane concentration falls with time.

From these observations, it would seem that given enough time, the concentrations and concentration gradients obtained in an enclosed tent will be the same, within experimental errors, for a pool of diesel underneath more than 1 m of sand and pans filled with diesel on the surface.

This points to the use of pans filled with liquid petroleum as good indicators of concentration and concentration gradients to be expected in the presence of real leaks.

Also, from these observations, it can be concluded that for a representative concentration and composition, *fresh liquid petroleum product must flow continuously, to replenish the more volatile compounds*.

And last, but not least, *there is a higher concentration close to the ground than from 1 m and above*.

Enclosing the vapor in a sealed tent also affects the simulation. It would have been preferable not to have a tent above the simulated leak. In the work presented here, the tent was necessary because the container was indoors and the vapors had to be contained and vented to the exterior for health and safety reasons. This was also done to minimize the environmental effects such as temperature changes and wind. A better scenario would be to put pans outside, as was done with the windowless gas cell of the previous phase, but to look down towards at a simulated soil surface. Methods to control temperature and wind would need to be devised.

The tests with the leak simulator and a static pool of liquid petroleum gave some interesting insight into the behavior of leaks in a sandy environment.

- The soil/sand over a leak acts as a cap to the vapors, at least in the initial stages of the leak.
- The vapor concentration is largest close to the leak, at least in the initial stages.
- The vapor concentration falls when the sampling is done away from the leak, towards the surface.
- There is a significant drop of vapor concentration at the surface.
- Diffusion in the ground is much slower than in the air.
- Ambient air acts as a powerful pump for the vapors (concentration gradient).
- The effective area from which vapor is emanating is small, corresponding to the "pores" in the ground.
- There is a compositional change, at least initially, between the vapor close to the underground leak and the vapor close to the surface of the ground.

The leak simulator was used to both study the transient behavior of a leak and the steady state of a pool of liquid petroleum (diesel) under ~ 5 feet of sand. The actual rate of migration of the liquid petroleum horizontally and vertically could not be ascertained. The fact that the simulated leak was at the bottom of the container did not allow for liquid to migrate downwards. This likely has an impact on the results of the transient behavior.

In conclusion, *pools of liquid petroleum in pans on a surface are good simulators of actual leaks as long as fresh liquid petroleum is pumped into the pools while the older liquid petroleum is pumped out. As gravity strongly affect vapor spatial distribution, with a larger concentration near the surface, representative simulations of an airborne leak detector must be performed vertically over the simulated leak. Techniques that measure very close to the ground are better than those that do not. The vapors must not be enclosed for a realistic scenario*.

3.6 Outdoor Set-Up

UV-DiAL Measurements

The measurements presented here were taken using a windowless gas cell with a hard target less than 1 m behind the exit from the cell. The hard target is made of the same sand as that used for the leak simulator. The measurement procedure is a lot like that for the IR LiDAR measurements. The output from the tunable UV laser is directed through the windowless gas cell, hits the hard target and generates a return that is collected by the receiver telescope collocated with the laser. The light collected by the receiver is optically filtered to isolate the return from the laser. A photomultiplier tube is used to detect the return light. There are unfortunately no measurements with the leak simulator in diesel injection mode. There are thus no numbers for

the amount of benzene in the windowless gas cell. The analysis will be done in light of the samples taken during the leak simulator run and that were later analyzed.

The return from the hard target at >40 m is strong enough to saturate the photomultiplier tube at close to maximum gain. To avoid saturation, the voltage used on the photomultiplier tube was set to - 425 V, which is fairly low for this type of detector. This indicates that using a silicon avalanche photodiode would be sufficient for this approach. The return has a high signal-to-noise ratio. Noise on the measurement will come from effects other than signal strength. Moreover, since the measurement is in the solar blind region, ambient light, is not an issue when well filtered. In the measurements presented here, the entirety of the return waveform is measured, using the high sampling rate digitizer. No return waveform is presented here. Suffice it to say that the spatial resolution is limited by the laser pulse duration of 6 ns. For each emitted wavelength, the area under the ground return peak is 1234211 with the emitted laser pulse energy as measured with a pyroelectric detector. A reference detector with a better signal-to-noise ratio, such as a silicon photodiode, would be preferred.

In this discussion of UV absorption measurements, it is not necessary to have a pulsed emitter and electronics to digitize a nanosecond long pulse. Any absorption technique that allows for the measurement of the absorption by benzene (or toluene, or both) in the allocated 300 ms that was determined in the CONOPS, from the return from the ground, would be acceptable. This opens up the technological possibilities.

Figure 25 shows a spectrum taken with the gasoline pan heated to 20 °C inside the windowless cell. The estimated benzene concentration-length product is between 125 and 150 ppm-m. This makes for a relative absorption, at maximum, of ~ 40% (for 250 to 300 ppm-m, since the laser and the return pass through the cell), which is significant. The features in the spectrum are limited by the laser linewidth of 0.017 nm. The sampling step, or the laser wavelength step, is 0.01 nm. It is probable that the absorption feature is narrower, spectrally, than the laser. This makes for a reduced level of absorption. On the other hand, in the two wavelength DiAL approach, the laser need not to be as stabilized as if the laser line was much smaller than the absorption line, in order to perform a measurement.

Three different measurements were taken, all fairly similar. Figure 25 is an average of the three measurements.

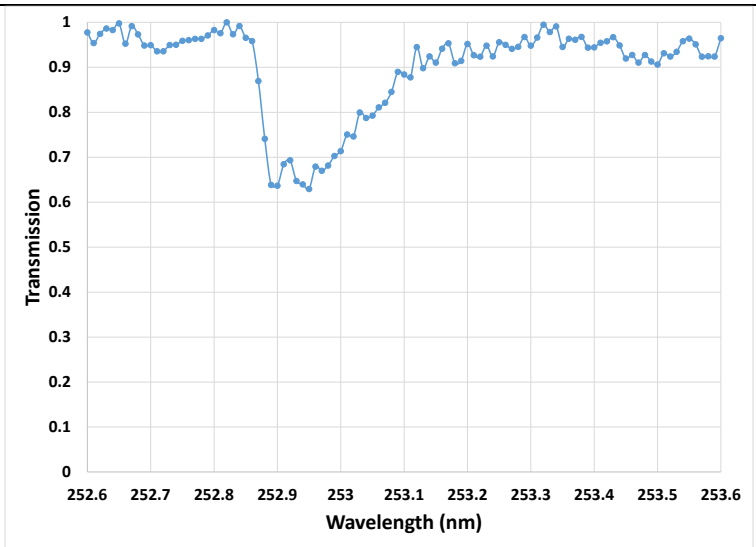

Figure 25. UV absorption spectrum of benzene above a heated gasoline pan.

In a UV-DiAL setup designed for leak detection, there would ideally be two laser lines, one for a wavelength at peak benzene absorption and one at a wavelength of little absorption. The difference between the two would indicate the likely presence of benzene and thus of a leak in the pipeline.

A better approach would probably be one of correlation spectroscopy, in which spectrally broader light is emitted and the detection is made with a high resolution spectrograph with a sensitive camera, or better, measuring through a gas cell containing benzene and comparing to the same measurement without going through a benzene gas cell. There are multiple UV sources that could be used for the purpose. Gas correlation spectroscopy detection (cameras) is routinely done for NO_2 and SO_2 [18]. This is potentially simpler than a two line laser system working in the deep UV region. It is thus conceivable with the set-up as is, because of the laser line being larger or equivalent to the absorption line, to perform a gas correlation measurement. It would then be sufficient to install, in one of two paths, a gas cell filled with benzene.

Figure 25 represents the measurement of a spectrum. This spectrum shows a relatively high level of measurement noise. This is caused by the measurement sequencing. At each wavelength, 50 pulse returns (5 seconds) are acquired and stored. The wavelength is then changed, which is not instantaneous, taking a bit less than 1s. The atmosphere between the LiDAR apparatus and the windowless cell most probably changes in that time. The laser beam experiences varying degrees of loss before being scattered by the ground and the return also experiences varying degrees of loss. The result is a noisy spectrum.

In the context of the CONOPS, a spectrum would not be measured with 0.01 nm wavelength steps. A restricted number of wavelengths would be chosen, two being the minimum. The two wavelengths would be emitted serially at a very high repetition rate, preferably in the kHz range. In that sense, our present UV-DiAL system is not optimal, having a very low 10 Hz repetition frequency. Conceivably, the two wavelengths would be 252.6 and 252.88 nm. The wavelength separation is only 0.28 nm, much too small for a significant change in ground reflectivity. Varying ground spectral reflectivities is not a problem here. Even if a greater number of wavelengths is chosen, 3 to 5 wavelengths for example, the total spread would not cover more than 1 nm. The measurement of benzene in the UV spectrum is much more selective than the measurement of alkanes in the IR spectrum.

There are no libraries of ground spectral reflectivities in the deep UV region because there has never been a need for such libraries. When it is stated that varying ground spectral reflectivities is not a problem, this is more or less an extrapolation of known solid surface behaviors. However, there will be varying ground reflectivities, even though it does not change within the spectral interval being scanned. This must be considered in the design of a leak detection system using the optical absorption of benzene (or toluene, or both) as the marker for a leak.

The problem is not with the apparatus: it is with the very small concentration of benzene measured over the ground in the leak simulator. After injecting diesel in the ground and waiting for 8 days after last injection, there were only 130 ppb of benzene just above ground. Benzene is one of the most volatile compounds of diesel. When testing with pans of gasoline, or measuring the vapor phase benzene from diesel in the ground or in a jerrican, the concentration is closer to 4 to 5 ppm. This is the value that should be expected when searching for an active leak. If we assume the 5 m height plume with an average of 5 ppm, the concentration-length product to detect would be 50 ppm-m. Since the vapors tend to stay closer to the ground, a smaller value is to be expected, closer to 30 ppm-m.

The measurements presented previously were for 250 to 300 ppm-m. A measurement was done with 10 ppm-m in a closed gas cell. The benzene signature was barely measurable, but it was perceptible. The measurement can be greatly enhanced by using detectors with higher resolution (photodiodes instead of pyroelectric detectors). However, this is not a measurement done from 50 m with a reflection from the ground: it is a measurement on a calibration/reference cell, inside the mobile laboratory. In order to measure a leak with any kind of certainty would require measuring an absorption of less than 1% from a reflection from the ground at 50 m. This is feasible, even though it was not shown to be possible with the INO platform in its current state. 10 ppm-m corresponds to approximately 2% absorption. 30 ppm-m would represent 6 to 7% absorption at 0.017 nm measurement resolution.

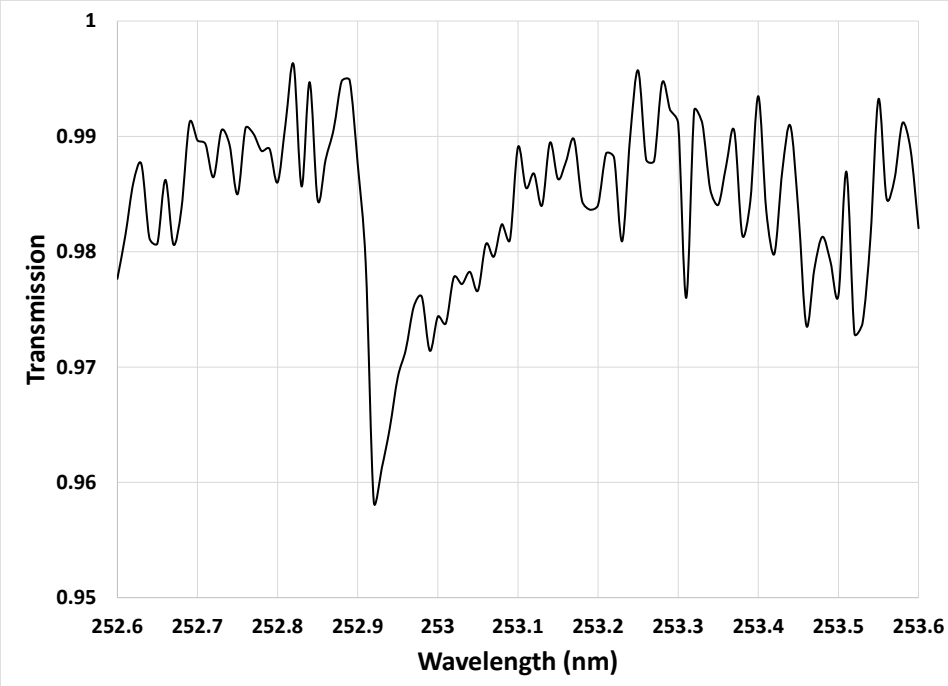

Figure 26. UV absorption spectrum of benzene in a 10 ppm-m reference gas cell.

In the air samples that were taken inside the leak simulator, toluene was in greater amount than benzene: the concentration varied from 7 to 15 ppm. On the other hand, the absorption cross-section is smaller. It is not clear that toluene would be a better candidate, but it is an alternate molecule to look for in the UV. It could also be imagined that the LiDAR be designed to detect both molecules in the UV.

In report 3, the UV-DiAL sensitivity for benzene at 247 nm was estimated at 0.15 ppm-m. This was for an absorption of 0.0006 and in the absence of atmospheric and detector noise, and not 0.01 at 253 nm as used here in an outdoors test. This being said, the results agree within a factor of 2 with the conclusions of report 3. *Our revised sensitivity*, for an hardware as described in report 3, and in the presence of atmospheric, ground reflectivity and detector noise, would be *3 to 5 ppm-m*.

In conclusion, *absorption of benzene in the UV is more selective than absorption of alkanes in the IR, but the very small concentrations in the presence of a leak renders the leak detection more challenging. It has not been proven that it is a better approach*.

3.7 Conclusion

Based on the work done in the previous phases of this project, and especially in light of the concordance between modeling and testing for Raman UV-DiAL and IR absorption, it is clear that optical remote sensing techniques are feasible approaches for the detection of leaks in liquid

petroleum pipelines. Using the molecular parameters determined in the preliminary testing, and introducing these numbers into the modeling with realistic platform and noise parameters, limits of detection were determined for the platforms as they stand and for enhanced platforms. This was verified in an outdoors experiment with a windowless gas cell as discussed in report 4.

The results from Report 1 led us to pentane and benzene for the testing phase. Based on a very simplified hydrocarbon diffusion model, it was determined in the same report that the average concentration of pentane vapor in the vicinity of a small liquid pipeline leak of 0.1 L/min – from 1 m to 6 m high – would lie in the range of 300 ppm. This concentration was deemed to be representative of a real weeper/seeper leak and the defined CONOPS was then considered for LOD computations.

For UV Raman, both alkanes and aromatics can be detected. In the case of Raman spectroscopy, the contribution to the signal of nearly all hydrocarbons of a complex crude mixture are detected at the same time, in the same spectral region, thereby increasing the sensitivity of the technique. The absence of interference in the spectrum and the presence of Raman active bands around 3000 cm^{-1} (C-H bonds) for all hydrocarbons are responsible for this. Preliminary testing with the INO breadboard on pentane and crude indicate that the report 1 modeling, and thus the Raman cross-sections used, was correct within an order of magnitude at 355 nm (probably within a factor of ~2).

Within the tasks summarized in report 4, INO modified the Raman platform to have better sensitivity along with a simplified platform. The modifications were tested in indoors and outdoors settings. A windowless gas cell was designed and manufactured for the outdoors tests. These tests indicated that further modifications were required to the platform, the major changes being a gated PMT gain, a smaller laser footprint along with a smaller diameter core collection fiber and reduced optical detection bandwidth.

The modifications that have been completed before the last testing phase are a simplified optical filtering unit with 10 nm bandwidth, photomultiplier tubes as detectors, a current integrator or a transient digitizer for the detection electronics and a reduced diameter core collection fiber. The remaining proposed modifications requiring either a more powerful excitation laser or more time (delivery of components).

Work done in this last phase showed a major concern as to the validity of the vapor plume model used in the previous phases. The outdoors tests performed in the previous phase were done by going through a 2 m long windowless gas cell horizontally, which made for a uniform 2 m of interaction. Moreover, there was no solid target immediately at the exit to the cell. The leak simulator built in this phase allowed for measurements from above towards the ground, as it would be if the sensor was on an airborne platform. Measurements with the different optical

sensor modalities and with an FID/PID showed that there were **strong vertical concentration gradients with the highest concentration very close to the ground**. Our use of a tent to enclose the vapor plume probably reduced the gradients with respect to what it would be without the tent, in open air, with drafts and wind. Moreover, in the case of the sand used in these tests at least, simulating a leak directly in the sand, and waiting a very long period for the leak effects to stabilize, generates vapor concentrations of the same order as pans filled with liquid petroleum placed on the sand surface. Finally, replenishing the liquid petroleum is important for a more realistic leak simulation.

It is thus recommended that for future leak simulations, pans of liquid petroleum be used instead of leak in soils, placed on the surface of the ground, and with a slow replenishing flow equal to the leak rate. These pans should be placed in a non-enclosed surroundings to allow strong horizontal diffusion of the vapor. Measurements need to be performed after a steady state has been established. More reflection needs to be put into the best approach/geometry (size, number of pans, etc.).

Although this has no effect on the estimates of limits of detection in terms of number of molecules, it does have an impact on the estimate of the number of molecules with which an excitation laser beam will interact. **It has an impact on the minimum detectable leak size**. It also has an impact on the eventual design of an optimized measurement hardware.

For leak detection from an airborne platform using optical techniques, the leak needs to have persisted for some period of time: a leak cannot be detected instantaneously. The vapor plume that starts in the ground, close to the liquid petroleum product, needs to migrate towards the surface. This can take quite a while, on the order of multiple days. In addition, and even though most of the techniques described here try to detect all alkanes, lighter components will evaporate more rapidly and diffuse into the atmosphere more readily, depleting the vapor plume over the leak of the more volatile fraction when the leak is very small. The leak must have created a large enough pool for the vapor plume to be detected.

The measurements of soil vapor concentrations and compositions presented in this report tend to indicate that leak detection in the ground would be much more efficient than from the air. This was discussed in part in the first report, but not in the context of actual performed concentration measurements. What was presented in the first report is that underground leak detection is costly, both to install and to maintain, on a per mile basis. But it is clear that it would be much more efficient.

As for the testing of the Raman platform for leak detection, it can be concluded that, again, the sensitivity is as modeled. The problem is that a large number of the molecules to be detected are very close to the ground. Raman and FID/PID control measurements done in this phase, in the

tent over the leak simulator container, showed that there was a strong vertical gradient in concentration. The hardware, as built, could not resolve the portion just above ground where the concentration is maximum. Both with the current integrator and the transient digitizer, spatial resolution was insufficient. It is recommended to go with the transient digitizer and a laser with a shorter pulse length (<1 ns) unless a fast gateable MCP-PMT is used with the current integrator. Both these avenues raise the cost of the hardware. In addition, and as stated in the previous reports, a high pulse energy, high power (10 W) laser is needed. But even with the platform as is, with the transient digitizer, and without the contribution of the molecules closest to the ground, *Raman could eventually detect better than concentration length products between 100 and 500 ppm-m* as measured with the PID and FID if measurement time was not an issue.

In light of the additional cost of the proposed hardware, and of the weak concentration encountered over the simulated leak, INO suggests to abandon the Raman technique for remote leak detection from an airborne platform.

INO performed IR LiDAR measurements in addition to Raman measurements with the leak simulator. The IR LiDAR does path integrated measurements, unlike the Raman approach, which is spatially resolved. The infrared wavelengths used for the tests on the leak simulator were the same as those used with the windowless gas cell of the previous phases of the project. A sandblasted aluminum target was used, not the sand surface. This should not change the conclusions: this was done to have measurements completed with similar parameters as the windowless gas cell measurements. A major advantage of IR absorption measurements is that the laser beam travels all the way to the surface and back, going through the entire plume twice.

As expected, the IR measurements are very sensitive, having the best limit of detection for a reasonably sized hardware. The infrared measurements were the more precise and the less noisy of the measurements, including FID/PID measurements. It measures the molecules that are in the largest quantity, the molecules containing an alkane portion. It shows the constant rise of the alkanes' height integrated concentration. It even becomes non-linear because of too strong of an absorption signal in the case of the pentane. It was not even used in the case of the gasoline pans.

The problem with the IR LiDAR remains. It is the variation of the ground spectral reflectivity within the same spectral range as for the measurement of the alkanes. INO attacked this problem by searching for the wavelengths and procedures that would minimize the impact of the ground reflectivity using a spectral library of ground spectral reflectivities. INO tried both with wavelength pairs in a classic two wavelength DiAL approach, and a multi-wavelength (9 wavelengths) pulsed DOAS approach. Both approaches came up with the same conclusion: *it is not possible to ascertain that the measured signal is due to absorption by hydrocarbons when the concentration obtained is below 465 ppm-m. When the measurement gives more than ~ 500 ppm-m (250 ppm-m of actual molecules), it is indicative of the very probable presence of alkanes*.

In light of this, IR LiDAR should be revisited as a viable approach to leak detection as long as one is looking for a leak generating a vapor concentration higher than 250 ppm-m.

The last modality to be tried was UV-DiAL. It was proposed in the previous phases without being truly tested. In this approach, only benzene is detected, and benzene has a more selective signature than alkanes, which practically eliminates the problem of varying ground spectral reflectivities. However, benzene is in much smaller concentration than the whole of the alkanes. UV-DiAL was not tested with the leak simulator, but with the windowless gas cell. The INO platform for UV-DiAL is not optimized for the leak detection application. Wavelength switching is very slow, and needs to be very fast. Nevertheless, an estimate of limit of detection of 3 to 5 ppm-m was found, giving a more realistic number than the one calculated in a previous report. *This amounts to 1.5 to 2.5 ppm-m of benzene molecules*, as in this modality the laser also travels to ground and back to the receiver, giving an integrated path measurement. Benzene represents 1.71 % of vapor molecules, whereas hydrocarbons containing at least an alkanes portion represent 94.75 % in the vapor sampled 8 days after injection in the bottom of the sand container. In fresh vapor (as in a diesel jerrican), benzene is 2.85 %, whereas hydrocarbons containing alkane are 82%. In alkanes equivalent, this would give a limit of detection between 40 and 140 ppm-m. Toluene would also be a candidate for UV-DiAL detection. There is more toluene than benzene in air samples from diesel fuel, but the absorption cross-section is slightly smaller. The net gain is not clear.

In light of this, UV-DiAL of benzene would be the most sensitive approach, even though the effective LODs of the different techniques are all in the same range (if we consider the performance limitations related to type of soils and background for IR-DiAL).

Because of the work done in this phase, the assumption that using Raman scattering would have the best sensitivity has to be revisited. Raman still has the advantage of being scalable with laser power. Absorption, be it IR or UV, does not have that advantage. But this is only an advantage on paper since using very high power UV lasers would be an issue. Limit of detection is not the only parameter to take into account, although one of the most important. The three techniques are very close when looking at vapor plume detection, be it through alkanes or aromatics or both. Other requirements such as cost, mass, size, power, false alarms, ease of use need to be considered.

Moreover, the right technique might differ from pipeline to pipeline, depending on vapor migration through the ground, soil temperature (in particular frozen ground), soil cover (in particular snow) and other similar restrictions. None of this is considered in the feasibility presented here. Clearly, leak detection through a generated vapor plume will work best in warm climates.

As in many instances, only field trials will determine the most adequate approach. Follow on work could focus on looking at better ways of detecting through absorption in the UV. There could be ways to simplify the approach by not using costly stabilized laser systems. INO is looking into promising alternatives and would appreciate the opportunity to participate in field trials, on simulated leaks or real pipelines.

Finally, in the course of this project, we determined that there is not much vapor over an underground leak spot and that there is a strong concentration gradient over the soil surface; the most concentrated fraction being in the first centimeters over the surface. To ensure a maximum sensitivity, the chosen technique should be able to collect signal coming from every centimeter along the probing path. This gives serious advantage to absorption techniques. Raman and fluorescence are therefore abandoned. Although UV-DiAL seems very interesting at this point, the technique has not been studied in details within this project. Having better idea of the vapors behavior over a leak, it would be interesting to complete a new pros and cons exercise considering only the two absorption techniques.

Considering these conclusions, INO's recommendations for further studies would be concentrated around simulated tests and studies of absorption measurements only. For IR absorption, the uncertainty lies in the encountered soils reflectivity variations. Validation of INO's theoretical evaluation is therefore proposed as a future development. Experimental measurements of ground reflectivity over a pipeline right-of-way are proposed. For UV absorption technique, more tests are proposed. Data analysis algorithms need to be refined and independence of the approach to soil variation is also to be demonstrated. At this point, measurements done over a given number of soil types may be sufficient. UV source alternatives also need to be evaluated in order to reduce size, cost and complexity of the actual laser source.

Suggested tasks for a follow-on work on optically remote leak detection would be:

- To investigate about the UV light source alternatives for DiAL applications
- To perform more tests using the UV-DiAL approach in realistic conditions
- To refine the analytical approach and algorithm
- To make measurements of the ground reflectivity in the IR along a typical right-of-way
- To complete a new pros and cons of the approaches using information gathered during this last test campaign
- Based on the pros and cons results, to adapt the selected platform for further testing
- To perform tests on simulated or real leak

4.0 References

1. Elliott, R.W. and H. Watts, *Diffusion of some Hydrocarbons in Air: a Regularity in the Diffusion Coefficients of a Homologous Series.* Canadian Journal of Chemistry, 1972. 50(31): p. 31-34.

2. Fingas, M.F., *Studies on the evaporation of crude oil and petroleum products II Boundary layer regulation.* Journal of Harardous Materials, 1998. 57: p. 41-58.

3. Fingas, M.F., *Studies on the evaporation of crude oil and petroleum products I the relationship between evaporation rate and time.* Journal of Hazardous Materials, 1997. 56: p. 227-236.

4. Thorley, F.C., et al., *Dependence of the Raman spectra of drug substances upon laser excitation wavelength.* Journal of Raman Spectroscopy, 2006. 37(1-3): p. 335-341.

5. DePersia, A.T., et al. *Phenomenology considerations for hyperspectral mine detection*. in *Proc. of SPIE 2496, Detection Technologies for Mines and Minelike Targets, 159*. 1995.

6. Lesaignoux, A., et al. *Influence of Surface Soil Moisture On Spectral Reflectance of Bare Soil in the 0.4 – 15 µM Domain* in *6th EARSeL Imaging Spectroscopy SIG Workshop*. 2009. Tel Aviv, Israel.

7. Mével, R., P.A. Boettcher, and J.E. Shepherd, *Absorption cross section at 3.39 µm of alkanes, aromatics and substituted hydrocarbons.* Chemical Physics Letters, 2012. 531(0): p. 22-27.

8. Bertie, J.E. and C.D. Keefe, *Comparison of infrared absorption intensities of benzene in the liquid and gas phases.* The Journal of Chemical Physics, 1994. 101(6): p. 4610-4616.

9. Mével, R., P.A. Boettcher, and J.E. Shepherd, *Erratum: Absorption cross section at 3.39 µm of alkanes, aromatics and substituted hydrocarbons (Chemical Physics Letters (2012) 22 (531)).* Chemical Physics Letters, 2012. 539-540: p. 253.

10. Pyun, S.H., *Mid-IR Laser Absorption Diagnostics for Hydrocarbon Fuel Vapor Sensing and Decomposition Species Measurements*, in *Departement of Mechanical Engineering* 2012, Stanford University. p. 116.

11. Klingbeil, A.E., *Mid-IR Laser Absorption Diagnostics for Hydrocarbon Vapor Sensing in Harsh Environments*, in *Departement of Mechanical Engineering*. 2007, Stanford University. p. 209.

12. Skinner, J.G. and W.G. Nilsen, *Absolute Raman Scattering Cross-Section Measurement of the 992 cm^{-1} Line of Benzene.* Journal of the Optical Society of America, 1968. 58(1): p. 113-118.

13. Ekoto, I.W. and R.S. Barlow, *Development of a Raman Spectroscopy Technique to Detect Alternate Transportation Fuel Hydrocarbon Intermediates in Complex Combustion Environments*. 2012: Albuquerque, New Mexico 87185 and Livermore, California 94550 p. 67.

14. Harmon, P.A. and S.A. Asher, *Environmental dependence of preresonance Raman cross-section dispersions: Benzene vapor-phase excitation profiles*. The Journal of Chemical Physics, 1990. 93(5): p. 3094-3100.

15. Stephenson, D.A. *Raman Spectroscopy of Some Hydrocarbons and Freons in the Gas Phase*. in *Laser raman gas diagnostics, proceedings workshop*. 1974.

16. Willitsford, A., et al., *Resonance enhanced Raman scatter in liquid benzene at vapor-phase absorption peaks*. Optics Express, 2013. 21(22): p. 26150-26161.

17. Lambert-Girard, S., et al. *Proposal for a standoff bio-agent detection SWIR/MWIR differential scattering lidar*. in *SPIE Defense, Security, and Sensing* 2012. Orlando.

18. Kabashnikov, V.P. and N.S. Metel'skaya, *A Passive Method of Nondispersion Correlation Spectroscopy for Remote Monitoring of the Content of CO, SO2, and NO2 in the Atmosphere*. Journal of Applied Spectroscopy, 2005. 72(2): p. 276-279.

5.0 Appendix 1 - Petroleum Hydrocarbon Leak Simulation in a Realistic Intermediate Scale Physical Model

This Page is Intentionally Left Blank.

Petroleum Hydrocarbon Leak Simulation in a Realistic

Intermediate Scale Physical Model

Final Report

By

Thomas Robert
Ph.D. Candidate

Richard Martel
Professor

Luc Trépanier
Research professionnal

Richard Lévesque
Analytical technician

December 10, 2014

1. Introduction

The Institut national de la recherche scientifique (INRS) was asked by the Institut national d'optique (INO) to provide an intermediate scale sand tank model with the ability to simulate a diesel fuel leak under a thickness of 1.2 m of dry sand. The requested model had to allow vapor monitoring in soil as well as in the air column located above the sand surface up to a height of 5 m. The mandate also required that INRS monitor diesel vapor migration both in the sand and in the air column located above the sand tank during the experiment.

The intermediate scale model was set up during the week of September 1st 2014. The experiment took place between September 9th and 18th 2014. At the same time INO was performing measurements of volatiles organic compounds with their LIDAR system under development. This report presents the experimental apparatus provided by INRS to INO and the methodology followed, as well as the analytical results of the vapor migration monitoring program. A photomontage showing the experimental setup is presented in Appendix A.

2. Experimental setup and methodology

2.1 Tank

The physical model used for the experiment was a rectangular watertight steel tank lined with a PVC flexible membrane of 4mx5mx3mm (Figure 1). The size of the tank was:

- Interior height : 1.372 m
- Width : 1.880 m
- Length : 2.565 m
- Area : 4.822 m^2
- Internal volume : 6.616 m^3

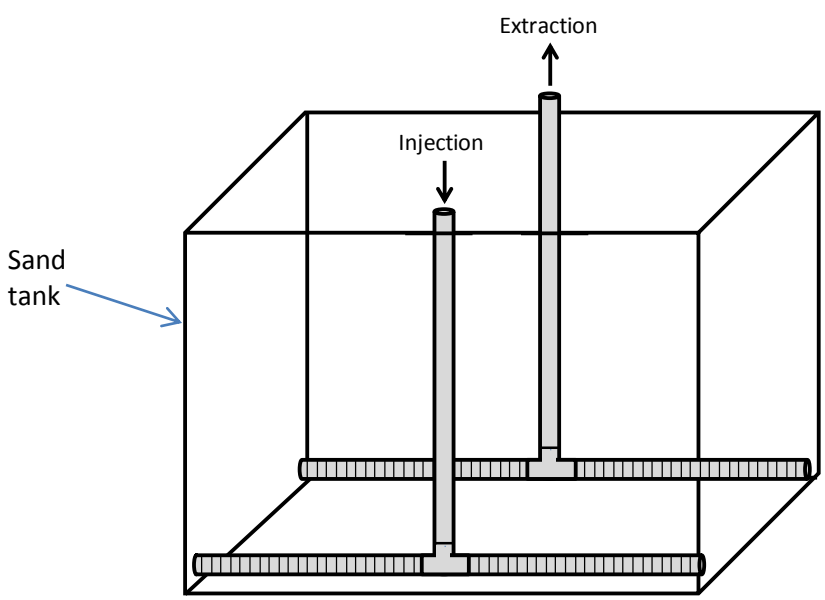

Figure 1. Tank layout prior to sand filling (not to scale)

A fuel injection and extraction system was installed inside the tank before it was filled with sand. The system was designed to simulate a continuous leak at the base of the sand tank. The system is illustrated on Figure 1 and was composed of the following:

- Two horizontal wells located at the base of the tank, against opposite sides. The wells were constructed with slotted 1-inch PVC pipe (slot size 0,010 inch). Both ends of each wells were caped;

- Two vertical solid 1-inch PVC pipes connected to the middle of each horizontal well with a tee and rising along the tank wall to a height of 1.5-m.

2.2 Sand filling

Temisca grade #18 silica sand obtained from Opta Minerals (Waterdown, Ont. Canada) was used as the experimental soil. The grain size distribution provided by the supplier is presented in Table 1.

Table 1. Grain size distribution provided by Opta Mimerals

Mesh size (mm)	% retained
1,18	53
0,85	43
0,60	4

A qualitative mineralogy test was performed on the sand and results showed the presence of 70% quartz and carbonate mineral in proportions of 30 %.The mean grain size is approximately 1,05 mm and corresponds to a medium sand.

The tank was filled by successive and identical sand layers. Each layers consisted of 565.2 kg of sand (25 bags of 22.5 kg each), resulting in a thickness of 0.09 m. The bags were manually emptied on the surface of the previous layer, and the sand was levelled evenly with shovels and rakes. Each layer was compacted using a 2 HP electrical Vibco plate TPE-1830 compactor. The compactor plate was 0.45 m by 0.45 m. It was circulated once over the entire sand layer at a speed of 0,5 m/s approximately. Following compaction, a rake was used to scarify the sand surface in order to make a link between layers and to avoid the formation of preferential vapor flow along horizontal paths.

A total of 14 layers were required to fill the tank to a height of 1.28 m, which represents 7875 kg and 6.172 m^3 of sand. The resulting sand density was 1276 kg/m^3. This value is considered low with regard to usual soil density (around 1750 kg/m^3). The lower density is explained by the uniform sand grains diameter, resulting in lower compaction and high porosity.

2.3 Fuel supply and injection

Three types of fuel were used in the course of this experiment: diesel fuel, pentane and unleaded regular gasoline.

Both diesel fuel and gasoline were obtained at the same Esso service station located in Quebec City, at the intersection between Hamel Boulevard and Saint-Jean-Baptiste Street. Clean 20L Jerri cans were used to carry the fuel to the laboratory. Pentane was laboratory grade and supplied by INO in original 2L amber glass bottle .

Two peristaltic pumps were used for injection and extraction of the diesel fuel. Fexible Viton and high density polyethylene tubings (¼ inch outside diameter) ran from each pump to their respective horizontal well (see Figure 1). The diesel fuel was injected directly from the 20L Jerri cans. The Jerri can used for injection was placed on a scale (Ohaus 3000 series ± 1 g) in order to calculate the injection rate. During the injection phase of the experiment, the injection flow rate was an average of 0.30 kg/min or 0.36 L/min if a density of 0.83 kg/L is considered for diesel fuel. During the recirculation phase, the flow rate was set at 0.1 kg/min (0.12 L/min) for both injection and extraction pumps.

The fuel Jerri cans and the scale were located inside a small tent kept under negative pressure with the air evacuation system of the building in order to prevent contamination of ambient air. The extracted diesel was pumped into a 1000L waste disposal reservoir located outside of the building.

A pan experiment was also made with 5 to 6 pans (Pyrex pan of 30cmx30cmx 5cm), filled with 1 cm of fresh product (diesel, pentane or gasoline) set uniformly at the surface of the sand tank in order to measure the VOC/air vapor concentrations generated by those hydrocarbons in the air column above them with the Lidar instrument.

2.4 Vapor control system

A vapor control system was operated during segments of the experiment. The system was composed of the following:

- A 5m-high polythene tent set above the tank. The base of the tent had the same size as the area of the tank. The base of the tent was taped to the tank in order to limit vapor migration. The materials used were clear polythene and a 1-inch PVC piping frame;

- The top of the tent consisted of a 1 m x 1 m frame built with 1-inch slotted PVC tubing (slot size of 0.010 inch);

- A ½ HP vacuum pump connected to the top slotted PVC frame through the tent structure;

- A 205 L steel barrel filled with granular activated carbon for vapor treatment prior to its release into the atmosphere.

The vapor treatment unit was located outside of the building. When in operation, the pump was set at the highest achievable vacuum pressure (-50 inch H_2O). The periods when the vapor control system was on are specified in the experimental procedures section.

2.5 Monitoring wells and air sampling ports

The monitoring wells used for vapor monitoring inside the sand tank consisted of stainless steel rods with an inside diameter of 6,4 mm (¼ in.). The end tips of each rod were perforated with 2 mm holes over a length of 0.01 m. A stainless screen was set inside the rods along their perforated sections. The end tips were tapered and the rods were hammered into the sand at the desired location and depth.

Three clusters of 3 monitoring wells each were installed inside the sand, for a total of 9 soil vapor monitoring wells. The clusters were place along an axe parallel to diesel fuel flow during the recirculation operation, as shown in Figure 2. The first cluster was located at 0.2 m from the upgradient wall of the tank, the second cluster was located in the center of the tank, and the third cluster was located 0.2 m from the downgradient wall of the tank. In each cluster, the total depth of the 3 wells was 0.18 m, 0.68 m and 1.18 m from the surface of the soil. The corresponding elevations from the floor of the tank were 1.10 m, 0.60 m and 0.10 m respectively (Figure 2(b)).

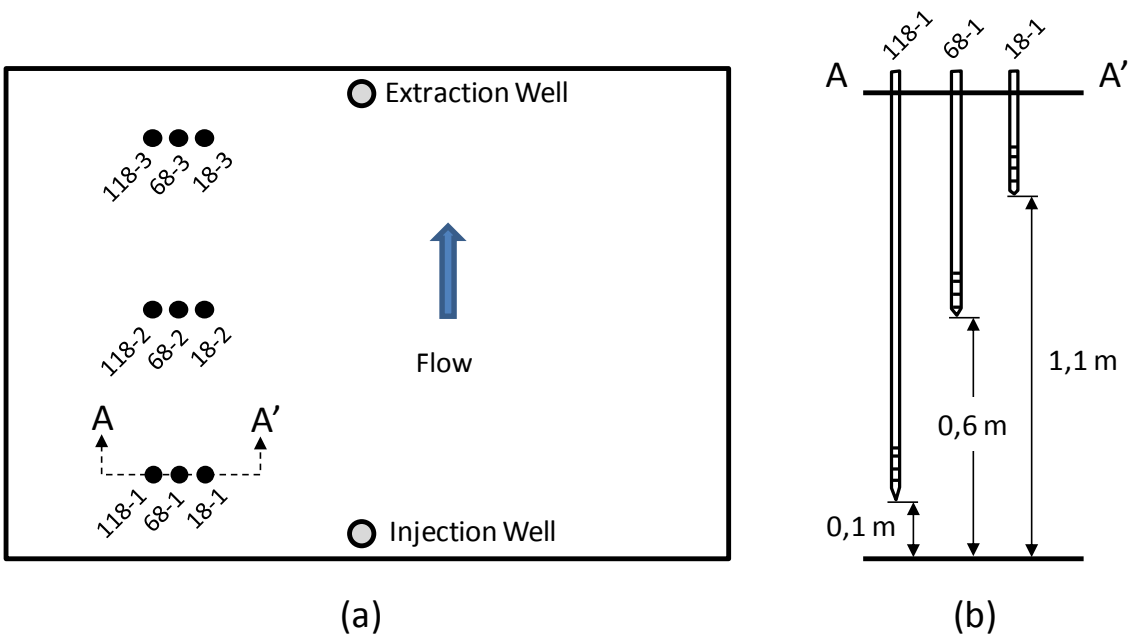

Figure 2. Soil vapor monitoring wells in the sand tank. Plan view (a) and cross-section (b).

An air monitoring tower was set above the surface of the sand in order to collect air samples at 5 different heights. Each sampling port attached to the tower consisted of a 25 feet (7.62m) ¼ in. (6 mm) polyethylene tubing extremity held in place at the desired height by a tie-wrap. Figure 3 presents the ports which were set at heights of 0.03 m, 0.98 m, 2.18 m, 3.38 m and 4.58 m from the surface of the soil.

Each sample port, both in soil and in the air, was connected to a 25 feet (7.62m) polyethylene tubing (Watts, part#SPEB25). All the tubings were regrouped on a table located besides the tank. A 6-inch (15 cm) adaptor made with Masterflex Norprene tubing (part#6404-24) was inserted at the tip of the polyethylene tubing to allow vapor readings.

2.6 Analytical instruments and sampling procedures

Volatile petroleum hydrocarbon (VPH) in soil vapor and air were measured using a Thermo/Foxboro TVA 1000B PID/FID Vapor Analyzer rented from Pine Environmental (Mississauga, Ont., Canada). The Flame Ionization Detector (FID) of the analyzer was supplied with grade 5.0 Hydrogen obtained from Linde (Québec, Qc., Canada). The samples were collected by inserting the analyser sampling tip directly into the Norprene adaptors. Sampled air was introduced into the analyzer using the internal pump at a flow rate of 1 L/min. All measures were taken following a 45 seconds purge allowing the analyser to flush the sampled line and to stabilize. In between each reading, the analyser was left in ambient air for 15 seconds before connecting it to the next sampling line. This flush was extended to at least 1 minute if the concentration was above 400 ppm by photoionisation detector (PID) or 8000 ppm by flame ionisation detector (FID).

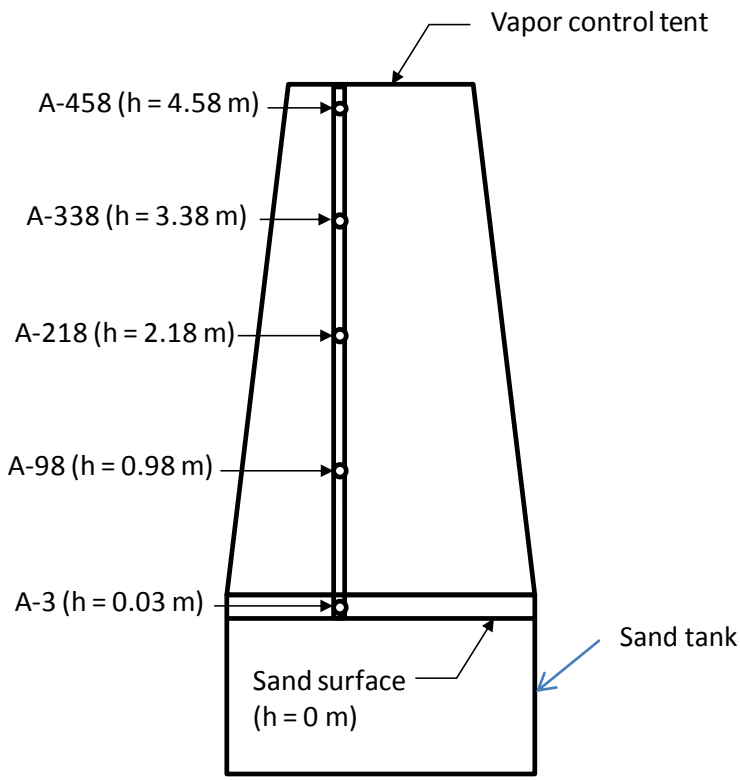

Figure 3. Air monitoring ports above the sand surface (not to scale)
(h = height measured from the sand surface)

The flame ionization detector (FID) detects ions formed during the combustion of a molecule by an hydrogen flame. During combustion, the hydrogen-carbon bonds of the molecule are broken and ions are produced proportionally to the number of carbon atoms in the molecule (only for non-oxygenated and non-halogenated molecules). For example, 1 mmoles of dodecane ($C_{12}H_{26}$) will produce twice as much ions than 1 mmoles of hexane (C_6H_{14}). On the other hand, the photoionization detector (PID) uses UV light to ionize molecules that have a similar or lower ionization energy that the photons produced by the PID lamp. PID readings do not depend on the number of carbons, but on the capacity of the high-energy photons emitted from the PID lamp to

ionize target molecules. According to the literature provided with the instrument, a FID reading of pure n-heptane gas will give an average relative response 16.6 times higher than PID reading.

Thermal desorption tubes (TDT) packed with Carbopack B and shipped by CASSEN Testing Laboratories (Toronto, Ont., Canada) were also used for vapor analysis in order to obtain more information on the vapor composition of selected samples. A total of 29 out of 36 target compounds identified as majors vapor components were quantified by CASSEN Testing Laboratories using Method M.2402.R4 (Reference Method: EPA TO-17 and NIOSH 2549). The sampling system for the sorption of VPH on TDT was composed of an Aircheck sampler (part# 224-PCXR4) connected with a Tygon R3603 tubing to a primary calibrator Defender 510-L (part# 717-510L) rented from Concept Controls Inc. (Ville St-Laurent, Qc., Canada). Sampling was done by connecting the line adaptor to the TDT attached to the single adjustable low flow holder (part# 224-26-01) in line with the primary calibrator in sampling data mode and the Aircheck sampler. This configuration allowed to precisely measure the flow rate during the sampling of each TDT. Sampling flow rate was adjusted to 50 mL/min using the dedicated calibrator tube. Before each sampling, measurement was done with the TVA 1000B analyzer in order to both purge the line and estimate the sampling time on sorbent tube. Temperature and humidity was monitored with a Springfield Precise Temp instrument and measures of the atmospheric pressure were taken from Jean-Lesage International Airport (YQB) meteorological station. This station is located 6 km to the northwest of the INRS Laboratory.

2.7 Experimental procedures

The procedures undertaken during the experiment are presented in Table 2. Vapor monitoring results presented in the following sections are all reported as a function of the cumulative time of the experiment (hr), as presented in the table.

Table 2. Experimental procedure

Date	Time	Cumul. time (hr)	Events
2014-09-09	09:58	0,00	Start diesel injection at the base of the tank
2014-09-09	14:57	4,90	End of diesel injection at the base of the sand tank (100 L injected)
2014-09-10	09:28	23,50	Start of diesel injection/extraction from the base of the tank
2014-09-10	11:20	25,37	End of diesel injection/extraction (15 L)
2014-09-10	11:25	25,46	Positionning of 5 diesel pans on the surface of the sand
2014-09-10	12:00	26,03	The base of the vapor control tent was sealed to the tank perimeter
2014-09-10	15:25	29,45	Positionning of 5 pentane pans on the surface of the sand
2014-09-10	16:00	30,03	Retrieval of pans
2014-09-18	11:05	217,12	Positionning of 6 gasoline pans on the surface of the sand
2014-09-18	16:00	222,03	Retrieval of pans

Notes: - the cumulative time is from the start of the diesel fuel injection in soil;
- the vapor recovery system was in operation during the initial diesel injection;
- the vapor recovery system was always shut off overnight, and a cover was set on the tent;
- the vapor recovery system was always in operation when pans were set on the sand surface.

3. Results

3.1 Soil vapor monitoring during and after diesel fuel injection

A total of 100 L of diesel fuel were initially injected at the base of the sand tank. The average thickness of diesel fuel in the sand accumulated at the base of the tank, estimated from measurements made inside the injection and extraction wells, was 2.5 cm. Figure 4 presents soil vapor monitoring results obtained during and after diesel fuel injection at the base of the tank for the whole duration of the test.

Early FID and PID data measured at a depth of 118 cm clearly show that the vapor migration front is following the diesel fuel flow in the tank during the initial injection phase. Vapor concentrations reached sampling point 118-1 before sampling point 118-2 and sampling point 118-3. The same was observed, but to a lesser extent, with data collected at a depth of 68 cm. After 24 hours however, the vapor composition is similar for a given depth.

PID results show a stabilisation of the soil vapor profile after 2 to 3 days (48 to 72 hours). FID results show a decrease of soil vapor concentrations after a period of 24h. It is hypothesized that this decrease is representative of a compositional change in the vapor composition occurring with time.

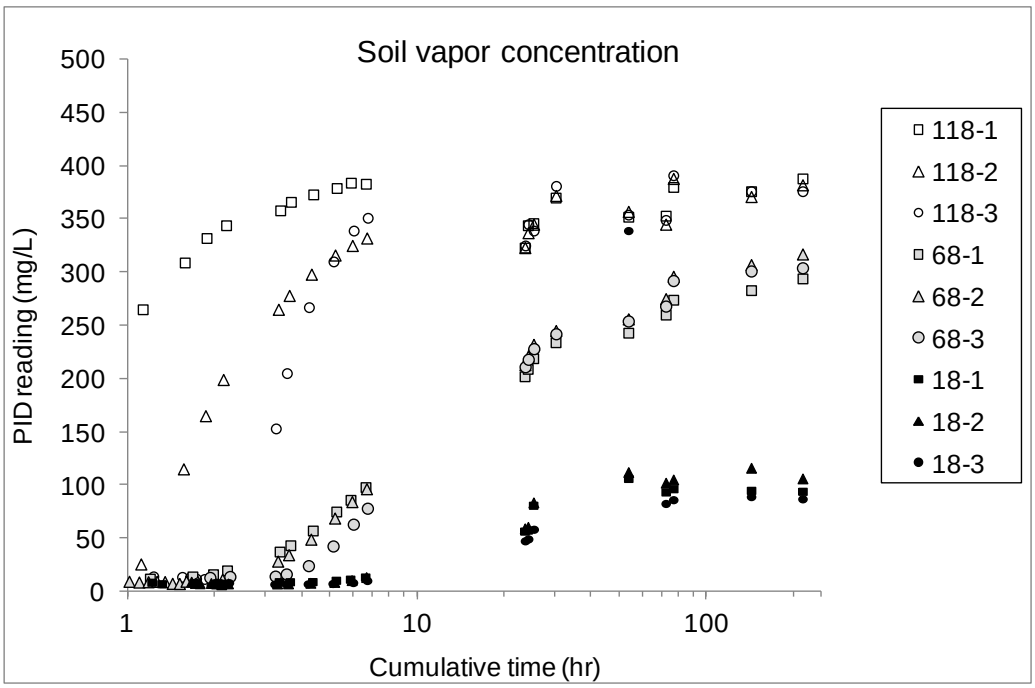

(a)

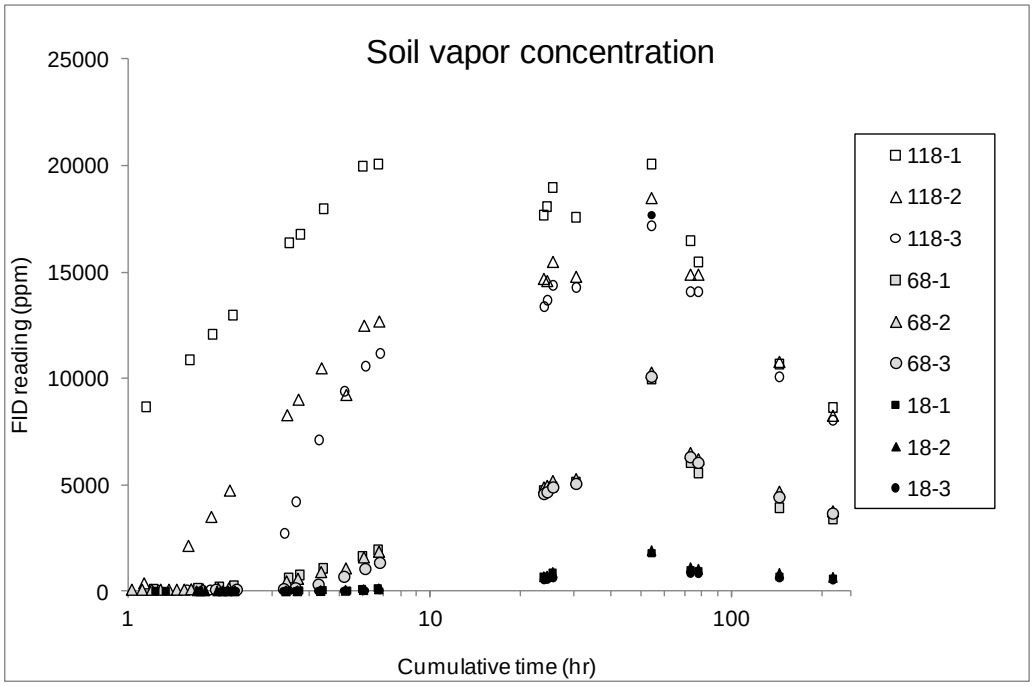

(b)

Figure 4. Soil vapor monitoring in sand during the experiment ((a) PID readings; (b) FID readings).

3.2 Air vapor monitoring

A total of 6 blanks were collected in ambient air during the experiment. Blank PID readings varied between -0.54 and 0.26 mg/L, while blank FID readings varied between 1.28 and 3.65 ppm. Based on these low values detected in ambient air, air vapor results presented in this report were not corrected.

Figure 5 shows air vapor concentrations inside the vapor control tent with diesel fuel present only at the base of the sand tank. It shows that air vapor concentrations inside the tent are diluted when compared with soil vapor concentrations measured at a depth of 0.18 m from the soil surface. The dilution factor obtained from PID readings in soil (depth of 0.18 m) vs. in air (height of 0.03 m) is approximately 10 (100 mg/L in soil (18-1, 18-2, 18-3) vs. 10 mg/L in the air (A-3).

Figure 6, 7 and 8 show the air-monitoring results for the pan experiments. During those experiments, 5 to 6 pans filled with 10 cm of fresh product (diesel, pentane or gasoline) were set uniformly inside the tent, on the sand surface.

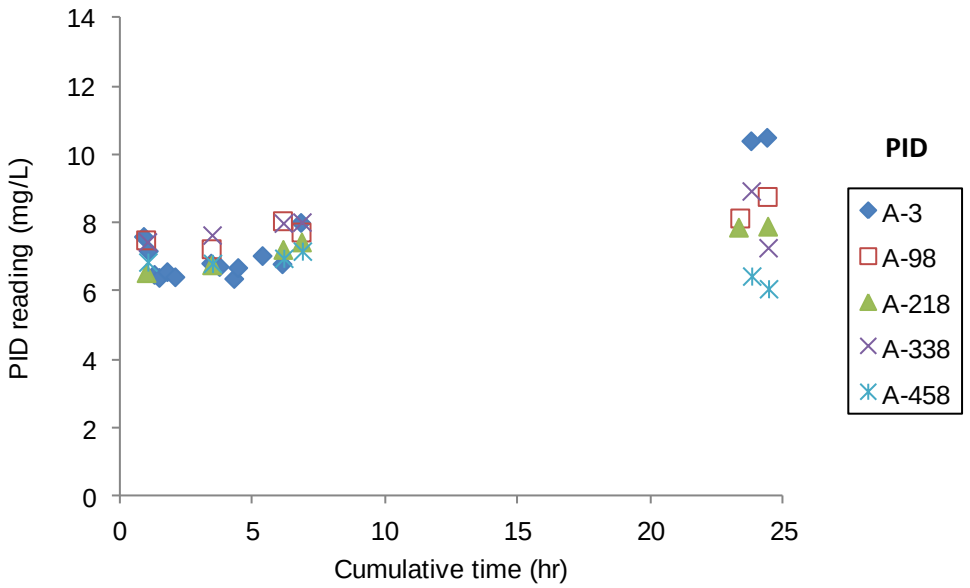

(a)

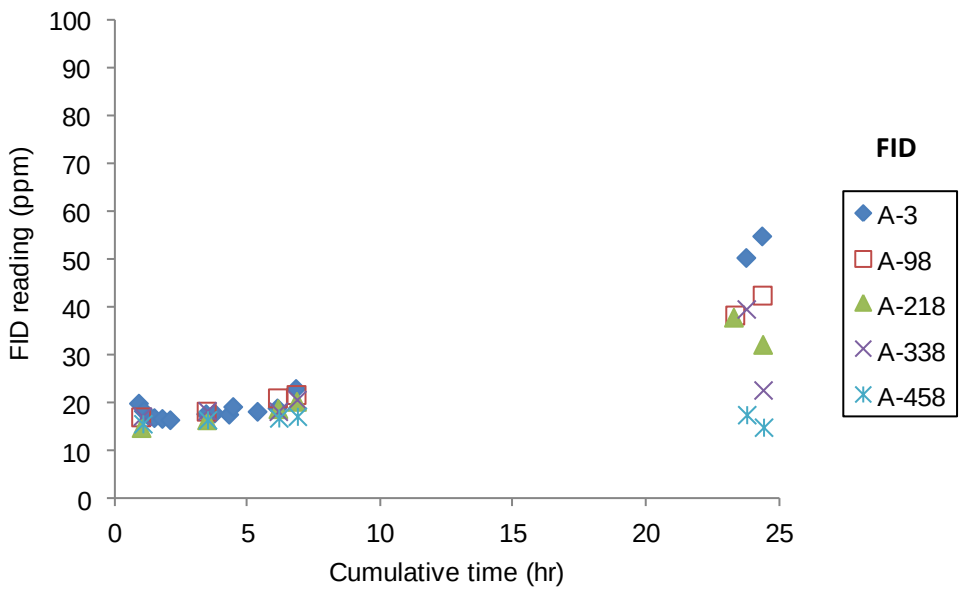

(b)

Figure 5. Air-vapor monitoring with diesel fuel present at the base of the soil in the sand tank ((a) PID readings; (b) FID readings)

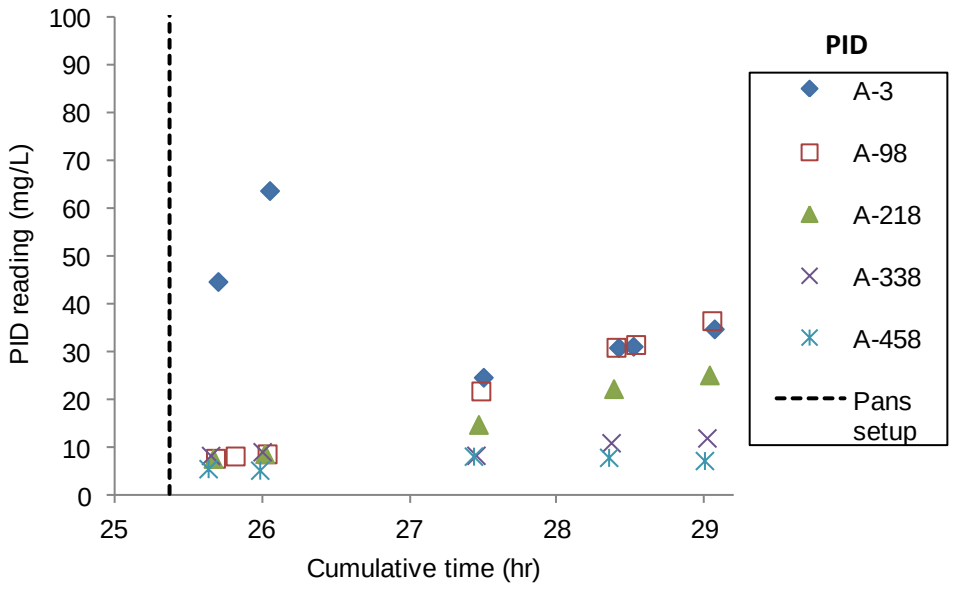

(a)

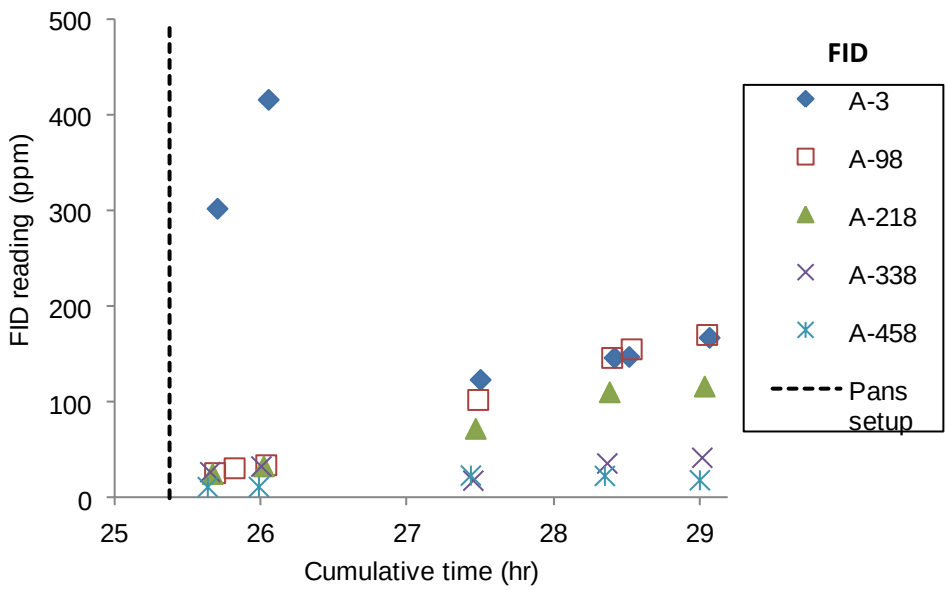

(b)

Figure 6. Air-vapor monitoring with diesel fuel pans located on the surface of the sand tank ((a) PID readings; (b) FID readings)

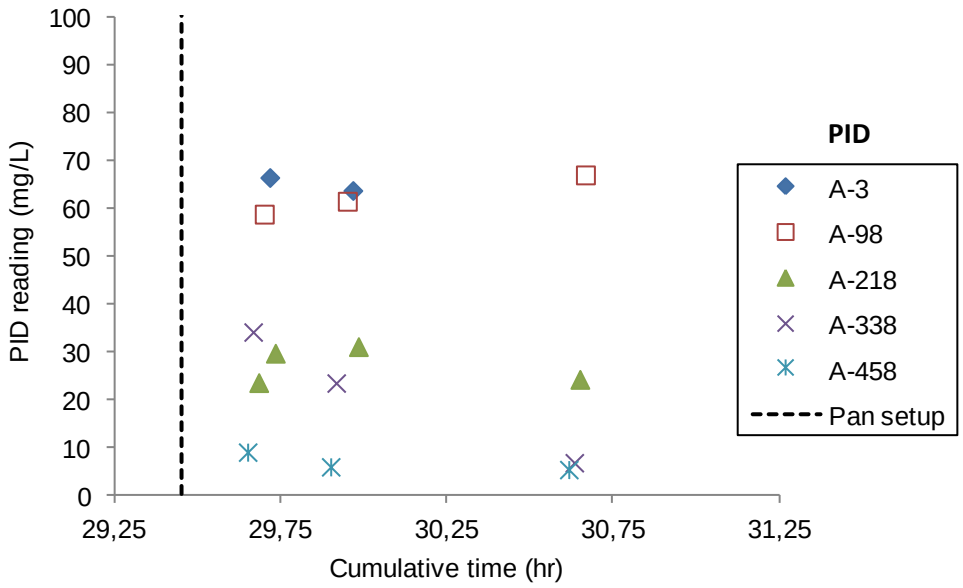

(a)

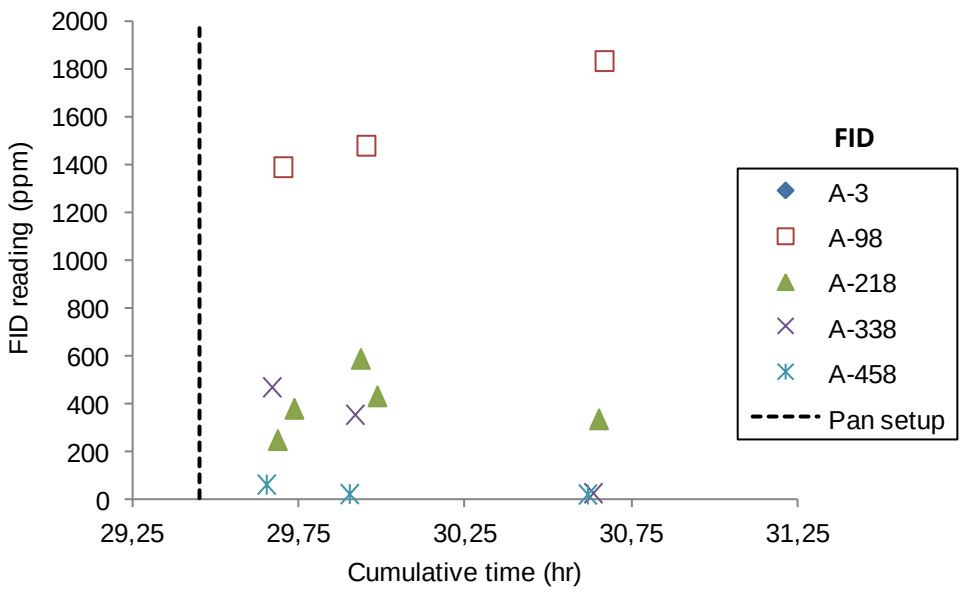

(b)

Figure 7. Air vapor monitoring with pentane pans located on the surface of the sand tank ((a) PID readings; (b) FID readings)

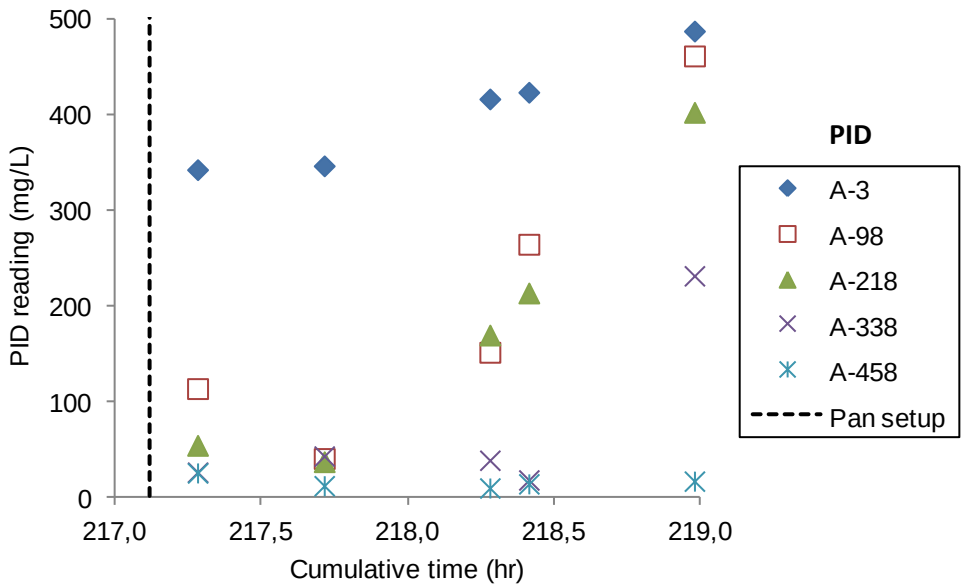

(a)

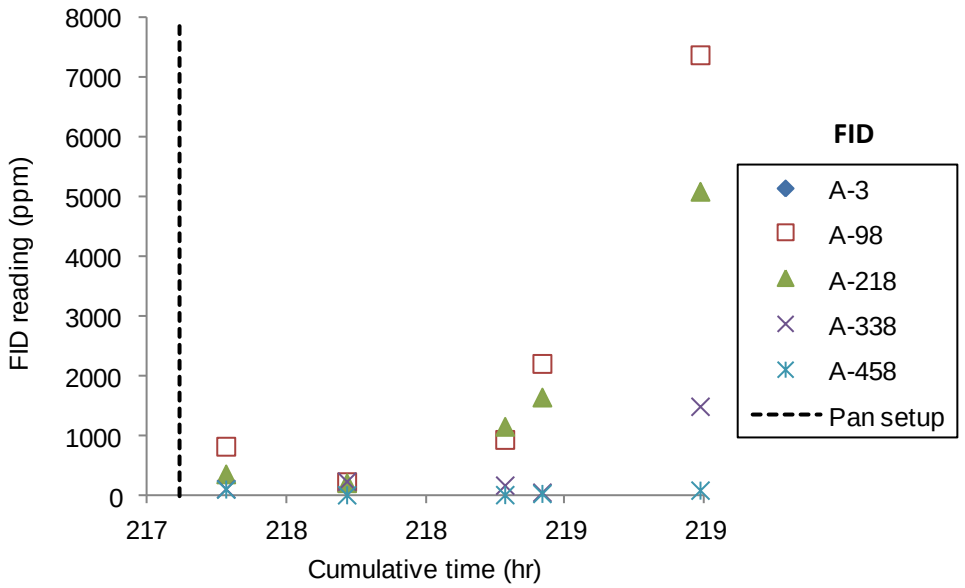

(b)

Figure 8. Air vapor monitoring with gasoline pans located on the surface of the sand tank ((a) PID readings; (b) FID readings)

4. Detailed vapor compounds analysis

Concentrations of VOCs obtained from the thermal desorption tubes are presented in Tables 3 to 5. The objective was to obtain the detailed composition of diesel-fuel and gasoline used at different times of the experiment. Overall, 20 different compounds were analysed. Table 3 presents the blank results (background) measured inside the vapor control tent prior to the initial diesel-fuel release. Table 4 presents the concentrations of compounds in diesel vapor: the fresh product vapor composition can be compared with soil vapor in the middle of the sand profile and air vapor measured at 3 cm above the soil in the vapor control tent. Table 5 presents the compound analysis for the gasoline pan experiment measured at 98 cm above the pans, but at two different times.

Table 3. Background hydrocarbons concentration in air

Sample type:	**Air (blank)**	
Hydrocarbon source:	**-**	
Location:	**A-218**	
Tube number	Tube 7	
Tube ID No.	G0121496	
Date	08-sept	
Hour	14h40	
Average Flow Rate (mL/min)	43,2	
Sampling Time (min)	20	
Sample Volume (L)	0,864	
Temperature (°C)	21,3	
Ambiant pressure (mm Hg)	764,9	
Humidity (%)	43	
PID value (ppm)	**4,38**	
FID value (ppm)	**8,83**	
Analytical results	Concentration	Proportion
	(ug/m^3)	(%-mass)
Cyclohexane	n.d.	n.d.
Benzene	n.d.	n.d.
n-Heptane	n.d.	n.d.
Methylcyclohexane	n.d.	n.d.
n-Octane	n.d.	n.d.
Toluene	24,6	42,86
Ethylcyclohexane	n.d.	n.d.
Ethylbenzene	n.d.	n.d.
n-Nonane	n.d.	n.d.
m/p-Xylene	23,1	40,24
o-Xylene	n.d.	n.d.
Isopropylbenzene	n.d.	n.d.
n-Propylbenzene	n.d.	n.d.
n-Decane	1,3	2,26
4-Ethyltoluene	n.d.	n.d.
1,3,5-Trimethylbenzene	n.d.	n.d.
n-Butane	8,4	14,63
Isobutane	n.d.	n.d.
n-Pentane	n.d.	n.d.
2-Methylbutane	n.d.	n.d.
Total Mass in 1 m^3 (ug)	57,4	100

Note: n.d. = below detection limit

Table 4. Composition of fresh diesel fuel vapor in air of Jerri can, and weathered diesel fuel vapor in soil in the middle of sand tank and in the air 3 cm above the sand tank

Sample type:	**Air-vapor**		**Soil-vapor**		**Air-vapor**	
Hydrocarbon source:	**Fresh diesel fuel**		**Diesel in soil**		**Diesel in soil**	
Location:	**Diesel Jerri can**		**68-2**		**A-3**	
Tube number	Tube 3		Tube 2		Tube 1	
Tube ID No.	G0162177		G0139870		G0139876	
Date	18-sept		18-sept		18-sept	
Hour	10h53		10h35		10h10	
Average Flow Rate (mL/min)	54,4		51,6		47,4	
Sampling Time (min)	1		1		20	
Sample Volume (L)	0,0544		0,0516		0,948	
Temperature (°C)	18,1		18,1		17,5	
Ambiant pressure (mm Hg)	757,4		757,4		757,2	
Humidity (%)	46		46		48	
PID value (ppm)	**6700**		**345**		**18,73**	
FID value (ppm)	**56200**		**3871**		**95**	
Analytical results	Conc.	Proportion	Conc.	Proportion	Conc.	Proportion
	ug/m^3	(%-mass)	ug/m^3	(%-mass)	ug/m^3	(%-mass)
Cyclohexane	31600	5,88	24300	7,30	861	3,54
Benzene	15300	2,85	12900	3,87	416	1,71
n-Heptane	8300	1,54	39000	11,71	1310	5,38
Methylcyclohexane	158000	29,41	73500	22,07	2870	11,79
n-Octane	68100	12,67	34000	10,21	768	3,15
Toluene	56100	10,44	27800	8,35	723	2,97
Ethylcyclohexane	30300	5,64	20200	6,07	526	2,16
Ethylbenzene	6070	1,13	2810	0,84	26,4	0,11
n-Nonane	12700	2,36	5330	1,60	45,8	0,19
m/p-Xylene	19900	3,70	8120	2,44	85,6	0,35
o-Xylene	5360	1,00	2390	0,72	26,5	0,11
Isopropylbenzene	824	0,15	279	0,08	n.d.	n.d.
n-Propylbenzene	197	0,04	n.d.	n.d.	n.d.	n.d.
n-Decane	n.d.	n.d.	n.d.	n.d.	7,3	0,03
4-Ethyltoluene	102	0,02	n.d.	n.d.	n.d.	n.d.
1,3,5-Trimethylbenzene	136	0,03	n.d.	n.d.	n.d.	n.d.
n-Butane	7400	1,38	1960	0,59	59	0,24
Isobutane	3670	0,68	444	0,13	16,2	0,07
n-Pentane	110000	20,47	61200	18,38	16300	66,95
2-Methylbutane	3240	0,60	18800	5,65	306	1,26
Total Mass in 1 m^3 (ug)	537299	100	333033	100	24347	100

Note: n.d. = below detection limit

Table 5. Composition of gasoline fuel vapor in air at 98 cm above pans at two different times

Sample type: **Hydrocarbon source:** **Location:**	**Air-vapor** **Gasoline pans** **A-98**		**Air-vapor** **Gasoline pans** **A-98**	
Tube number	Tube 5		Tube 6	
Tube ID No.	G0160448		G0160552	
Date	18-sept		18-sept	
Hour	11h29		13h52	
Average Flow Rate (mL/min)	53,1		51,9	
Sampling Time (min)	3		1	
Sample Volume (L)	0,159		0,0519	
Temperature (°C)	17,9		16,2	
Ambiant pressure (mm Hg)	759,1		762,1	
Humidity (%)	43		40	
PID value (ppm)	**62,5**		**502**	
FID value (ppm)	**403**		**8964**	
Analytical results	Concentration	Proportion	Concentration	Proportion
	ug/m^3	(%-mass)	ug/m^3	(%-mass)
Cyclohexane	3180	3,77	21400	12,99
Benzene	1500	1,78	17600	10,68
n-Heptane	1350	1,60	14900	9,05
Methylcyclohexane	2040	2,42	20700	12,57
n-Octane	340	0,40	2330	1,41
Toluene	5610	6,64	47700	28,96
Ethylcyclohexane	153	0,18	882	0,54
Ethylbenzene	252	0,30	2940	1,78
n-Nonane	36	0,04	220	0,13
m/p-Xylene	810	0,96	1940	1,18
o-Xylene	274	0,32	673	0,41
Isopropylbenzene	n.d.	n.d.	n.d.	n.d.
n-Propylbenzene	n.d.	n.d.	n.d.	n.d.
n-Decane	n.d.	n.d.	n.d.	n.d.
4-Ethyltoluene	n.d.	n.d.	n.d.	n.d.
1,3,5-Trimethylbenzene	n.d.	n.d.	n.d.	n.d.
n-Butane	1710	2,03	1350	0,82
Isobutane	772	0,91	297	0,18
n-Pentane	32600	38,61	30400	18,46
2-Methylbutane	33800	40,03	1390	0,84
Total Mass in 1 m^3 (ug)	84427	100	164722	100

Note: n.d. = below detection limit

Appendix B presents the certificates of analysis. Chromatograms are presented for each analysed sample.

5. Data Interpretation

An analytical solution was used to determine the vapor-diffusion properties of the experimental model. In the case of a semi-infinite solid (z > 0) initially at zero concentration (c = 0) everywhere and whose surface (z = 0) is maintained at a constant concentration ($c = c_S$) during the whole experiment (t > 0), the statement of the problem is :

$$\frac{1}{D}\frac{\partial c}{\partial t} = \frac{\partial^2 c}{\partial z^2}$$

The solution of this differential equation is obtained using the Laplace transform. The concentration at any elevation *z* and time *t* in the model (sand tank) is :

$$c(z,t) = c_s erfc(\frac{z}{2\sqrt{Dt}})$$

D is the effective diffusion coefficient in soil for the experiment. In this case it includes every mechanisms potentially controlling vapor migration such as vapor adsorption onto soil grains. Erfc is the complementary error function. It is of sigmoid shape and occurs in differential equations. It is implemented in Excel spreadsheets as erfc(). Erfc (x) is equal to 1 – erf (x).

This analytical diffusion model excludes any vapor concentration change due to convection under a pressure gradient. Thus, air pressure was considered constant at all time inside the model (sand tank).

The differential equation solution was fitted to the measured PID data by adjusting the parameters c_S and D. Results are presented in Figure 9. The best match was obtained for a c_S of 400 mg/L, and a D of 0,045 cm^2/s. The experimental data measured at a depth of 1,18 m were used for the curve matching since this data is the least influenced by potential convection of air under pressure gradients.

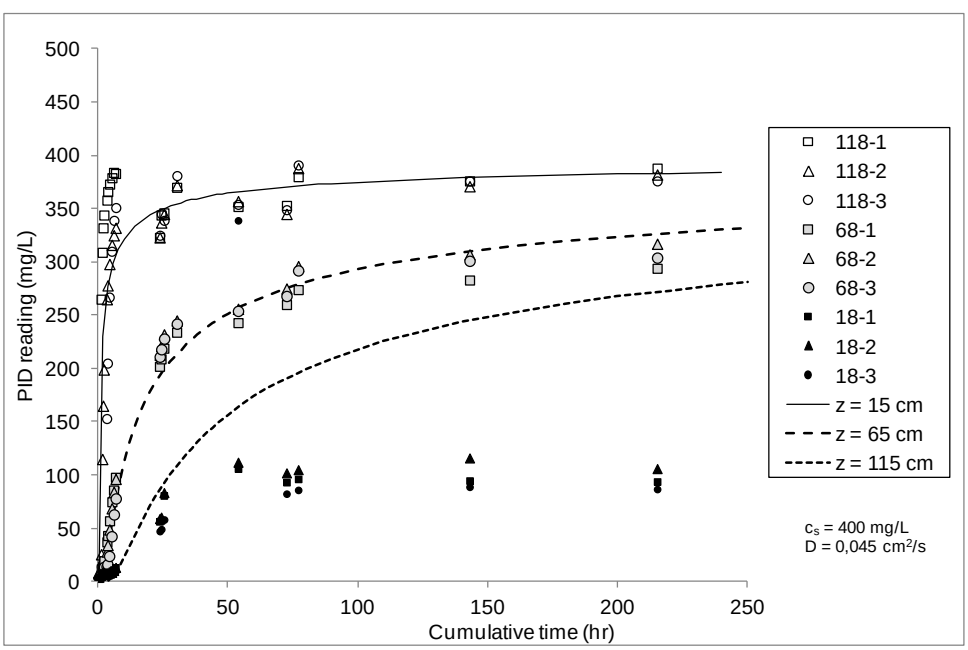

Figure 9. Analytical solution vs. experimental data. The curve matching was done with the set of data obtained at a depth of 1,18 m (elevation of 0,15 m) in the sand tank

Results show that the analytical model fitted to the data measured at the bottom of the sand tank (118-1, 118-2, 118-3), it also fits in a relatively good way the data measured in the center of the tank (68-1, 68-2, 68-3). However, the data measured near the sand surface (18-1, 18-2, 18-3) differs significantly from the model prediction. This shows that soil vapor in the upper half of the soil is diluted by the air located above the sand surface. The mechanism of dilution is operating not only in the air above the soil but also in the upper part of the soil profile explaining the relatively low vapor concentration measured in the air column located above the sand tank. This phenomenon should be considered in the development of the LIDAR technology.

The rate of vapor concentration change over time due to diffusion will be reduced if the soil contains a fraction of water. In this case, the water present in the soil pores will dissolve fuel compounds proportionally to the liquid-gas partitioning coefficient. The readers are referred to the theory section presented in Johnson and Kreamer (1994) for additional information.

6. Conclusion

A sand tank with a vapor control tent was built to reproduce a leak from a pipeline. Diesel-fuel was first used as a model oil. Concentrations up to 10 mg/L (PID reading) of diesel were generated in the air above the surface of the sand tank. Other tests were made with pans of diesel, gasoline and pentane at the surface of the sand tank. INO was able to test their LIDAR system with this experimental setup.

7. References

API, 2004. API interactive LNAPL guide. Version 2.0.

Hess. Diesel Fuel Safety Data Sheet. http://www.hess.com/docs/us-safety-data-sheets/dieselfuel_alltypes_includingultralowsulfur_diesel(ulsd).pdf?sfvrsn=2

Jo-Yu Chin, Stuart A. Batterman, 2012. VOC composition of current motor vehicle fuels and vapors, and collinearity analyses for receptor modeling. Chemosphere 86, 951-958.

Johnson, T.E. and Kreamer, D.K. 1994. Physical and mathematical modeling of diesel fuel liquid and vapor movement in porous media. Groundwater, Vol. 32, No. 4, 551-560.

Peng, C.-Y., Lan, C.-H., Dai, Y.-T., 2006. Speciation and quantification of vapor phases in soy biodiesel and waste cooking oil biodiesel. Chemosphere 65, 2054-2062.